AN INVESTIGATION OF THE SPATIALLY DEPENDENT REACTOR SOURCE TRANSFER FUNCTION WITH TEMPERATURE FEEDBACK

A THESIS

Presented to

The Faculty of the Graduate Division

by

Donald Norris Bridges

In Partial Fulfillment

of the Requirements for the Degree

Doctor of Philosophy

in the School of Nuclear Engineering

Georgia Institute of Technology

October, 1970

AN INVESTIGATION OF THE SPATIALLY DEPENDENT REACTOR SOURCE TRANSFER FUNCTION WITH TEMPERATURE FEEDBACK

Approved:

Chairman

Date approved by Chairman: 10/15/70

In presenting the dissertation as a partial fulfillment of the requirements for an advanced degree from the Georgia Institute of Technology, I agree that the Library of the Institute shall make it available for inspection and circulation in accordance with its regulations governing materials of this type. I agree that permission to copy from, or to publish from, this dissertation may be granted by the professor under whose direction it was written, or, in his absence, by the Dean of the Graduate Division when such copying or publication is solely for scholarly purposes and does not involve potential financial gain. It is understood that any copying from, or publication of, this dissertation which involves potential financial gain will not be allowed without written permission.

_____

7/25/68

ACKNOWLEDGMENTS

The research described in this thesis was made possible through the support and assistance of a large number of individuals. Acknowledgments and special thanks are heartily extended for these contributions. In particular, I wish to express sincere appreciation to my thesis advisor, Dr. J. D. Clement for his encouragement, support, and invaluable assistance in this research effort. A great deal of this assistance was provided at the sacrifice of his personal time. Dr. W. W. Graham, III, Dr. R. J. Johnson, and Dr. L. J. Gallaher served on my reading committee and provided many helpful suggestions both throughout the period of investigation and through their review of the manuscript. The assistance of Dr. G. G. Eichholz in his careful review of the manuscript is appreciated. Dr. C. J. Roberts, Director of the School of Nuclear Engineering, generously supported this work, providing both moral and financial support and enduring many tales of woe.

I am particularly grateful to my good friends, Mr. G. H. Weaver and Mr. D. D. Ebert, for their continuing assistance and interest in this work from inception to completion. Mr. J. P. Renier provided much needed encouragement and support and for this I am appreciative. Mr. J. M. Reynolds generously offered his time in assisting with the data analysis both in preparing the data for analysis and writing the Fast Fourier Transform Program for the analysis. A great deal of his personal time was expended in problems unique to this experiment. I am also grateful

for the many hours of discussion and assistance provided by Mr. John C. Alderman. The assistance of Mr. Alderman in the experimental planning and preparation stage made a seemingly impossible task become very reasonable and doable. Special thanks are in order for the generous assistance provided by Mr. J. W. Biddy and Mr. J. M. Burke in the design and construction of the pile oscillator. The inspired suggestions and interest in this work by Mr. Burke contributed significantly to the successful operation of the experimental equipment. The outstanding assistance by the GTRR Reactor Operations Group headed by Mr. R. S. Kirkland and Mr. F. C. Apple is gratefully acknowledged. Each of these men, Mr. L. D. McDowell, Mr. S. H. Kirbo, Mr. J. T. Moon, Mr. W. A. Pruett, and Mr. J. M. Sullivan, worked long night shifts in order that these experiments be conducted. The cooperativeness and "can do" attitude of this entire group deserves the highest accolade. Appreciation is extended to Mr. John Wright and the rest of the Health Physics staff for their assistance during the experimental program. The assistance of Mr. R. E. Meek and Mr. Billy D. Statham in testing and maintaining the electronic components in this experimental work is gratefully acknowledged. A word of thanks is extended to Mr. A. J. Foltman for photographing the equipment. I am very appreciative to Dr. N. J. Ackerman of the Oak Ridge National Laboratory for the loan of fission chambers during the latter stages of this program. The assistance of Mrs. Lydia Geeslin in the typing of the manuscript is appreciated.

Financial support for this research was provided by a Special Atomic Energy Commission Fellowship and a Georgia Tech Graduate Research Assistantship.

To my parents, I express deep appreciation for their confidence and encouragement over this period of graduate study. Finally, and certainly most importantly, I extend my sincerest appreciation to my wife, Charlene, and our children, Denise and David, for their love, support, and understanding during a difficult time when family life always seemed to come second to "books."

TABLE OF CONTENTS

TABLE OF CONTENTS (Concluded)

LIST OF TABLES

LIST OF ILLUSTRATIONS

LIST OF ILLUSTRATIONS (Continued)

LIST OF ILLUSTRATIONS (Continued)

LIST OF ILLUSTRATIONS (Concluded)

SUMMARY

The nature of this investigation lies in the area of transfer functions in the general field of nuclear reactor dynamics. Transfer functions indicate the linear dynamic characteristics of a system and are used frequently in control and stability studies. The specific nature of this research involved the study, both theoretically and experimentally, of the space-dependent reactor source transfer function with temperature feedback.

An existing theoretical model, known as the complex source method and capable of predicting neutron flux response to a small periodic disturbance, was extended to include temperature feedback effects. Temperature feedback terms were included by relating reactor parameter changes to the fluctuating flux levels. This derivation based on two-group diffusion theory resulted in two sets of nonhomogeneous complex equations. These general equations were applied to a one-dimensional model of the Georgia Tech Research Reactor (GTRR) and a computer program, SPARE, was developed for computing the source transfer function as a function of the reactor power level. The validity of the SPARE calculations was tested over six orders of frequency magnitude from 1×10^{-4} Hz to $1 \times 10^{+2}$ Hz for both no feedback (zero-power) and temperature feedback (full-power) conditions. The results of the checks against the SPARE calculations were very good and served to validate the SPARE calculations.

The experimental portion of this investigation involved the design and construction of an in-core pile oscillator. The pile oscillator was

located in the center of the reactor since this arrangement permitted the experimental verification of a one-dimensional calculation. The pile oscillator employed a pseudo-random binary sequence for introducing flux disturbances with the desired frequency components. This approach offered the advantage of investigating a broad band of frequencies in a single experimental run. Measurements were made for several spatial detector locations within the reactor for zero-power and at-power (900 kW) conditions. The frequency range from 4×10^{-4} Hz to 8.5 Hz was investigated. Data were taken and stored on magnetic tape using a network of two PDP-8 computers and a magnetic tape unit. Data analysis was done using a Fast Fourier Transform program on a Univac 1108 computer.

The results from the SPARE calculations and the experiments agreed quite closely. Temperature feedback effects for the GTRR were observed to occur at frequencies of 2×10^{-2} Hz and less, and to become quite pronounced at frequencies of 1×10^{-3} Hz and smaller. The extent of temperature feedback over the frequency spectrum was correctly predicted by the SPARE calculations.

Spatial effects were observed to be significant only for the higher frequencies. For the frequency range less than one Hz the experimental results indicated a point model response for the GTRR. SPARE calculations indicated true point model response at low frequencies of 1×10^{-3} Hz and less, with only slight spatial response over the limits of the reactor for frequencies as high as one Hz. The amplitude calculation over this frequency range showed no spatial dependence and the calculated phase angle variation over the spatial limits of the reactor increased from less than one degree variation at 1×10^{-3} Hz to slightly over six degrees variation

at one Hz. Further, the majority of the phase angle variation in this frequency range was calculated to occur between the oscillator and the first detector location (R=15 cm). The phase angle variation over the limits of the reactor for this frequency range was not large enough to be significant. In this sense the experimental measurements confirmed the SPARE calculations.

Spatial effects were observed for frequencies above one Hz. The higher frequency end of this study was investigated to a maximum of 8.5 Hz since this frequency region was found to be well outside the range of interest for temperature feedback and this frequency region had been the subject of an earlier investigation.

From the results of this investigation it was concluded that this approach for predicting the spatial source transfer function with temperature feedback is valid. This technique should be useful for predicting at-power spatial transfer functions for reactor system stability studies where temperature feedback and spatial effects are much more pronounced than in the GTRR. Also, this approach should be useful in dynamic studies for predicting at-power flux response to reactivity fluctuations. In general, this technique should find application in the study of space and energy effects in the area of reactor system dynamics.

CHAPTER I

INTRODUCTION

In recent years much interest has developed in the area of nuclear reactor dynamic behavior. The study of nuclear reactor dynamics is concerned with the spatial and transient behavior of the reactor and is usually called space-time kinetics. This interest in space-time behavior has been stimulated by the practical need to understand and control complex nuclear reactor systems. The subject of space-time kinetics becomes more important as nuclear reactor cores grow larger because of reduced neutron coupling between parts of the larger system.[1] With the advent of larger power reactors it has become necessary from a safety standpoint to understand more thoroughly the space-time effects in reactor performance. Results of kinetics studies indicate clearly that space effects can be important and a priori cannot be neglected in the interpretation of reactor experiments or in the analysis of reactor behavior, safety, or stability.[2]

The material in this chapter presents a background discussion in the space-time kinetics area and states the objective of this particular kinetics investigation. Specifically, the background discussion includes a rather brief, general discussion on the major space-time analysis methods, a review of work in the more specialized area of spatial transfer functions, and a review of modulated experiments which is the experimental technique for measurement of transfer functions. The concept and use of reactor

transfer functions are presented in detail in the chapter on Theoretical Development; however, consider for now that the use of transfer functions is a specialized technique for studying certain dynamic characteristics of the reactor system.

Space-Time Kinetics

Factors important in reactor kinetic studies include the energy generated in the system; its distribution between fuel, moderator, and coolant; and the time rate of change of energy production and its spatial distribution. Comprehensively describing these complex interactions, experimentally evaluating certain parameters, and the difficulty of handling analytically or numerically the time-dependent transport equations have led to the wide use of the space-independent conventional kinetics equations.[2] The space-independent equations have subsequently been used extensively, both for the interpretation of experimental data and for the prediction of dynamic response.

The development of larger reactor cores for higher power reactors led to an emphasis on spatial effects. Theoretical work in this area was assisted by the increased capability of larger and faster computers. Studies in the slow transient region for the investigation of spatial xenon oscillations were among the first space-time investigations. Emphasis in this area of space-time work was on determining conditions for stability. Methods for analyzing these slow transients have been thoroughly reviewed by Stone[3] and Wilson.[4]

In a review paper by Hsu and Mulcahey[5] on space-dependent reactor dynamics it was pointed out that spatial methods developed to date have

indicated the need for more complete methods to calculate spatial effects. These methods are needed for predicting the existence of potentially hazardous conditions in reactors due to spatial effects. For instance, large discrepancies have been reported in reactor transients calculated with and without considering spatial effects.[6,7] It was concluded

> that, for large reactors, the standard non-spatial methods for calculating reactor kinetics are inadequate to predict some situations. To insure the safe operation of an advanced power reactor throughout its life it is necessary to consider spatial dynamics in the design of reactor and plant control and safety systems.[5]

It was also pointed out that the spatial methods should be capable of taking into account for heat transfer, fluid flow, and multiple-energy-group kinetics considerations.

The present principal methods have been discussed thoroughly in the review papers of Hsu and Mulcahey[5] and Kerlin.[8] Among the methods discussed is the point-model reactor kinetics method. The concept of this model is the study of reactor dynamic behavior by means of spatially averaged or weighted-average quantities of system variables. The basic assumption is that the space-time solution of the system variables can be separated into a single product of a space-dependent function and a time-dependent function. The most general discussion on the derivation of the point model kinetics equations is given by Henry.[9] The most often used weighting function for this model is the steady-state adjoint solution of the system equations.[10] The basic assumption used in deriving the point model implies that no knowledge of the spatial variation is obtainable with this model, so this approach is not suitable for studying large-size power reactors, fast or thermal.

Another common method of space-time analysis is the "adiabatic method." This method introduced by Henry and Curlee[11] is essentially based on the same principle as the point model. The difference is that the adiabatic method modifies the solution of the system variables as well as the spatial weighting function at various time intervals while retaining the point model formulation. This method implies that the flux shape responds instantaneously to the change of reactor properties. The application of this approach to large power reactors has similar drawbacks as the point model, although to a lesser extent.

The "modal method"[1,12] is another frequently used method of space-time analysis. In concept this method approximates the space-time solution of the system variables by a linear combination of some known space functions (modes) with undetermined time-dependent coefficients. The space-time system equations can be reduced to a set of time-dependent equations of the modal coefficients by performing spatial integration over the reactor. The various types of modal methods involve the selection or construction of the space functions. It has been noted that the modal method is adequate for simple linear space-time reactor systems. For more complex or nonlinear systems, the method becomes undesirable because of the amount of effort required in the analysis.

The "nodal method"[1] is another common method. This approach (coupled core) considers a space-time reactor system as a finite number of points (nodes) or smaller reactor systems coupled by the interaction between adjacent nodes (e.g., due to flux leakage or heat transfer between interface boundaries). The procedure is to divide the entire reactor system into strategically located smaller regions or zones. The same basic

assumption used in the point model is imposed in each and every region, and the final node equations are derived by the same procedure as in the point model formulation. The coupling coefficients are obtained by means of the boundary conditions given for each region. The adequacy of this approach is limited only by the number of regions that can be considered in practice. The number of node equations becomes very large and the determination of coupling coefficients usually poses a problem for the desired accuracy.

Another principal method described is the "transfer function method." This method is applicable for linear dynamic processes only and, although limited in general application, does have wide application in the field of stability analysis. The transfer function approach is a method for studying the reactor dynamic characteristics by relating the system response to a sinusoidal input forcing function. This general method is used in this investigation and will be discussed in greater detail in the chapters on the theoretical and experimental portions of this work.

Other methods include Flux Synthesis,[13] the Direct Method,[14,15] and a number of other methods in related disciplines.[5] These methods have lesser applicability than the previously described methods and will not be discussed herein.

The general opinion seems to be that the theoretical investigations have reached a state of maturity and the current need is for practical application of these theories.[5]

Review of Spatial Transfer Function Methods

In practice the most widely used approach for determining stability is the method of transfer function analysis employing Bode or Nyquist plots.[16] Transfer functions simplify the study of stability by the use of highly developed analytical and graphical methods. The transfer function is frequency dependent and is described qualitatively as the ratio of the system response to a sinusoidal input signal.

The transfer function approach to reactor system response dates back as early as 1949.[17] The analysis of reactor control using transfer functions was given early justification as a result of experimental transfer function measurements on the Argonne CP-2 reactor.[18] Transfer function representation and utilization has played a vital role in the development of reactor systems. The concept of transfer function representation of nuclear power plants has proved a very fruitful tool both from points of view of dynamic analysis and the interpretation of experimental data.[19] A vast amount of stability analysis has been based on transfer function equations derived from the conventional point reactor kinetics equations and suffers the same spatial shortcomings as do the point-kinetics flux space-time analysis.

The experimental technique for transfer function measurements makes use of a modulated source and dates back to the paper of Weinberg and Schweinler.[20] The pile oscillator technique has been used many times for reactor studies and transfer function measurements. The uses are far too numerous to list; however, a few outstanding transfer function experiments are referenced.[21,22,23,24,25]

Hanson and Foulke[26] have done significant experimental work using

a pile oscillator to observe spatial effects in the zero power transfer function for a reflected reactor (NORA Reactor). Experimental results compared favorably with two-group theory spatial calculations by the method of finite differences using an analog computer.

Nomura[27] did extensive work on developing a technique for predicting space-dependent transfer functions using a modal expansion technique with orthogonal functions. This work was applied to one- and two-energy group equations and, in addition, the evaluation of the transfer function was utilized to determine subcriticality as well as fast and thermal lifetimes. A somewhat similar method was developed by Sanathanan.[28]

Loewe[29] developed a theoretical model for the spatial source transfer function by considering the two-group neutron diffusion equations in a multiregion reactor for an arbitrarily located oscillatory absorber and detector. The modal method of analysis was employed with the space functions expanded in terms of solutions to the Helmholtz equation. Loewe found that there was not general agreement between the space-dependent and the space-independent functions and that particularly high-frequency transfer function data must be interpreted in terms of space-dependent effects. He concluded that the evaluation of data using several detector locations in terms of the conventional model could give results quite different.

Kylstra and Uhrig[30] obtained the spatial source transfer function in a manner similar to Loewe. The general equation was developed for a single region, isotropic, homogeneous medium using the time-dependent Fermi age and diffusion theories. They found that, in general, there was

no agreement between the frequency response obtained with the lumped-parameter (conventional) model and the space-dependent model. The results obtained from experiments with a light and heavy water subcritical assembly indicated that the lumped-parameter model is not capable of accurate results.

Hoshino, Wakabayashi, and Hayashi[31] have also developed a theoretical model for predicting the source transfer function using a modal expansion technique with the Laplace transformed diffusion equations. An example was presented for a single group model with the theory amenable for extension to multienergy, multiregion systems.

Cohn, Johnson, and Macdonald[32,33,34] introduced a technique for calculating the zero-power source transfer function using a sinusoidal source input with the time varying flux and source expressed as complex quantities. This approach permitted solution of the spatial transfer function using normal statics techniques. Results from experiments conducted on the heavy water-moderated Georgia Tech Research Reactor and the NORA Reactor closely reproduced the calculations for the zero-power spatial source transfer function.

Poncelet[35,36] developed an approach for calculating the spatial source transfer function using the multienergy, multiregion diffusion equations. Poncelet's equations were expressed in the frequency regime by Laplace transformations of the diffusion equations. This approach was extended to include feedback effects for predicting at-power source transfer functions.

Bridges, Clement, and Renier[37] extended the zero-power model of Johnson[33] to include feedback terms. This permitted an approach for

calculating the power-dependent source transfer function taking into account temperature feedback terms. The equations derived in this manner were similar to the equations developed by Poncelet[35] using a different approach. Some of the constants in the equations were slightly different since a few of the constants evaluated by Bridges, Clement, and Renier[37] were developed considering additional terms beyond those of Poncelet.

Review of Noise Analysis and Modulated Neutron Experiments

As pointed out earlier, the idea of modulated sources dates back to 1948 with subsequent oscillator experiments on the Oak Ridge reactor and the original University of Chicago reactor.[18,20] Transfer function measurements through oscillation tests have been used for the measurement of prompt neutron lifetimes, coefficients of reactivity and associated time constants, cross sections, the prediction of power level at which linear stability no longer exists, shut down reactivity, etc.[38] As one might expect, the large majority of pile oscillator experiments was done with sinusoidal absorber input signals. This sinusoidal approach proved to be rather time consuming since such a method examines each frequency separately. The introduction of noise analysis techniques alleviated the requirement for single frequency experimental runs. Noise analysis as such has been employed in the study of reactor "noise" or the random nature of neutron fluctuations. The technique for analyzing the data normally involves a correlation process and then a conversion of these data from the time regime to the frequency regime by a Fourier transform.

It has long been recognized[39,40] that, in the zero power (and sub-critical) condition, the reactor neutron population fluctuates and that

qualitative studies of these fluctuations give information about reactor kinetic parameters. Despite the promise of the early zero-power studies the application of noise analysis to power reactors was dormant until Moore[41] suggested the determination of reactor transfer functions from measurements at steady operation. This suggestion was applied shortly thereafter to the analysis of the Experimental Boiling Water Reactor (EBWR).[42] Subsequently, Cohn[43,44] made several contributions in this field related to the determination of kinetic parameters.

Numerous noise spectra have since been measured in both zero-and full-power reactors,[45] mostly for the purpose of determining transfer function measurements for stability analysis. This experimental tool has had particular use in power reactors whose experimental programs could not conveniently include a rod oscillator test. Thie[46] pointed out significant advantages for the determination of transfer functions by noise analysis methods rather than by the more conventional pile oscillator technique. Among these advantages were the investigation of a broad band of frequencies in an experimental run rather than a single frequency. This determination can be made by frequency analyzing the input and response signals for any given phenomenon, such as flux response to input reactivity, etc. over the frequency bands of interest. This information then provides the basis for the transfer function determination.

The use of noise analysis techniques can, of course, be applied whether the noise is introduced as in the case of modulated sources or whether the noise is normal self excitation governed by stochastic processes. The introduction of input perturbations of reactivity to measure the dynamic characteristics of a high-power nuclear reactor system was

pioneered by Balcomb, et al.[47] The input chosen was the pseudo-random binary sequence which was used to perturb the reactivity by introducing the signal into the control loop. This type of testing has been carried out in subsequent nuclear rocket reactor and engine tests (NERVA, KIWI, and Phoebus). Perturbations of both reactivity and coolant flow rate were used. The technique gave good results even under adverse experimental conditions.

Hara and Suda[48] used the pseudo-random binary sequence for dynamics measurements on the Japanese Research Reactor-3. Results were not very good and it was conjectured that this was due to the difficulty in maintaining the zero-power reactor at exactly critical and in maintaining a constant power level without drift for the power low-frequency runs. The frequency response measurements agreed fairly well in medium and high frequency regions but rather poorly in low frequency regions (frequency < 0.01 radians/sec).

A number of other experiments has used external excitation.[49,50,51] External excitation such as a pile oscillator device provides the distinct advantage of selectively permitting investigation of a band of frequencies in a desired interval. A discussion of the various methods used in frequency response testing is presented by Kerlin.[52] The specific approach of using a binary sequence for frequency testing is presented in Appendix B.

Recent developments in the application of the Fast Fourier Transform[53,54,55] to signal analysis have resulted in greatly improved techniques for analyzing noise analysis data. The Fast Fourier Transform (hereafter referred to as FFT) method is a technique for efficiently

computing the discrete Fourier transform of a series of data samples. The FFT takes advantage of the fact that calculation of the coefficients of the discrete Fourier transform can be carried out iteratively resulting in considerable savings of computation time. The FFT is a scheme of sequentially combining progressively larger weighted sums of data samples that, at the start, may be considered as a series of two-point data samples. This procedure is continued until all data points are considered using the recursion techniques inherent to the method. The main advantages in the application of the FFT to noise analysis are due to the fact that this approach permits analysis of much larger data records with appreciably less computational round off error than before. Reynolds[56] has applied the FFT to work on the spectral analysis of the Georgia Tech Research Reactor.

With a great deal of zero-power noise analysis completed[57,58,59] the most recent effort is a concentration of noise analysis work in the field of power reactors with the problems of spatial effects, feedback, and stability analysis.[60,61] This includes the practical application of the existing spatial techniques with multidimensional analysis and experimental verification.

Objective of this Research

The objective of this investigation was to study theoretically and experimentally the zero-power and the at-power reactor source transfer functions. Emphasis of this research was on measuring and predicting the effect of temperature feedback on the spatial source transfer function values for the Georgia Tech Research Reactor.

The theoretical aspect of this investigation consisted of extending a model for predicting the spatially dependent source transfer function to include feedback terms which are necessary to describe at-power operation. In support of this model a computer code has been developed for a one-dimensional theoretical calculation of the source transfer function as a function of the reactor power level.

The experimental aspect of this investigation consisted of measuring the source transfer function of the Georgia Tech Research Reactor over a wide range of spatial locations with emphasis in the low-frequency range. Measurements have been made both at 900 kW power level and at zero-power level. For this experiment a pile oscillator for perturbing the reactor flux has been designed and constructed for insertion and operation in a fuel element position in the reactor core. The pile oscillator was driven in a pseudo-random binary sequence which permitted the selective investigation of desirable frequency ranges.

Experimental data have been taken on a system of PDP-8 computers with the analysis done on the Univac 1108 computer using a Fast Fourier Transform Program. The experimental results were then used to test the validity and accuracy of the theoretical predictions.

CHAPTER II

THEORETICAL DEVELOPMENT

The investigation of a dynamic system considering feedback effects and spatial response is desirable since an adequate consideration of these factors can lead to a satisfactory prediction of system performance. In the development of equations describing such a system one is inherently limited to assumptions and considerations intrinsic to the approach taken. In this discussion the system under consideration is a nuclear reactor and one such condition is that of at-power operation, since feedback effects are under investigation. The development in this chapter will proceed from a basic definition of terms and concepts employed to a final set of equations for predicting the spatially dependent reactor response under the influence of feedback mechanisms. Throughout this discussion care will be taken to point out the approximations and limitations of this approach and, hence, establish the applicability of such a technique.

The approach taken in this presentation for calculating the spatially dependent response with feedback will be similar to the development by Johnson[33] for the zero-power case. However, the model herein is extended to include feedback effects.[37] The general approach lends itself to multigroup, multiregion analysis with the capability for the introduction of any number of feedback mechanisms such as temperature feedback, xenon feedback, void formation, etc. For the purposes of this research the analysis and experimental investigation was restricted to the consid-

eration of two-group equations with temperature feedback only.

Before proceeding with the development of the equations, a brief introduction to the physical phenomenon causing temperature feedback in a thermal reactor will be presented. Temperature feedback occurs in such a reactor when the operating temperature changes for some reason, such as an increase in power over the steady state level. This change in temperature introduces a slight reactivity and this reactivity change per degree temperature is called the temperature coefficient of reactivity. Temperature changes in a reactor introduce reactivity primarily in three ways[62]: (1) by altering the mean energy of thermal neutrons in the reactor, (2) by changing reactor core densities, and (3) by changing the overall size of the reactor. The temperature coefficient of a reactor can be separated into three parts: a nuclear temperature coefficient, a density temperature coefficient, and a volume temperature coefficient. The nuclear temperature coefficient is an effect related to the change in nuclear cross sections with the change in temperature. In many cases the thermal absorption cross sections follow the 1/V law and thus sharply decrease with an increase in temperature. The primary result is that this effect reduces the microscopic cross sections and increases the thermal leakage. In addition, the increase in temperature causes a slight decrease in the value of the resonance escape probability. This is due to the increased resonance absorption of neutrons in the resonance energy range (the Doppler effect) and because more thermal neutrons, on shifting of energy spectrum with temperature, enter the resonance energy range. Both the increase in leakage and decrease in resonance escape probability contribute to a negative tempera-

ture coefficient. Other factors contribute to the negative nuclear temperature coefficient, however, they are lesser in magnitude.

The density temperature coefficient is related to the change in reactor material density with temperature. An increase in temperature reduces densities and macroscopic absorption and scattering cross sections. This increases the corresponding mean free paths and therefore increases leakage. This, likewise, contributes to a negative temperature coefficient.

The volume temperature coefficient is an effect related to the increase in the size of the reactor with an increase in temperature. This increased size tends to reduce leakage with increased temperature and, hence, contributes in a positive manner with increasing temperature. This volume effect is usually the smallest of the three effects. The net result from the combination of these three effects is a negative temperature coefficient for the reactor.

The Transfer Function

The use of transfer functions has become widespread in frequency response studies and stability analysis and, hence, has become a standard tool in nuclear reactor analysis. The concept of the transfer function as presented herein will be in the traditional sense as a measure of the response at a given point in a linear system to the input at another point in the system for a given frequency of sinusoidal excitation. This approach linearizes the equations by means of the small signal approximation.[1] Consider the input parameter P of a system and subject this parameter to a small sinusoidal variation. Thus, if P_0 is the steady state value of P,

then $$P = P_o + \delta P = P_o + |\delta P| \, e^{j\omega t}$$

where it is understood that only the real part of P is interpreted to have physical significance.[1]

Now if R represents another parameter within the system, the variation of P will result in an oscillation in R since the two are related by the physical system. The variation will be of amplitude $|R|$ and of the same frequency ω. Thus, if R_o is the steady state value of R, then

$$R = R_o + \delta R = R_o + |\delta R| \, e^{j(\omega t+\alpha)}$$

where α is a phase shift which is in general a function of ω.

The quantity P is called the input and is the independent variable or the so-called driving function. The quantity R is the output or response which is a dependent variable. The transfer function is frequently designated by the notation

$$G(\omega) = \delta R/\delta P = (|\delta R|/|\delta P|) \, e^{j\alpha}$$

where α is the phase shift.

Thus, in general, a transfer function is a mathematical expression which describes the effect of a physical system on the information transferred through it, e.g. $\delta R = G(\omega) \, \delta P$. More specifically, the transfer function is obtained by Laplace transformation of the generalized differential equations describing a linear system. The transfer function is then defined as the ratio of the transformed output to the transformed input with the Laplace transformation variable, s, replaced by $j\omega$.[63] The

prior notation reflects this approach where $G(\omega) = G(j\omega)$ for notational purposes.

The transfer function $G(\omega)$ is clearly a complex quantity where the amplitude of $G(\omega)$ represents the gain, or the ratio of the amplitude of the output sinusoid to the input sinusoid, and the phase angle of $G(\omega)$ represents the phase shift or the phase angle difference between the input and output sinusoids.

Cohn[64] has pointed out that small changes in the absorption of the reactor, i.e. reactivity changes, may be treated as external sources for the case of small signal disturbances. Therefore, an oscillating absorber in a reactor environment meeting the small signal criteria may appropriately be called a negative source. Considering this disturbance as the source, the term "source transfer function" then follows in observing the spatial response to such a disturbance or source.

Derivation of Equations for the Source Transfer Function

In the development of the equations for the source transfer functions the reactor is assumed to operate at steady state at an average power P_o. A small sinusoidal reactivity disturbance is then introduced by oscillating an absorber in the reactor. The equations used in this development will proceed from the two-group diffusion theory equations. However, the general approach could equally well proceed from a more complex equation such as the telegrapher's equation.[65] The equations thus developed will be limited to the conditions and validity of diffusion theory. In addition, the source disturbance must be of sufficiently small magnitude as to meet the criteria for small signal approximation.

The time-dependent two-group diffusion equations for a critical reactor are written as follows:

Fast group:

$$\nabla \cdot D_1(\bar{x},t)\ \nabla\Phi_1(\bar{x},t) - \Sigma_r(\bar{x},t)\ \Phi_1(\bar{x},t) - \Sigma_{a_1}(\bar{x},t)\ \Phi_1(\bar{x},t) \qquad (1)$$

$$+ (1/k)(1-\beta)[\nu\,\Sigma_{f_1}(\bar{x},t)\ \Phi_1(\bar{x},t) + \nu\,\Sigma_{f_2}(\bar{x},t)\ \Phi_2(\bar{x},t)]$$

$$+ \sum_n \lambda_n\ C_n(\bar{x},t) + S_1(\bar{x},t) = \frac{1}{v_1}\frac{\partial\Phi_1(\bar{x},t)}{\partial t}$$

Thermal group:

$$\nabla \cdot D_2(\bar{x},t)\ \nabla\Phi_2(\bar{x},t) - \Sigma_{a_2}(\bar{x},t)\ \Phi_2(\bar{x},t) + \Sigma_r(\bar{x},t)\ \Phi_1(\bar{x},t) \qquad (2)$$

$$+ S_2(\bar{x},t) = \frac{1}{v_2}\frac{\partial\Phi_2(\bar{x},t)}{\partial t}$$

Precursor densities:

$$\beta_n[\nu\,\Sigma_{f_1}(\bar{x},t)\ \Phi_1(\bar{x},t) + \nu\,\Sigma_{f_2}(\bar{x},t)\ \Phi_2(\bar{x},t)] - \lambda_n\ C_n(\bar{x},t) \qquad (3)$$

$$= \frac{\partial\ C_n(\bar{x},t)}{\partial t}$$

where

$\Phi(\bar{x},t)$ is the space- and time-dependent flux

$D(\bar{x},t)$ is the space- and time-dependent diffusion coefficient

$\Sigma_r(\bar{x},t)$ is the space- and time-dependent fast removal cross section

$\Sigma_a(\bar{x},t)$ is the space- and time-dependent macroscopic absorption cross section

v is the neutron velocity

ν is the mean number of neutrons per fission

$\Sigma_f(\bar{x},t)$ is the space- and time-dependent macroscopic fission cross section

$S(\bar{x},t)$ is the external source term (independent of neutron flux)

β_n is the fraction of neutrons from the n^{th} delayed neutron precursor $\left(\sum_{n=1}^{N} \beta_n = \beta\right)$

λ_n is the decay constant of the n^{th} delayed neutron precursor

$C_n(\bar{x},t)$ is the space- and time-dependent concentration of the n^{th} delayed neutron precursor

subscripts 1 and 2 indicate fast and thermal groups, respectively

$\bar{x}$ is the three-dimensional coordinate.

The factor $1/k$ in equation (1) was introduced for mathematical convenience. By adjusting k, the eigenvalue, corrections can be made for slight errors in the values of the reactor parameters. For the remainder of the derivation the value of k will be taken as 1.00 with the implicit assumption that the reactor constants and cross sections used predict the stationary state with the reactor critical.

As mentioned earlier the power level or flux is subjected to a small time-dependent disturbance about some steady state value. Consider now the resolution of the time varying flux and neutron precursor densities into a steady part, dependent only on position (denoted by subscript 0), and a fluctuating part dependent on both position and time and represented by

$$\Phi_i(\bar{x},t) = \Phi_{i_0}(\bar{x}) + \delta\ \Phi_i(\bar{x},t) \tag{4}$$

and

$$C_n(\bar{x},t) = C_{n_0}(\bar{x}) + \delta\ C_n(\bar{x},t) \tag{5}$$

respectively.

With the time variation of the flux and neutron precursor density, the rate of heat or energy generation will vary, causing some fluctuation in the reactor core temperatures which will in turn lead to temperature feedback effects. The effect of temperature feedback effects will be considered for the diffusion coefficients and the removal, absorption, and fission cross sections. Feedback effects are considered for both moderator and fuel temperature changes. The time-dependent parameters mentioned above will be considered as having a steady state value which, of course, is dependent on position with a small time varying component superimposed upon their steady state values. The parameters, considering feedback, are represented in the following manner for energy group i (i=1,2):

$$D_i(\bar{x},t) = D_i(\bar{x}) + \delta D_i(\bar{x},t) \tag{6}$$

$$= D_i(\bar{x}) + [K^F_{D_i}(\bar{x})\ \delta T_F(\bar{x},t) + K^M_{D_i}(\bar{x})\ \delta T_M(\bar{x},t)]$$

$$\Sigma_r(\bar{x},t) = \Sigma_r(\bar{x}) + \delta \Sigma_r(\bar{x},t) \tag{7}$$

$$= \Sigma_r(\bar{x}) + [K^F_r(\bar{x})\ \delta T_F(\bar{x},t) + K^M_r(\bar{x})\ \delta T_M(\bar{x},t)]$$

$$\Sigma_{a_i}(\bar{x},t) = \Sigma_{a_i}(\bar{x}) + \delta \Sigma_{a_i}(\bar{x},t) \tag{8}$$

$$= \Sigma_{a_i}(\bar{x}) + [K^F_{a_i}(\bar{x})\ \delta T_F(\bar{x},t) + K^M_{a_i}(\bar{x})\ \delta T_M(\bar{x},t)]$$

$$\Sigma_{f_i}(\bar{x},t) = \Sigma_{f_i}(\bar{x}) + \delta \Sigma_{f_i}(\bar{x},t) \tag{9}$$

$$= \Sigma_{f_i}(\bar{x}) + [K^F_{f_i}(\bar{x})\ \delta T_F(\bar{x},t) + K^M_{f_i}(\bar{x})\ \delta T_M(\bar{x},t)]$$

where

δT_f is the variation in fuel temperature

δT_M is the variation in moderator temperature

K is the coefficient that relates change in temperature to a change in value of the parameter under consideration

K^F is the fuel coefficient

K^M is the moderator coefficient

subscripts D, r, a, f, F, and M indicate diffusion coefficient, removal, absorption, fission cross sections, fuel, and moderator, respectively, and

superscripts F and M indicate fuel and moderator, respectively.

Similar equations could be written for any other parameters subject to feedback.

The substitution of the steady state plus time-dependent component representation of equations (4) through (9) is made in the time-dependent diffusion equations (equations (1) through (3)). The resulting equations are then

$$\nabla\cdot(D_1(\bar{x}) + \delta D_1(\bar{x},t))\nabla(\Phi_{1_o}(\bar{x}) + \delta\Phi_1(\bar{x},t)) - (\Sigma_r(\bar{x}) \tag{10}$$

$$+ \delta\Sigma_r(\bar{x},t))(\Phi_{1_o}(\bar{x}) + \delta\Phi_1(\bar{x},t)) - (\Sigma_{a_1}(\bar{x}) + \delta\Sigma_{a_1}(\bar{x},t))$$

$$\times (\Phi_{1_o}(\bar{x}) + \delta\Phi_1(\bar{x},t)) + (1-\beta)[\nu(\Sigma_{f_1}(\bar{x}) + \delta\Sigma_{f_1}(\bar{x},t))$$

$$\times (\Phi_{1_o}(\bar{x}) + \delta\Phi_1(\bar{x},t)) + \nu(\Sigma_{f_2}(\bar{x}) + \delta\Sigma_{f_2}(\bar{x},t))(\Phi_{2_o}(\bar{x}) + \delta\Phi_2(\bar{x},t))]$$

$$+ \sum_n \lambda_n(C_{n_o}(\bar{x}) + \delta C_n(\bar{x},t)) + S_1(\bar{x},t) = \frac{1}{v_1}\frac{\partial}{\partial t}(\Phi_{1_o}(\bar{x}) + \delta\Phi_1(\bar{x},t))$$

$$\nabla\cdot(D_2(\bar{x}) + \delta D_2(\bar{x},t))\nabla(\Phi_{2_o}(\bar{x}) + \delta\Phi_2(\bar{x},t)) - (\Sigma_{a_2}(\bar{x}) \tag{11}$$

$$+ \delta\Sigma_{a_2}(\bar{x},t))(\Phi_{2_o}(\bar{x}) + \delta\Phi_2(\bar{x},t)) + (\Sigma_r(\bar{x}) + \delta\Sigma_r(\bar{x},t))$$

$$\times (\Phi_{1_o}(\bar{x}) + \delta\Phi_1(\bar{x},t)) + S_2(\bar{x},t) = \frac{1}{v_2}\frac{\partial}{\partial t}(\Phi_{2_o}(\bar{x}) + \delta\Phi_2(\bar{x},t))$$

$$\beta_n[\nu(\Sigma_{f_1}(\bar{x}) + \delta\Sigma_{f_1}(\bar{x},t))(\Phi_{1_o}(\bar{x}) + \delta\Phi_1(\bar{x},t)) + \nu(\Sigma_{f_2}(\bar{x}) \tag{12}$$

$$+ \delta\Sigma_{f_2}(\bar{x},t))(\Phi_{2_o}(\bar{x}) + \delta\Phi_2(\bar{x},t))] - \lambda_n(C_{n_o}(\bar{x}) + \delta C_n(\bar{x},t))$$

$$= \frac{\partial}{\partial t}(C_{n_o}(\bar{x}) + \delta C_n(\bar{x},t))$$

In carrying out the algebra it is seen that terms involving the steady state parameters describe the steady state condition of the reactor which in turn has all time derivatives equal to zero. Now by subtracting the steady state portion and linearizing the solution one obtains

$$\nabla\cdot D_1(\bar{x})\ \nabla\delta\Phi_1(\bar{x},t) + \nabla\cdot\delta D_1(\bar{x},t)\ \nabla\Phi_{1_o}(\bar{x}) - \delta\ \Sigma_{a_1}(\bar{x},t)\ \Phi_{1_o}(\bar{x}) \tag{13}$$

$$- \Sigma_{a_1}(\bar{x})\ \delta\Phi_1(\bar{x},t) - \delta\ \Sigma_r(\bar{x},t)\ \Phi_{1_o}(\bar{x}) - \Sigma_r(\bar{x})\ \delta\Phi_1(\bar{x},t)$$

$$+ (1-\beta)[\nu\ \delta\ \Sigma_{f_1}(\bar{x},t)\ \Phi_{1_o}(\bar{x}) + \nu\ \Sigma_{f_1}(\bar{x})\ \delta\Phi_1(\bar{x},t)$$

$$+ \nu\ \delta\ \Sigma_{f_2}(\bar{x},t)\ \Phi_{2_o}(\bar{x}) + \nu\ \Sigma_{f_2}(\bar{x})\ \delta\Phi_2(\bar{x},t)] + \sum_n \lambda_n\ \delta\ C_n(\bar{x},t)$$

$$+ S_1(\bar{x},t) = \frac{1}{v_1}\frac{\partial\ \delta\ \Phi_1(\bar{x},t)}{\partial t}$$

$$\nabla\cdot D_2(\bar{x})\ \nabla\delta\Phi_2(\bar{x},t) + \nabla\cdot\delta D_2(\bar{x},t)\ \nabla\Phi_{2_o}(\bar{x}) - \Sigma_{a_2}(\bar{x})\ \delta\Phi_2(\bar{x},t) \tag{14}$$

$$- \delta\ \Sigma_{a_2}(\bar{x},t)\ \Phi_{2_o}(\bar{x}) + \Sigma_r(\bar{x})\ \delta\Phi_1(\bar{x},t) + \delta\Sigma_r(\bar{x},t)\ \Phi_{1_o}(\bar{x})$$

$$+ S_2(\bar{x},t) = \frac{1}{v_2}\frac{\partial\ \delta\ \Phi_2(\bar{x},t)}{\partial t}$$

$$\beta_n[\nu\ \delta\ \Sigma_{f_1}(\bar{x},t)\ \Phi_{1_o}(\bar{x}) + \nu\ \Sigma_{f_1}(\bar{x})\ \delta\Phi_1(\bar{x},t) + \nu\ \delta\ \Sigma_{f_2}(\bar{x},t) \quad (15)$$

$$\times\ \Phi_{2_o}(\bar{x}) + \nu\ \Sigma_{f_2}(\bar{x})\ \delta\Phi_2(\bar{x},t)] - \lambda_n\ \delta\ C_n(\bar{x},t) = \frac{\partial\ \delta\ C_n(\bar{x},t)}{\partial t}\ .$$

Further substitutions are now made in equations (13) through (15) for the linearized time-dependent reactor parameter variations as a function of the varying moderator and fuel temperature values. The functional relationships between the time-dependent parameter values and the slight fuel and moderator temperature changes are spelled out in equations (6) through (9). This substitution results in the following equations.

$$\nabla\cdot D_1(\bar{x})\ \nabla\delta\Phi_1(\bar{x},t) + \nabla\cdot(K^F_{D_1}(\bar{x})\ \delta T_F(\bar{x},t) + K^M_{D_1}\ \delta T_M(\bar{x},t))\nabla\Phi_{1_o}(\bar{x}) \quad (16)$$

$$- (K^F_{a_1}(\bar{x})\ \delta T_F(\bar{x},t) + K^M_{a_1}\ \delta T_M(\bar{x},t))\Phi_{1_o}(\bar{x}) - \Sigma_{a_1}(\bar{x})\ \delta\Phi_1(\bar{x},t)$$

$$- (K^F_r(\bar{x})\ \delta T_F(\bar{x},t) + K^M_r\ \delta T_M(\bar{x},t))\Phi_{1_o}(\bar{x}) - \Sigma_r(\bar{x})\ \delta\Phi_1(\bar{x},t)$$

$$+ (1-\beta)[\nu(K^F_{f_1}(\bar{x})\ \delta T_F(\bar{x},t) + K^M_{f_1}(\bar{x})\ \delta T_M(\bar{x},t))\Phi_{1_o}(\bar{x}) + \nu\ \Sigma_{f_1}(\bar{x})$$

$$\times\ \delta\Phi_1(\bar{x},t) + \nu\ (K^F_{f_2}(\bar{x})\ \delta T_F(\bar{x},t) + K^M_{f_2}(\bar{x})\ \delta T_M(\bar{x},t))\ \Phi_{2_o}(\bar{x})$$

$$+ \nu\ \Sigma_{f_2}(\bar{x})\ \delta\Phi_2(\bar{x},t)] + \sum_n \lambda_n\ \delta\ C_n(\bar{x},t) + S_1(\bar{x},t)$$

$$= \frac{1}{v_1}\frac{\partial}{\partial t}(\delta\Phi_1(\bar{x},t))$$

$$\nabla\cdot D_2(\bar{x})\ \nabla\delta\Phi_2(\bar{x},t) + \nabla\cdot(K^F_{D_2}(\bar{x})\ \delta T_F(\bar{x},t) + K^M_{D_2}(\bar{x})\ \delta T_M(\bar{x},t))\nabla\Phi_{2_o} \quad (17)$$

$$- \Sigma_{a_2}(\bar{x})\ \delta\Phi_2(\bar{x}) - (K^F_{a_2}(\bar{x})\ \delta T_F(\bar{x},t) + K^M_{a_2}(\bar{x})\ \delta T_M(\bar{x},t))\ \Phi_{2_o}(\bar{x})$$

$$+ \Sigma_r(\bar{x})\ \delta\Phi_1(\bar{x},t) + (K^F_r(\bar{x})\ \delta T_F(\bar{x},t) + K^M_r(\bar{x})\ \delta T_M(\bar{x},t))\ \Phi_{1_o}(\bar{x})$$

(continued)

$$+ S_2(\bar{x},t) = \frac{1}{v_2} \frac{\partial}{\partial t} (\delta\Phi_2(\bar{x},t))$$

$$\beta_n[\nu(K_{f_1}^F(\bar{x})\ \delta T_F(\bar{x},t) + K_{f_1}^M(\bar{x})\ \delta T_M(\bar{x},t))\Phi_{1_0}(\bar{x}) + \nu\Sigma_{f_1}(\bar{x}) \tag{18}$$

$$\times\ \delta\Phi_1(\bar{x},t) + \nu\ (K_{f_2}^F(\bar{x})\ \delta T_F(\bar{x},t) + K_{f_2}^M(\bar{x})\ \delta T_M(\bar{x},t))\Phi_{2_0}(\bar{x})$$

$$+ \nu\Sigma_{f_2}(\bar{x})\ \delta\Phi_2(\bar{x},t)] - \lambda_n\ \delta\ C_n(\bar{x},t) = \frac{\partial}{\partial t}(\delta\ C_n(\bar{x},t))$$

The above equations are rather cumbersome and contain both time-dependent temperature variations and time-dependent flux variations. An attempt will now be made to simplify these equations somewhat. First, by expressing the time-dependent flux variation in the frequency regime and then in turn relating the temperature variations with the flux variations for eventual substitution in and simplification of equations (16) through (18).

As noted earlier, for the purposes of the development we have restricted the analysis to the consideration of small sinusoidal disturbances. This approach is adequate for other types of disturbances since a nonsinusoidal disturbance could be Fourier analyzed and each frequency component considered individually. As a matter of interest the experimental measurements were done in such a manner using a periodic binary input disturbance. This is the subject of considerable discussion in the chapter on experimental procedure.

With the sinusoidal external source, the fluxes, precursor densities, and parameter responses are also sinusoidal with the same frequency. We then have

$$\delta\Phi_i(\bar{x},t) = \underline{\Phi}_i(\bar{x},\omega)\ \exp(j\omega t) \tag{19}$$

$$\delta C_n(\bar{x},t) = \underline{C}_n(\bar{x},\omega)\ \exp(j\omega t) \tag{20}$$

$$S_i(\bar{x},t) = \underline{S}_i(\bar{x})\ \exp(j\omega t) \tag{21}$$

where $\underline{\Phi}_i(\bar{x},\omega)$ and $\underline{C}_n(\bar{x},\omega)$ are the complex representation, dependent on position and frequency, for the flux and precursor densities, respectively. $\underline{S}_i(\bar{x})$ is the complex representation of the source or disturbance term dependent on location.

At this point a number of time-dependent quantities can be shifted to the frequency domain by the use of equations (19) through (21). However, equations (16) through (18) still contain time-dependent temperature fluctuations of moderator and fuel. These time varying temperature values will now be examined more closely in an effort to reduce equations (16) through (18) to a set of equations that can be solved for the thermal and fast $\underline{\Phi}(\bar{x},\omega)$ terms.

For the fuel region the moderator and fuel will be smeared together as in a homogenized mixture analysis. However, both $\delta T_F(\bar{x},t)$ and $\delta T_M(\bar{x},t)$ will retain their unique values as arrived at from conventional reactor heat transfer calculations. For the relationship between flux and temperature variations consider now the following definitions.

$$F_F(\bar{x},t) \equiv \delta T_F(\bar{x},t)/\delta P(\bar{x},t)\ ,\ F_M(\bar{x},t) \equiv \delta T_M(\bar{x},t)/\delta P(\bar{x},t) \tag{22}$$

where

$\delta T_F(\bar{x},t)$ is the small variation of the space-dependent fuel temperature about the steady state value

$\delta T_M(\bar{x},t)$ is the small variation of the space-dependent moderator temperature about the steady state value

$\delta P(\bar{x},t)$ is the small variation of the space-dependent power density about the steady state value.

From the concepts of power generation introduced by these definitions, the subsequent analysis applies only to a homogeneous reactor core or a heterogeneous core which lends itself to a "homogenized mixture" analysis. This is true since the power density in the moderator alone is relatively small compared to the power generation in the fuel. The power density is defined in the following manner:

$$P_o(\bar{x}) = \xi[\nu \Sigma_{f_1}(\bar{x}) \Phi_{1_o}(\bar{x}) + \nu \Sigma_{f_2}(\bar{x}) \Phi_{2_o}(\bar{x})] \tag{23}$$

where ξ is the ratio of the power density to the neutron production rate.

The time-dependent power variation due to the sinusoidal perturbation is now introduced in equation (23) and the effect of feedback on the fission cross sections is considered. Temperature feedback is considered for both the fuel and the moderator. This is expressed as

$$P_o(\bar{x}) + \delta P(\bar{x},t) = \xi[\nu (\Sigma_{f_1}(\bar{x}) + \delta \Sigma_{f_1}(\bar{x},t))(\Phi_{1_o}(\bar{x}) + \delta\Phi_1(\bar{x},t)) \tag{24}$$

$$+ \nu (\Sigma_{f_2}(\bar{x}) + \delta \Sigma_{f_2}(\bar{x},t))(\Phi_{2_o}(\bar{x}) + \delta\Phi_2(\bar{x},t))]$$

$$\delta P(\bar{x},t) = \xi[\nu \Sigma_{f_1}(\bar{x}) \delta\Phi_1(\bar{x},t) + \nu \Sigma_{f_2}(\bar{x}) \delta\Phi_2(\bar{x},t) \tag{25}$$

$$+ \nu \Phi_{1_0}(\bar{x}) (K^F_{f_1}(\bar{x}) \delta T_F(\bar{x},t) + K^M_{f_1}(\bar{x}) \delta T_M(\bar{x},t))$$

$$+ \nu \Phi_{2_0}(\bar{x}) (K^F_{f_2}(\bar{x}) \delta T_F(\bar{x},t) + K^M_{f_2}(\bar{x}) \delta T_M(\bar{x},t))]$$

but from our prior definition

$$\delta P(\bar{x},t) = \frac{\delta T_F(\bar{x},t)}{F_F(\bar{x},t)} = \frac{\delta T_M(\bar{x},t)}{F_M(\bar{x},t)} \tag{26}$$

Therefore,

$$\delta T_F(\bar{x},t) = F_F(\bar{x},t) \xi[\nu \Sigma_{f_1}(\bar{x}) \delta\Phi_1(\bar{x},t) + \nu \Sigma_{f_2}(\bar{x}) \delta\Phi_2(\bar{x},t)] / \tag{27}$$

$$\{1 - F_F(\bar{x},t) \xi[\nu \Phi_{1_0}(\bar{x}) K^F_{f_1}(\bar{x}) + \nu \Phi_{2_0}(\bar{x}) K^F_{f_2}(\bar{x})] - F_M(\bar{x},t)$$

$$\xi[\nu \Phi_{1_0}(\bar{x}) K^M_{f_1}(\bar{x}) + \nu \Phi_{2_0}(\bar{x}) K^M_{f_2}(\bar{x})]\}$$

$$\delta T_M(\bar{x},t) = F_M(\bar{x},t) \xi[\nu \Sigma_{f_1}(\bar{x}) \delta\Phi_1(\bar{x},t) + \nu \Sigma_{f_2}(\bar{x}) \delta\Phi_2(\bar{x},t)] / \tag{28}$$

$$\{1 - F_F(\bar{x},t) \xi[\nu \Phi_{1_0}(\bar{x}) K^F_{f_1}(\bar{x}) + \nu \Phi_{2_0}(\bar{x}) K^F_{f_2}(\bar{x})] - F_M(\bar{x},t)$$

$$\xi[\nu \Phi_{1_0}(\bar{x}) K^M_{f_1}(\bar{x}) + \nu \Phi_{2_0}(\bar{x}) K^M_{f_2}(\bar{x})]\}.$$

The use of the definitions for $F_F(\bar{x},t)$ and $F_M(\bar{x},t)$ permits us to relate the variation in fuel and moderator temperatures to the flux variation in a rather direct manner. The values for $F_F(\bar{x},t)$ and $F_M(\bar{x},t)$ can now be considered in the frequency regime since $\delta T_F(\bar{x},t)$ for the fuel and $\delta T_M(\bar{x},t)$ for the moderator are the time varying responses or outputs for a given frequency of input perturbation. These definitions also fit the

conditions for a transfer function with a time-dependent temperature variation output of the fuel and moderator resulting from the source driven sinusoidal variation in the power level. Considering $F_F(\bar{x},t)$ and $F_M(\bar{x},t)$ in the frequency domain they become the fuel and moderator temperature to power transfer functions, respectively.

The transfer functions $F_F(\bar{x},\omega)$ and $F_M(\bar{x},\omega)$ have been defined by Schultz[63] and a number of other experimenters.[66,67,68] The fuel and moderator temperature to power transfer functions are derived for the GTRR model in Appendix A. The values for $F_F(\bar{x},\omega)$ and $F_M(\bar{x},\omega)$ are shown to be functions of the frequency and the reactor heat transfer characteristics.

The relationship between the fuel and moderator temperature variations and the flux variations is then

$$\delta T_F(\bar{x},t) = \alpha_1^F(\bar{x},\omega)\ \delta\Phi_1(\bar{x},t) + \alpha_2^F(\bar{x},\omega)\ \delta\Phi_2(\bar{x},t) \tag{29}$$

$$\delta T_M(\bar{x},t) = \alpha_1^M(\bar{x},\omega)\ \delta\Phi_1(\bar{x},t) + \alpha_2^M(\bar{x},\omega)\ \delta\Phi_2(\bar{x},t) \tag{30}$$

where

$$\alpha(\bar{x},\omega) = \{1 - F_F(\bar{x},\omega)\ \xi[\nu\ \Phi_{1_0}(\bar{x})\ K_{f_1}^F(\bar{x}) + \nu\ \Phi_{2_0}(\bar{x})\ K_{f_2}^F(\bar{x})] \tag{31}$$

$$- F_M(\bar{x},\omega)\ \xi[\nu\ \Phi_{1_0}(\bar{x})\ K_{f_1}^M(\bar{x}) + \nu\ \Phi_{2_0}(\bar{x})\ K_{f_2}^M(\bar{x})]\}$$

$$\alpha_1^F(\bar{x},\omega) = \frac{F_F(\bar{x},\omega)\ \xi\ \nu\ \Sigma_{f_1}(\bar{x})}{\alpha(\bar{x},\omega)} \tag{32}$$

$$\alpha_2^F(\bar{x},\omega) = \frac{F_F(\bar{x},\omega)\ \xi\ \nu\ \Sigma_{f_2}(\bar{x})}{\alpha(\bar{x},\omega)} \tag{33}$$

$$\alpha_1^M(\bar{x},\omega) = \frac{F_M(\bar{x},\omega)\ \xi\ \nu\ \Sigma_{f_1}(\bar{x})}{\alpha(\bar{x},\omega)} \tag{34}$$

$$\alpha_2^M(\bar{x},\omega) = \frac{F_M(\bar{x},\omega)\ \xi\ \nu\ \Sigma_{f_2}(\bar{x})}{\alpha(\bar{x},\omega)} \tag{35}$$

The fuel and moderator temperature to power transfer functions can be calculated on a unit cell basis much in the manner that a unit cell is homogenized for neutronic calculations. An extensive heat transfer analysis of a unit cell has been described by Hsu.[69]

At this point in the development it may be of some advantage to summarize briefly the steps taken to this stage and then provide some insight in the direction for the final development of the equations. The derivation started with the diffusion equations to describe the oscillator-driven reactor. The resulting flux was then assumed to consist of a steady state value plus a fluctuating component with the time-dependent flux and precursor densities expressed in complex representation, e.g. $\delta\Phi(\bar{x},t) = \underline{\Phi}(\bar{x},\omega)\ \exp(j\omega t)$. The reactor parameters used in the diffusion equations were also expressed in terms of a time-dependent fluctuation due to temperature feedback effects about some steady state value. This parameter variation was then related to the fluctuating fuel and moderator temperatures, e.g.

$$\begin{aligned} D_i(\bar{x},t) &= D_i(\bar{x}) + \delta D_i(\bar{x},t) \\ &= D_i(\bar{x}) + [K_{D_i}^F(\bar{x})\ \delta T_F(\bar{x},t) + K_{D_i}^M(\bar{x})\ \delta T_M(\bar{x},t)]. \end{aligned}$$

Substitution of the above representation into the diffusion equations

and subtraction of the steady state condition yielded equations that were a function of $\underline{\Phi}_i(\bar{x},\omega)$, reactor parameters, temperature coefficients, and the $\delta T(\bar{x},t)$ values for the fuel and moderator. A further observation regarding the temperature to power transfer functions related the $\delta T(\bar{x},t)$ in the fuel and moderator to the $\delta\Phi_i(\bar{x},t)$ or the $\underline{\Phi}_i(\bar{x},\omega)$.

Appropriate substitution as just noted will be made for the $\delta T_F(\bar{x},t)$ and $\delta T_M(\bar{x},t)$ terms. This then yields equations that are a function of $\underline{\Phi}_i(\bar{x},\omega)$, the reactor parameters and properties, and the temperature coefficients. More specifically, equations (6) through (9) (the time-dependent parameter equations) and equations (19) through (21) (the complex representation of the time-dependent fluctuating flux) are substituted into the modified diffusion equations, equations (16) through (18). In addition, the terms relating flux and temperature variation, equations (27) and (28) are further combined in these same equations.

In the manipulation of the equations by the previously noted substitutions, the time dependency is removed by cancellation of the common term, exp ($j\omega t$). It then requires only a series of algebraic operations to collect terms. The resulting frequency-dependent equations are as follows.

$$\nabla\cdot D_1(\bar{x})\ \nabla\underline{\Phi}_1(\bar{x},\omega) - \Sigma_r(\bar{x})\ \underline{\Phi}_1(\bar{x},\omega) - \Sigma_{A_1}(\bar{x},\omega)\ \underline{\Phi}_1(\bar{x},\omega) \tag{36}$$

$$+ [\nu\,\Sigma_{f_1}(\bar{x})\ W(\omega) + \tau_1(\bar{x},\omega)]\ \underline{\Phi}_1(\bar{x},\omega) + [\nu\,\Sigma_{f_2}(\bar{x})\ W(\omega)$$

$$+ \tau_2(\bar{x},\omega)]\ \underline{\Phi}_2(\bar{x},\omega) + \nabla\cdot\gamma_1(\bar{x},\omega)\ \underline{\Phi}_1(\bar{x},\omega) + \nabla\cdot\gamma_2(\bar{x},\omega)\ \underline{\Phi}_2(\bar{x},\omega)$$

$$+ \underline{S}_1(\bar{x}) = 0$$

$$\nabla\cdot D_2(\bar{x})\ \nabla\underline{\Phi}_2(\bar{x},\omega) - \Sigma_{A_2}(\bar{x},\omega)\ \underline{\Phi}_2(\bar{x},\omega) + \Sigma_r(\bar{x})\ \underline{\Phi}_1(\bar{x},\omega) \tag{37}$$

$$+ \epsilon_1(\bar{x},\omega)\ \underline{\Phi}_1(\bar{x},\omega) + \epsilon_2(\bar{x},\omega)\ \underline{\Phi}_2(\bar{x},\omega) + \nabla\cdot\rho_1(\bar{x},\omega)\ \underline{\Phi}_1(\bar{x},\omega)$$

$$+ \nabla\cdot\rho_2(\bar{x},\omega)\ \underline{\Phi}_2(\bar{x},\omega) + \underline{S}_2(\bar{x}) = 0$$

where

$$\gamma_1(\bar{x},\omega) = \sum_{j=F,M} K^j_{D_1}(\bar{x})\ \alpha^j_1(\bar{x},\omega)\ \nabla\Phi_{1_0}(\bar{x}) \tag{38}$$

$$\gamma_2(\bar{x},\omega) = \sum_{j=F,M} K^j_{D_1}(\bar{x})\ \alpha^j_2(\bar{x},\omega)\ \nabla\Phi_{1_0}(\bar{x}) \tag{39}$$

$$\Sigma_{A_i}(\bar{x},\omega) = \Sigma_{a_i}(\bar{x}) + \frac{j\omega}{v_i} \tag{40}$$

$$W(\omega) = 1 - \sum_n \frac{j\omega\ \beta_n}{\lambda_n + j\omega} \tag{41}$$

$$\tau_1(\bar{x},\omega) = \Big[- K^F_r(\bar{x})\ \alpha^F_1(\bar{x},\omega)\ \Phi_{1_0}(\bar{x}) - K^M_r(\bar{x})\ \alpha^M_1(\bar{x},\omega)\ \Phi_{1_0}(\bar{x}) \tag{42}$$

$$- K^F_{a_1}(\bar{x})\ \alpha^F_1(\bar{x},\omega)\ \Phi_{1_0}(\bar{x}) - K^M_{a_1}(\bar{x})\ \alpha^M_1(\bar{x},\omega)\ \Phi_{1_0}(\bar{x})$$

$$+ \left(1 - \sum_n \frac{j\omega\ \beta_n}{j\omega + \lambda_n}\right)(\nu\ \Phi_{1_0}(\bar{x})\ K^F_{f_1}(\bar{x})\ \alpha^F_1(\bar{x},\omega) + \nu\ \Phi_{1_0}(\bar{x})$$

$$K^M_{f_1}(\bar{x})\ \alpha^M_1(\bar{x},\omega) + \nu\ \Phi_{2_0}(\bar{x})\ K^F_{f_2}(\bar{x})\ \alpha^F_1(\bar{x},\omega)$$

$$+ \nu\ \Phi_{2_0}(\bar{x})\ K^M_{f_2}(\bar{x})\ \alpha^M_1(\bar{x},\omega))\Big]$$

$$\tau_2(\bar{x},\omega) = \Big[- K^F_r(\bar{x})\ \alpha^F_2(\bar{x},\omega)\ \Phi_{1_0}(\bar{x}) - K^M_r(\bar{x})\ \alpha^M_2(\bar{x},\omega)\ \Phi_{1_0}(\bar{x}) \tag{43}$$

$$- K^F_{a_1}(\bar{x})\ \alpha^F_2(\bar{x},\omega)\ \Phi_{1_0}(\bar{x}) - K^M_{a_1}(\bar{x})\ \alpha^M_2(\bar{x},\omega)\ \Phi_{1_0}(\bar{x})$$

$$+ \left(1 - \sum_n \frac{j\omega\ \beta_n}{j\omega + \lambda_n}\right)(\nu\ \Phi_{1_0}(\bar{x})\ K^F_{f_1}(\bar{x})\ \alpha^F_2(\bar{x},\omega)$$

(Continued)

$$+ \nu \Phi_{1_0}(\bar{x}) K^M_{f_1}(\bar{x}) \alpha^M_2(\bar{x},\omega) + \nu \Phi_{2_0}(\bar{x}) K^F_{f_2}(\bar{x}) \alpha^F_2(\bar{x},\omega)$$

$$+ \nu \Phi_{2_0}(\bar{x}) K^M_{f_2}(\bar{x}) \alpha^M_2(\bar{x},\omega))\Big]$$

$$\rho_1(\bar{x},\omega) = \sum_{j=F,M} K^j_{D_2}(\bar{x}) \alpha^j_1(\bar{x},\omega) \nabla\Phi_{2_0} \tag{44}$$

$$\rho_2(\bar{x},\omega) = \sum_{j=F,M} K^j_{D_2}(\bar{x}) \alpha^j_2(\bar{x},\omega) \nabla\Phi_{2_0} \tag{45}$$

$$\epsilon_1(\bar{x},\omega) = [- K^F_{a_2}(\bar{x}) \alpha^F_1(\bar{x},\omega) \Phi_{2_0}(\bar{x}) - K^M_{a_2}(\bar{x}) \alpha^M_1(\bar{x},\omega) \Phi_{2_0}(\bar{x}) \tag{46}$$

$$+ K^F_r(\bar{x}) \alpha^F_1(\bar{x},\omega) \Phi_{1_0}(\bar{x}) + K^M_r(\bar{x}) \alpha^M_1(\bar{x},\omega) \Phi_{1_0}(\bar{x})]$$

$$\epsilon_2(\bar{x},\omega) = [- K^F_{a_2}(\bar{x}) \alpha^F_2(\bar{x},\omega) \Phi_{2_0}(\bar{x}) - K^M_{a_2}(\bar{x}) \alpha^M_2(\bar{x},\omega) \Phi_{2_0}(\bar{x}) \tag{47}$$

$$+ K^F_r(\bar{x}) \alpha^F_2(\bar{x},\omega) \Phi_{1_0}(\bar{x}) + K^M_r(\bar{x}) \alpha^M_2(\bar{x},\omega) \Phi_{1_0}(\bar{x})]$$

These equations are complex, as noted earlier, and relate the response $\underline{\Phi}_i(\bar{x},\omega)$ due to the disturbance $\underline{S}_i(\bar{x}_d)$. The solution to these complex equations then provides the spatial source transfer function as it was defined at the beginning of this development. The output is the response $\underline{\Phi}_i(\bar{x},\omega)$ at some arbitrary position $\bar{x}$, and the input is the source or disturbance $\underline{S}_i(\bar{x}_d)$ at location $\bar{x}_d$. The ratio of the amplitudes of $\underline{\Phi}_i(x,\omega)$ to $\underline{S}_i(\bar{x}_d)$ provides the source transfer function amplitude or gain and the phase angle difference or phase shift represents the transfer function phase angle.

The practical approach in the solution of the spatial source transfer

function is to divide equations (36) and (37) by $\underline{S}_i(\bar{x}_d)$. This then provides for the direct solution for the source transfer function rather than the response alone. In addition, by making the $\underline{S}_i(\bar{x}_d)$ term a real number (say 1.00) with the imaginary component equal to zero, then the phase angle for the source term is then initially zero and the transfer function phase angle then represents the phase shift between the source and the response, $\underline{\Phi}_i(\bar{x},\omega)$. This approach results in a direct solution for the phase angle of $\underline{\Phi}_i(\bar{x},\omega)$. A more detailed description of the physical processes involved is presented by Johnson.[33]

The boundary conditions which must be satisfied by the equations for the source transfer function are the result of boundary conditions which must be satisfied by the true flux.

These boundary conditions for the solutions of the flux equations are

$$\Phi_i(\bar{x}_s,t) = 0 \qquad (i = 1,2) \quad \text{for} \quad t \geq 0 \tag{48}$$

where $\bar{x}_s$ denotes the extrapolated exterior boundary of the reactor,

$$\lim_{\epsilon\to 0} [\Phi_i(\bar{x}_{b-\epsilon},t) = \Phi_i(\bar{x}_{b+\epsilon},t)] \quad (i=1,2) \quad \text{for } t \geq 0 \tag{49}$$

i.e., the flux is continuous across a boundary, b,

$$\lim_{\epsilon\to 0} [D_i(\bar{x}_{b-\epsilon})\ \nabla\Phi_i(\bar{x}_{b-\epsilon},t) = D_i(\bar{x}_{b+\epsilon})\ \nabla\Phi_i(\bar{x}_{b+\epsilon},t)] \quad (i=1,2) \quad \text{for } t \geq 0 \tag{50}$$

i.e., the current is continuous across a boundary, b.

Substituting equation (4) into equation (48) through (50) and

subtracting the steady state components, which must be equal by definition, gives the boundary conditions for $\delta\Phi_i(\bar{x},t)$ which must be satisfied by $\underline{\Phi}_i(\bar{x},\omega)$ and are spelled out in equations (48) through (50). Replacing $\delta\Phi_i(\bar{x},t)$ by the complex representation and cancelling the $\exp(j\omega t)$ term results in the following boundary conditions for $\underline{\Phi}_i(\bar{x},\omega)$.

$$\underline{\Phi}_i(\bar{x}_s,\omega) = 0 \qquad (i=1,2) \quad \text{for } \omega > 0 \tag{51}$$

$$\lim_{\epsilon\to 0} [\underline{\Phi}_i(\bar{x}_{b-\epsilon},\omega) = \underline{\Phi}_i(\bar{x}_{b+\epsilon},\omega)] \qquad (i=1,2) \quad \text{for} \quad \omega > 0 \tag{52}$$

$$\lim_{\epsilon\to 0} [D_i(\bar{x}_{b-\epsilon})\ \nabla\underline{\Phi}_i(\bar{x}_{b-\epsilon},\omega) = D_i(\bar{x}_{b+\epsilon})\ \nabla\underline{\Phi}_i(\bar{x}_{b+\epsilon},\omega)] \qquad \begin{matrix}(i=1,2)\\ \text{for } \omega > 0\end{matrix} \tag{53}$$

The solution of equations (36) and (37) subject to the boundary conditions spelled out by equations (51) through (53) is somewhat similar to the solution of the ordinary diffusion equations. This is, however, considerably more difficult since the equations represented involve complex quantities.

As a matter of interest it may be pointed out that a similar set of equations not involving feedback strongly resembled the diffusion equations. As a result of this resemblance, Johnson[33] developed an approach for solving these complex equations by the separation of each equation into the real and imaginary parts which resulted in the solution of four coupled equations for the two groups. Two sets of equations were used to solve for the real components in each of the two groups and two sets of equations were used to solve for the imaginary components in each of the two groups. From the solution of the four equations, one was able

to predict both amplitude and phase angle for the source transfer function.

It should be noted that, in the general approach, the introduction of feedback mechanisms precludes the direct adoption of the method employed by Johnson since the general equation contains the normal diffusion type terms and, in addition, the $\nabla\cdot\gamma_{i-i}\Phi_i$ and $\nabla\cdot\rho_{i-i}\Phi_i$ terms. The introduction of these terms would involve the modification of a normal statics code to include these additional terms as "source terms." This was found to be difficult for the large two-dimensional statics codes now available and was not undertaken.

For these reasons a special one-dimensional computer code was written for the solutions to these equations. This solution, which involved direct complex arithmetic, is described at some length later in the text.

Concluding Remarks

Starting with the two group, multiregion representation of the diffusion equations, a derivation has been presented that results in two linear coupled, nonhomogeneous equations applicable to a power reactor system for predicting the spatial source transfer function under the influence of temperature feedback. This development was done under a number of approximations and assumptions which were pointed out throughout the discussion. A primary assumption was the linear system response to the small oscillatory "driver" signal.

CHAPTER III

COMPUTATIONAL SOLUTION OF THE TRANSFER FUNCTION EQUATIONS

The objective of this chapter is to describe the approach taken in solving the spatial source transfer function equations (equations (36) and (37)) for a one-dimensional (1D) model of the Georgia Tech Research Reactor (hereafter referred to as the GTRR). From the earliest stages of this research when it was deemed feasible that an oscillator could be placed in the geometrical center of the reactor core, it was decided to do a one-dimensional study of the GTRR spatial transfer function with temperature feedback. The one-dimensional study is obviously the simplest case and a reasonable first step. It will be shown presently that this case presents a formidable challenge. The computer code written to solve the spatial source transfer function equations was named SPARE, the mnemonic for spatial reactor effects.

As a matter of convenience in the discussion, the equations describing the spatial source transfer function with temperature feedback will be rewritten below. The definition of all the terms and coefficients is as presented in Chapter II. The equations are

$$\nabla \cdot D_1(\bar{x})\ \nabla \underline{\Phi}_1(\bar{x},\omega) - \Sigma_r(\bar{x})\ \underline{\Phi}_1(\bar{x},\omega) - \Sigma_{A_1}(\bar{x},\omega)\ \underline{\Phi}_1(\bar{x},\omega) \tag{54}$$

$$+ [\nu\ \Sigma_{f_1}(\bar{x})\ W(\omega) + \tau_1(\bar{x},\omega)]\ \underline{\Phi}_1(\bar{x},\omega) + [\nu\ \Sigma_{f_2}(\bar{x})\ W(\omega)$$

$$+ \tau_2(\bar{x},\omega)]\ \underline{\Phi}_2(\bar{x},\omega) + \nabla \cdot \gamma_1(\bar{x},\omega)\ \underline{\Phi}_1(\bar{x},\omega) + \nabla \cdot \gamma_2(\bar{x},\omega)\ \underline{\Phi}_2(\bar{x},\omega)$$

$$+ \underline{S}_1(\bar{x}) = 0$$

$$\nabla \cdot D_2(\bar{x})\ \nabla \underline{\Phi}_2(\bar{x},\omega) - \Sigma_{A_2}(\bar{x},\omega)\ \underline{\Phi}_2(\bar{x},\omega) + \Sigma_r(\bar{x})\ \underline{\Phi}_1(\bar{x},\omega) \tag{55}$$

$$+ \epsilon_1(\bar{x},\omega)\ \underline{\Phi}_1(\bar{x},\omega) + \epsilon_2(\bar{x},\omega)\ \underline{\Phi}_2(\bar{x},\omega) + \nabla \cdot \rho_1(\bar{x},\omega)\ \underline{\Phi}_1(\bar{x},\omega)$$

$$+ \nabla \cdot \rho_2(\bar{x},\omega)\ \underline{\Phi}_2(\bar{x},\omega) + \underline{S}_2(\bar{x}) = 0 \ .$$

A review of equations (54) and (55) indicates that, in addition to reactor parameters, many of the coefficients involve steady state fluxes (Φ_{1_0} and Φ_{2_0}). These coefficients include $\tau_1(\bar{x},\omega)$ and $\tau_2(\bar{x},\omega)$ and $\epsilon_1(\bar{x},\omega)$ and $\epsilon_2(\bar{x},\omega)$. Also many coefficients involve the gradient term for the steady state fluxes. In order to proceed with this development, it was first necessary to define the reactor in terms of zones with physical dimensions and properties. Based on this model the diffusion equations representing the neutronic properties of these zones were written and the solutions obtained. This information then served as an input data source for the computer code SPARE.

Reactor Model and Parameters

The model and dimensions chosen to physically approximate the GTRR in one-dimensional geometry are shown in Figure 1. This model has four regions with the first zone representing the region occupied by the pile oscillator, the second zone representing the fuel region, the third zone representing the heavy water moderator and reflector, and the fourth zone representing the graphite reflector. The third and fourth zones are based on the physical dimensions[70,71] of the reactor tank and the radius of the graphite reflector.

The dimensions of the first two regions were determined by cell

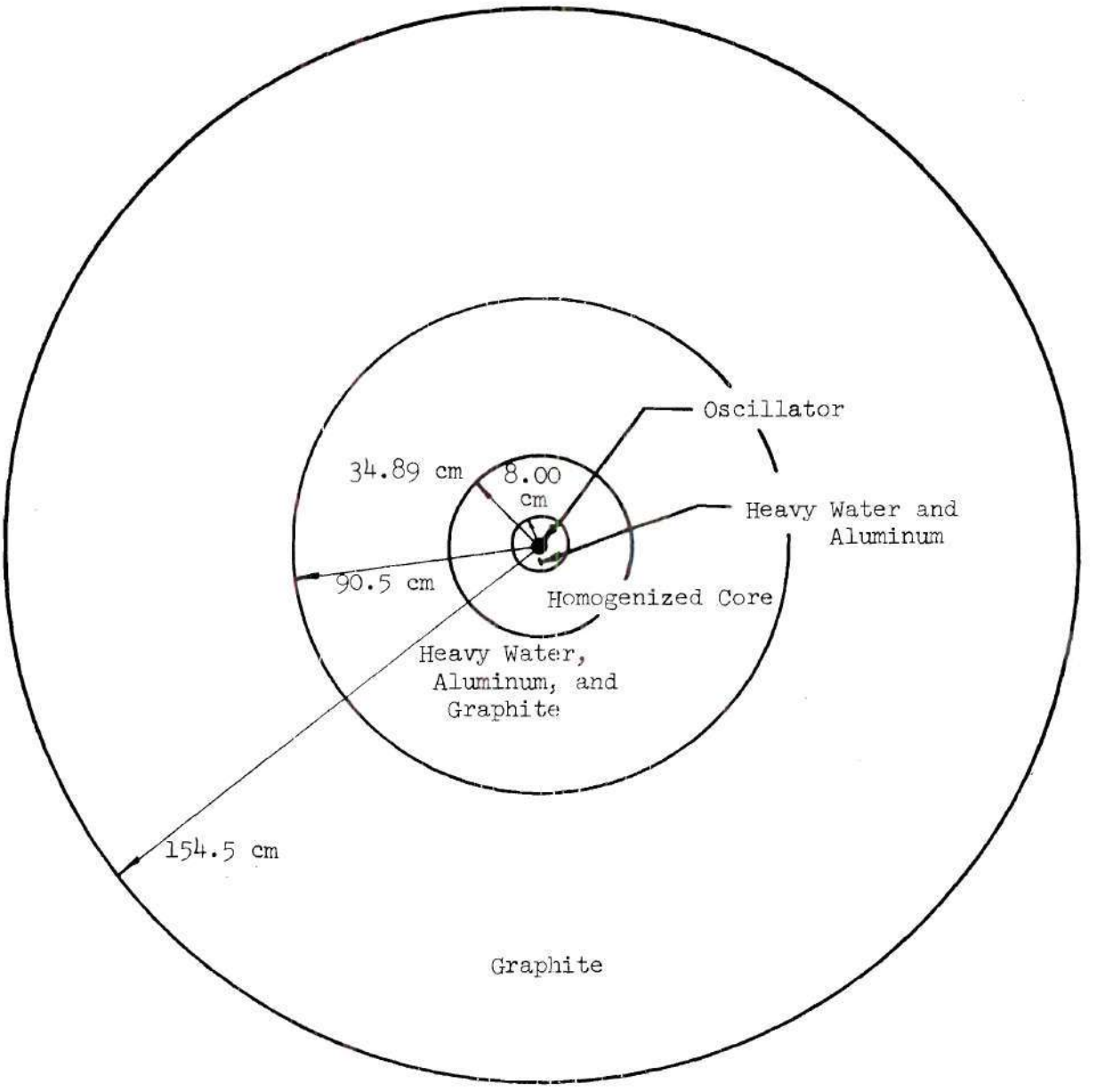

Figure 1. One-Dimensional Model of the GTRR Used in the Analytical Studies

calculations where a unit cell represents a fuel element and its surrounding moderator. Cell calculations have been made for the GTRR 1 MW fuel[72]; the unit cell area is 201.29 sq cm. This unit cell area results in a radius of 8.004 cm for the first region, which is a single unit cell occupied by the pile oscillator. Considering the pile oscillator to be at mid-plane in the reactor the first cell contains 1.9 percent aluminum and 98.1 percent heavy water by volume. The pile oscillator is represented by a seven-eighths inch diameter cross sectional area of aluminum with the remaining portion of the cell being the D_2O.

The second region consists of an area such that the remaining 18 fuel element unit cells are included in this zone. The properties of this zone have been determined earlier in a Reactor Physics Technical Report[72] by homogenizing and flux weighting the constants for the fuel, aluminum, and heavy water in a unit cell.

The third zone consists primarily of heavy water; however, the presence of aluminum in the beam tubes and structural members, and graphite in the beam holes was also considered. Based on prior studies the values used were 87.3 percent heavy water, 7.2 percent graphite, and 5.5 percent aluminum. The outer radius and limit of this region is the inside radius of the aluminum reactor vessel.

The fourth and last region is the graphite reflector region. The boundary of the reactor excluding any shielding has a total radius of 154.2 cm which consists of a physical dimension of 152.4 cm plus an extrapolation distance of 1.8 cm.

The reactor parameters for this analysis were used from an earlier study at a reactor temperature of 35°C with two exceptions. In the first

instance the thermal absorption cross section was increased slightly in the first zone in an attempt to match the analytical worth of the assembly to the experimentally measured value of 0.539 percent $\Delta k/k$. This approach provided a method for accounting for the presence of the cadmium rings in the oscillator. In the second instance the thermal absorption cross section was increased in the fuel zone to account for the poison buildup due to the normal fission process. This additional poisoning was determined by an external buckling calculation based on the normal fuel zone thermal absorption cross section and assumed criticality with 10 elements which was the case at initial criticality for the GTFR.[73] With the external buckling known it was then a matter of increasing the thermal absorption in the fuel zone for the 18-element core until the diffusion code measurements indicated a k_{eff} value of 1.000.

The values of the reactor parameters used in this study are tabulated and presented in Appendix C.

Diffusion Code Development

The one-dimensional form of the steady state neutron diffusion equations is then

$$D_1(\bar{x})\left(\frac{1}{x}\frac{\partial}{\partial x}\, x\, \frac{\partial}{\partial x}\, \Phi_{1_0}(\bar{x})\right) - \Sigma_r(\bar{x})\, \Phi_{1_0}(\bar{x}) - D_1(\bar{x})(B_Z^2)_1\, \Phi_{1_0}(\bar{x}) \tag{56}$$

$$- \Sigma_{a_1}(\bar{x})\, \Phi_{1_0}(\bar{x}) + (1/k)[\nu\, \Sigma_{f_1}(\bar{x})\, \Phi_{1_0}(\bar{x}) + \nu\, \Sigma_{f_2}(\bar{x})\, \Phi_{2_0}(\bar{x})] = 0$$

$$D_2(\bar{x})\left(\frac{1}{x}\frac{\partial}{\partial x}\, x\, \frac{\partial}{\partial x}\, \Phi_{2_0}(\bar{x})\right) - \Sigma_{a_2}(\bar{x})\, \Phi_{2_0}(\bar{x}) - D_2(\bar{x})(B_Z^2)_2\, \Phi_{2_0}(\bar{x}) \tag{57}$$

$$+ \Sigma_r(\bar{x})\, \Phi_{1_0}(\bar{x}) = 0$$

where $B^2_{Z_i}$ is the transverse buckling term. The other terms have been explained in the discussion in Chapter II.

The $D_i(\bar{x})\ B^2_{Z_i}$ term was added to account for leakage in the axial or Z direction and is based on the assumption

$$D_i(\bar{x})\ \frac{\partial^2 \Phi_i(\bar{x})}{\partial Z^2} = -\ D_i(\bar{x})(B^2_Z)_i\ \Phi_i(\bar{x}) \tag{58}$$

for slab geometry in the third direction.

For the solution of the GTRR model the radial dimensions were graduated such that grid points were established at 1 cm intervals the first 50 cm of the radial dimension, then at 2 cm intervals the next 50 cm, and finally at 3 cm intervals the remaining distance of approximately 55 cm. In addition, intermediate grid points were established near the reactor center and the outer edge and at the zone or region boundaries. This grid scheme resulted in approximately 110 grid points for the GTRR model.

At the zone or region boundaries a grid point was established, and, in addition, grid points on both sides of the boundary were established at a spacing of $1/40^{th}$ the normal grid spacing noted previously from the boundary. At the boundary the flux and current continuity equations were used and the arbitrary reduced grid spacing employed to more accurately describe the gradient term in the current continuity equations. The current continuity equations at the boundary, based on the numerical approximation to equation (50), were written in the following manner

$$D_i(x_{j-1})\left(\frac{\Phi_i(x_j) - \Phi_i(x_{j-1})}{h_{j-1}}\right) = D_i(x_{j+1})\left(\frac{\Phi_i(x_{j+1}) - \Phi_i(x_j)}{h_j}\right) \tag{59}$$

where

$\Phi_i(x_j)$ denotes the i^{th} flux at the j^{th} spatial location

x_j denotes the spatial location of the boundary

h_j denotes the distance from the j^{th} spatial point to the $(j+1)^{th}$ spatial point.

For the interior panels or grid points the numerical approximations to the leakage terms in equations (56) and (57) are presented in the following discussion. The $\nabla\cdot D_i(\bar{x})\ \nabla\Phi_i(\bar{x})$ leakage term is evaluated for cylindrical coordinates with $D_i(\bar{x})$ remaining constant over a given grid spacing; therefore,

$$\nabla\cdot D_i(\bar{x})\ \nabla\Phi_i(\bar{x}) = D_i(\bar{x})\left(\frac{\partial^2\Phi_i(\bar{x})}{\partial x^2} + \frac{1}{x}\frac{\partial\Phi_i(\bar{x})}{\partial x}\right) - D_i(\bar{x})(B_Z^2)_i\ \Phi_i(\bar{x}) \qquad (60)$$

The $\frac{\partial^2\Phi_i(\bar{x})}{\partial x^2}$ and $\frac{\partial\Phi_i(\bar{x})}{\partial x}$ terms were evaluated and related to adjacent grid points assuming a second degree curve and using Taylor's formula.[74] The first and second derivative approximations are shown in equations (61) and (62). This approach yielded the same result one would obtain using normal central difference equations with uniform spacing intervals.

$$\frac{\partial\Phi_i(x_j)}{\partial x} = \left(\frac{1}{h_{j-1}+h_j}\right)\left[\frac{h_{j-1}}{h_j}\left(\Phi_i(x_{j+1}) - \Phi_i(x_j)\right)\right. \qquad (61)$$

$$\left. + \frac{h_j}{h_{j-1}}\left(\Phi_i(x_j) - \Phi_i(x_{j-1})\right)\right]$$

$$\frac{\partial^2\Phi_i(x_j)}{\partial x^2} = \left(\frac{2}{h_{j-1}+h_j}\right)\left[\frac{1}{h_j}\left(\Phi_i(x_{j+1}) - \Phi_i(x_j)\right)\right. \qquad (62)$$

$$\left. - \frac{1}{h_{j-1}}\left(\Phi_i(x_j) - \Phi_i(x_{j-1})\right)\right]$$

where

$\Phi_i(x_j)$ denotes the i^{th} flux at the j^{th} spatial location

h_j denotes the distance from the j^{th} spatial point to the $(j+1)^{th}$ spatial point.

With the equations now written for each spatial point the approach taken for solution of the fluxes was the Gauss-Seidel iterative procedure. In this approach the fast flux was arbitrarily assigned a value at all spatial points. With the fast flux known from this assignment then the thermal flux could be solved. The thermal flux was solved using a Gauss reduction scheme on the individual thermal flux tridiagonal matrix. The solution proved to be quite straightforward. Then, with the thermal flux solved, the thermal flux values were used and solutions acquired for the fast fluxes. As in the earlier case of the thermal flux matrix the individual fast flux tridiagonal matrix was solved using the Gauss reduction method. The iterative scheme was then continued between the two fluxes until the eigenvalue, k, converged. The convergence criterion used in this particular case was that $\Delta k/k$ vary less than 1.0×10^{-7} with each additional iteration.

Convergence for the two group scheme was very good with only 12 to 15 iterations required for each group. The resultant power density using the flux solution was integrated over the volume of the reactor and normalized to the correct power level such that the flux values were then available as data input for the SPARE program which computed the source transfer function data.

In a similar manner the flux gradients were computed at each spatial point for data input for calculating the source transfer function.

The diffusion code flux values were run for several different models of the GTRR and compared with other diffusion code results.[75] The results were very good, with the resultant graphs in most cases providing also identical curves.

A flux plot of the GTRR using the diffusion code with an 18-element core and a dummy element in the center position is shown in Figure 2. The composition of the other zones is as discussed earlier in this chapter on the reactor model.

SPARE--A Program for Computation of Power-Dependent Source Transfer Function

The computer program SPARE is a one-dimensional program written in Fortran IV and implemented on the Univac 1108 computer for computation of the power-dependent reactor source transfer function. The equations used in the program involve complex numbers and calculations are done in normal complex arithmetic using the capability of the Univac for complex operations. This method is in contrast to that used by Johnson[33] and others of solving four groups of equations for a two-group analysis with a real and an imaginary equation for each group. This earlier approach was taken in order to utilize features of the existing diffusion codes.

The equations solved in the program are the two following equations derived in the theoretical analysis.

$$D_1(\bar{x})\left(\frac{1}{x}\frac{\partial}{\partial x}\, x\, \frac{\partial}{\partial x}\ \underline{\Phi}_1(\bar{x},\omega)\right) - \Sigma_r(\bar{x})\ \underline{\Phi}_1(\bar{x},\omega) - D_1(\bar{x})(B_Z^2)_1\ \underline{\Phi}_1(\bar{x},\omega) \quad (63)$$

$$- \Sigma_{A_1}(\bar{x},\omega)\ \underline{\Phi}_1(\bar{x},\omega) + [\nu\,\Sigma_{f_1}(\bar{x})\ W(\omega) + \tau_1(\bar{x},\omega)]\ \underline{\Phi}_1(\bar{x},\omega)$$

(Continued)

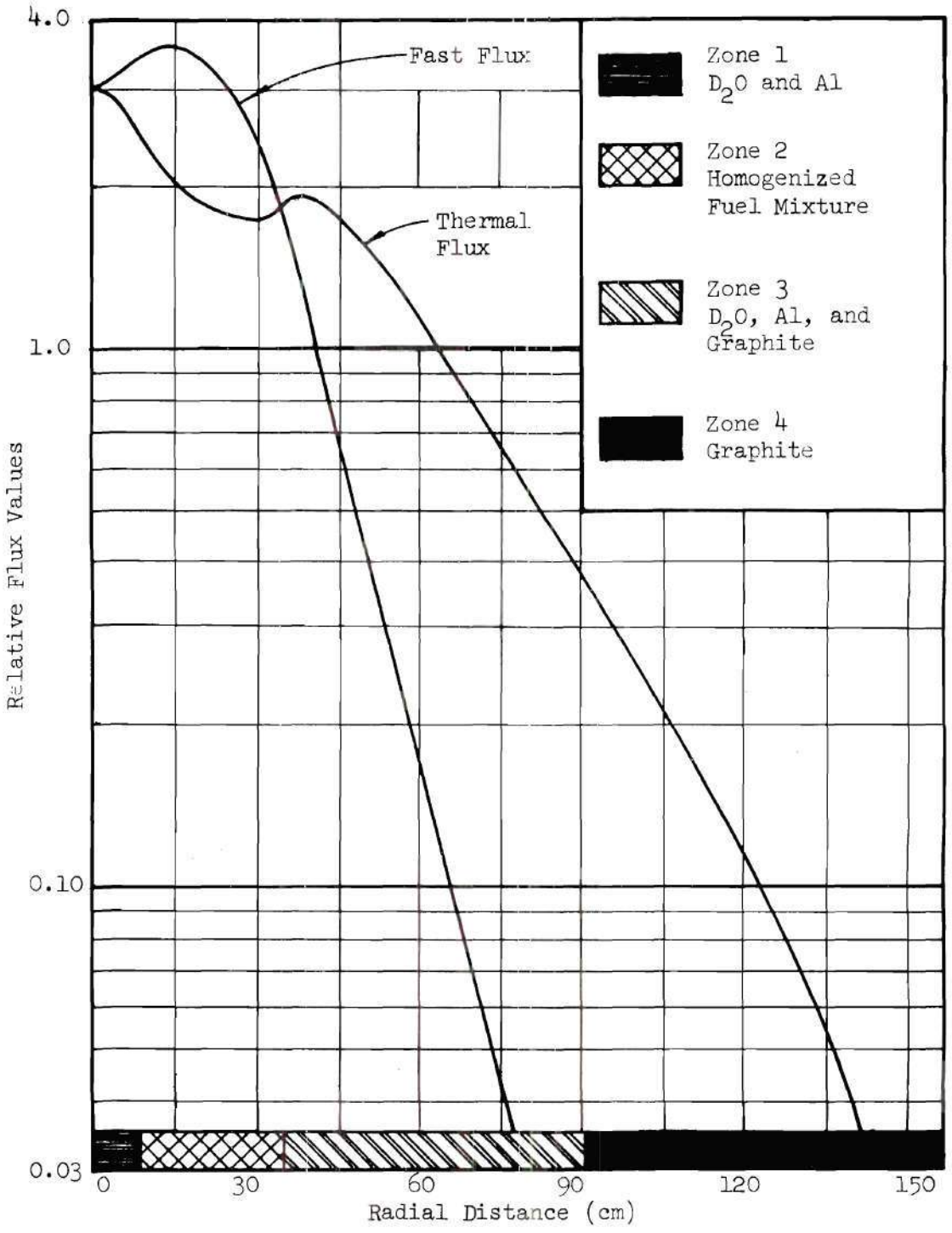

Figure 2. Flux Plots of the GTRR Model Using the SPARE Diffusion Code

$$+ [\nu \Sigma_{f_2}(\bar{x})\ W(\omega) + \tau_2(\bar{x},\omega)]\ \underline{\Phi}_2(\bar{x},\omega) + \nabla\cdot\gamma_1(\bar{x},\omega)\ \underline{\Phi}_1(\bar{x},\omega)$$

$$+ \nabla\cdot\gamma_2(\bar{x},\omega)\ \underline{\Phi}_2(\bar{x},\omega) = 0$$

$$D_2(\bar{x})\left(\frac{1}{x}\frac{\partial}{\partial x}\, x\, \frac{\partial}{\partial x}\, \underline{\Phi}_2(\bar{x},\omega)\right) - \Sigma_{A_2}(\bar{x},\omega)\ \underline{\Phi}_2(\bar{x},\omega) - D_2(B_Z^2)_2\ \underline{\Phi}_2(\bar{x},\omega) \quad (64)$$

$$+ \Sigma_r(\bar{x})\ \underline{\Phi}_1(\bar{x},\omega) + \epsilon_1(\bar{x},\omega)\ \underline{\Phi}_1(\bar{x},\omega) + \epsilon_2(\bar{x},\omega)\ \underline{\Phi}_2(\bar{x},\omega)$$

$$+ \nabla\cdot\rho_1(\bar{x},\omega)\ \underline{\Phi}_1(\bar{x},\omega) + \nabla\cdot\rho_2(\bar{x},\omega)\ \underline{\Phi}_2(\bar{x},\omega) + \underline{S}_2(\bar{x}) = 0$$

The terms are defined in Chapter II. Note that the $\underline{S}_1(\bar{x})$ term has been removed from equation (63). This theoretical analysis was intended to evaluate the source transfer function for subsequent comparison with experimental measurements. The pile oscillator used for the experimental measurements operated on the cadmium shading principle with cadmium movement serving to periodically disturb the flux levels. Since the ratio of the thermal to fast neutron absorption cross sections in cadmium is approximately 500 to one and the slow and fast flux values at the oscillator were very nearly equal, the fast neutron absorptions were only 0.2 percent of the thermal absorptions. The fast neutron absorptions have then been neglected and the numerical solution made for the thermal source transfer function. The $\underline{\Phi}_2(\bar{x},\omega)$ represents the thermal flux response to the source; therefore, the ratio, $\underline{\Phi}_2(\bar{x},\omega)/\underline{S}_2(x_c)$, represents the thermal source transfer function with the source at the center, x_c, of the reactor. By dividing equation (64) by $\underline{S}_2(x_c)$ and solving the two sets of simultaneous equations one then solved directly for the source transfer function. This was done by setting $\underline{S}_2(x_c) = (1.0 + 0.0j)$. This notation

indicates a real component of 1.0 and a zero imaginary component. The source $\underline{S_2}(x_c)$ was considered to be located at the reactor center since the experiments were conducted with the oscillator in that location. The source term $\underline{S_2}(x_c)$ was given the zero imaginary component since this served to give a starting point for the phase angle calculations, i.e. the source term had a zero phase angle; hence, further calculations indicated the true phase shift between the source and the response.

The program required a number of constants and values for input such as flux levels, heat transfer characteristics, reactor physics constants, etc. These were read in and computed in several subroutines prior to the transfer function calculations. The parameters used for the GTRR are presented in Appendix C.

The calculations for the complex fluxes were made in the same manner as in the case of the diffusion calculations, i.e. a Gauss-Seidel iterative procedure where one of the flux groups is assumed the next group computed and then continual iterations between the two groups until the calculations converge to a solution, always based on the latest calculations. The calculations involving complex numbers were much more time consuming and, in addition, convergence was much slower. This increased difficulty was to be expected since the two-group complex equations in essence represented a normal four-group approach.

The solution within each matrix is likewise similar to the diffusion calculations since the matrix contains a tridiagonal system of equations which can be readily solved by a Gauss elimination scheme even with complex numbers. As noted earlier the convergence did prove to be somewhat time consuming. For instance, the diffusion equations typically

required 10 to 20 iterations between each group for all spatial calculations before convergence. In the case of the complex flux calculations a typical calculation per frequency required 1500 iterations for both sets of equations, the fast complex and the thermal complex fluxes.

The convergence criterion applied for the transfer function calculations was that all thermal complex flux components, both real and imaginary, at every spatial point not exceed a fractional change with each iteration of 1×10^{-5}. This criterion meant that the maximum percent change at any given spatial point did not exceed 0.001 percent. Since some spatial points converge slightly quicker than others and one flux component (real or imaginary) converges slightly quicker than the other, then the more typical fractional change in the amplitude value was 0.0005 percent at convergence. This criterion was felt to be more than adequate. However, some of the computations were iterated until the fractional change for each spatial point did not exceed 1.0×10^{-6}. This latter criterion did not noticeably change the results but did require excessive amounts of computer time. For this more restrictive convergence criterion in the low frequency range a single frequency determination could require as much as 30 minutes of Univac time. For this reason the more restrictive convergence criterion was felt to be neither justifiable nor warranted.

Results of the SPARE Computations

The results of the SPARE computations for the GTRR model over a frequency range of five orders of magnitude are shown in Figures 3 and 4. Curves are presented both for zero power and for a power level of 900 kW.

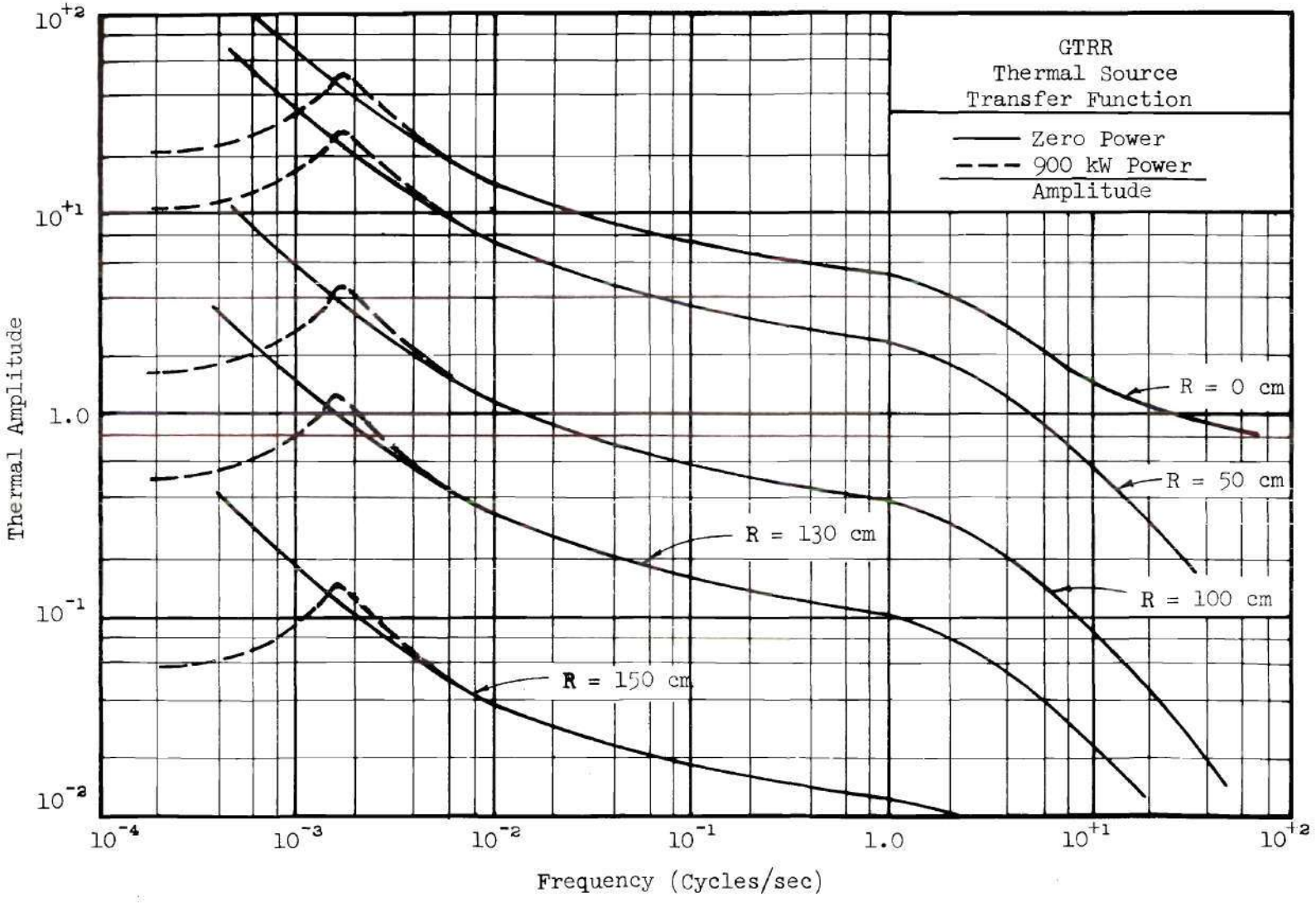

Figure 3. Amplitude Results Using SPARE for Spatial Source Transfer Function Calculations at 900 kW and Zero Power

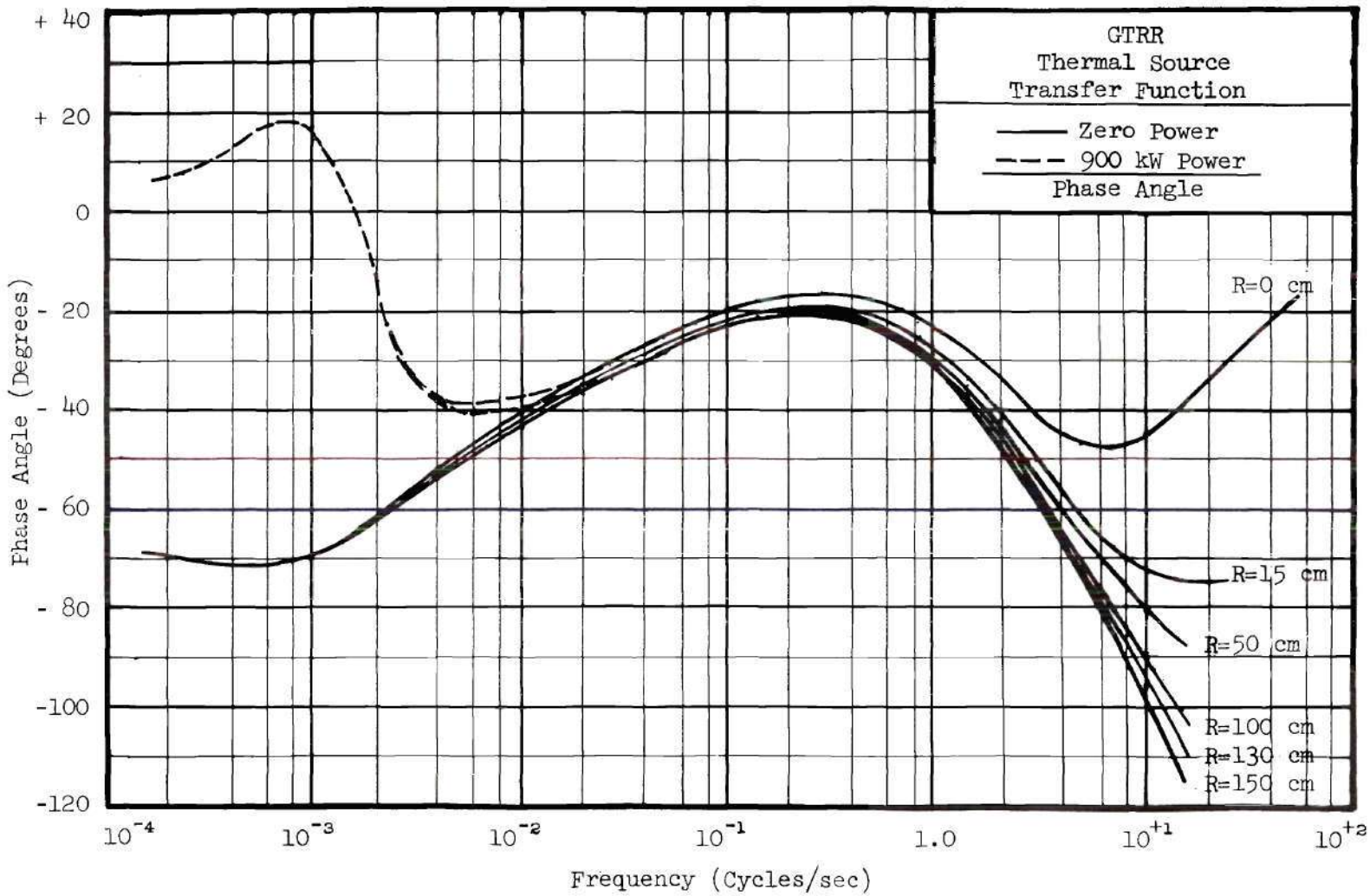

Figure 4. Phase Angle Results Using SPARE for Spatial Source Transfer Function Calculations at 900 kW and Zero Power

The amplitude results are presented in Figure 3 for five spatial positions varying from R=0 cm at the reactor center to R=150 cm at the outer edge of the reactor. Likewise, phase angle results are presented in Figure 4 over the same spatial range.

A detailed review of these curves indicates the presence of both temperature feedback effects and spatial effects. Each of these effects is quite pronounced in certain frequency ranges. Consider first the effect of temperature feedback by comparing the results of the zero-power calculations to those of the 900 kW power level. The results of the amplitude calculations indicate the beginning of temperature feedback at approximately 4×10^{-3} hertz (Hz).

The first effect of the temperature feedback is to increase the amplitude slightly over the zero-power case. Then, as the frequency is further reduced the amplitude is significantly reduced as compared with the zero-power case. This becomes significant as the frequency is reduced to 1×10^{-3} Hz and less. The first slight increase in amplitude is quite interesting and can be attributed to an optimal phase shift between the input signal and the feedback signal, which serves to boost the original input signal for the negative feedback case. However, this effect does not become very significant, as evidenced by the curves. The amplitude then decreases in value with decreasing frequency. The phase angle curves for the at-power condition indicate a departure from the zero-power case at approximately 2×10^{-2} Hz. As the frequency continues to decrease the phase angle differences become quite pronounced. The phase angle for the zero-power case approaches -90 degrees with very low frequencies whereas the at-power condition approaches a phase lead angle of +20 degrees and

then decreases asymptotically to zero degrees with decreasing frequency. One can conclude from these data that temperature effects for the GTRR are not appreciable at frequencies of 2×10^{-2} and higher. Above this frequency the at-power model reduces to a zero-power model.

It can further be observed from those curves that spatial effects are more significant in the high frequency ranges. At frequencies of one Hz and lower for the GTRR the transfer function amplitude curves remain constant in shape for all spatial positions, with the thermal amplitudes proportional to the spatial static thermal flux. The phase angle response varies slightly over six degrees over the spatial limits of the reactor at one Hz. This phase angle variation decreases to less than three degrees at 2×10^{-2} Hz and less than one degree at 1×10^{-3} Hz. These calculations indicate that the spatial model essentially degenerates to a point model for frequencies of 1×10^{-3} Hz and less.

For frequencies of 10 Hz and larger spatial effects become quite pronounced. At this point the amplitude curves begin to vary in shape depending on spatial position. Likewise, the phase angle variation over the spatial limits of the reactor becomes quite large with a phase angle variation of over 100 degrees at 30 Hz. Both amplitude and phase angle variations with spatial position increase with higher frequencies.

The primary objective of this investigation was to measure the at-power transfer function and observe the effects of temperature feedback. Experimentally the range of interest varied from 5×10^{-4} Hz to 5 Hz. This wide range of frequency investigation permitted comparison between experiment and theory for both feedback and non-feedback cases. This investigation, however, did not provide comparison in the high

frequency range of 10 Hz and higher. In this high frequency range SPARE was run and compared with both prior calculations[33] and experiments[26] on the NORA reactor. A brief description of this reactor is presented in Appendix C, and additional, more comprehensive information is available from references (26) and (34). The results of the comparison for the zero-power case were excellent. The experimental values were very close to the calculated values and the values obtained by SPARE were almost identical to earlier one-dimensional calculations by Johnson[33] in his investigation in this area. These results are displayed in Figures 5 and 6, which are graphs of the amplitude and phase angles, respectively. These results served to validate the computations from SPARE for the high end of the frequency spectrum.

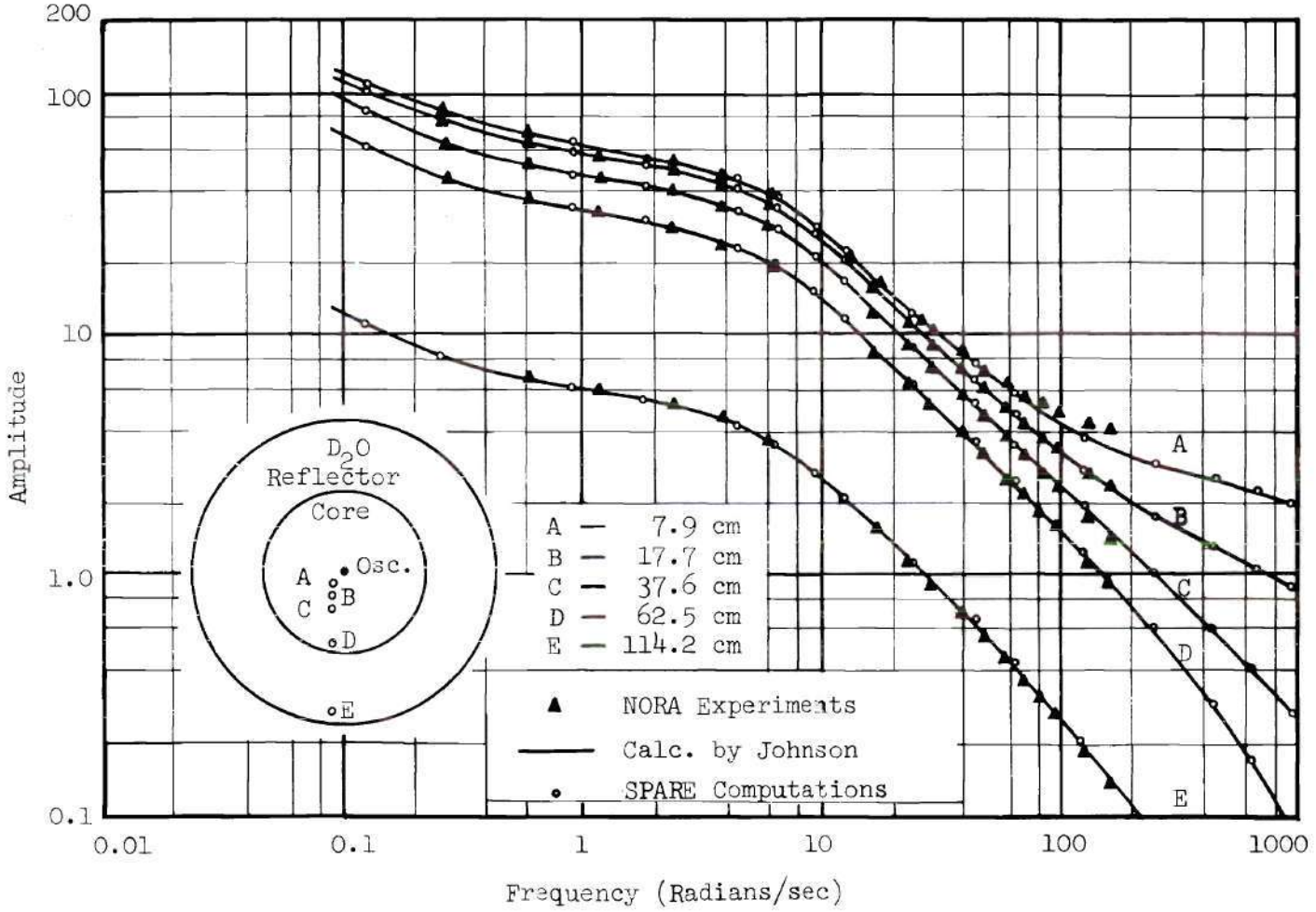

Figure 5. Experimental Amplitude Results Compared with Prior Digital Computations and with SPARE Computations for the NORA Reactor

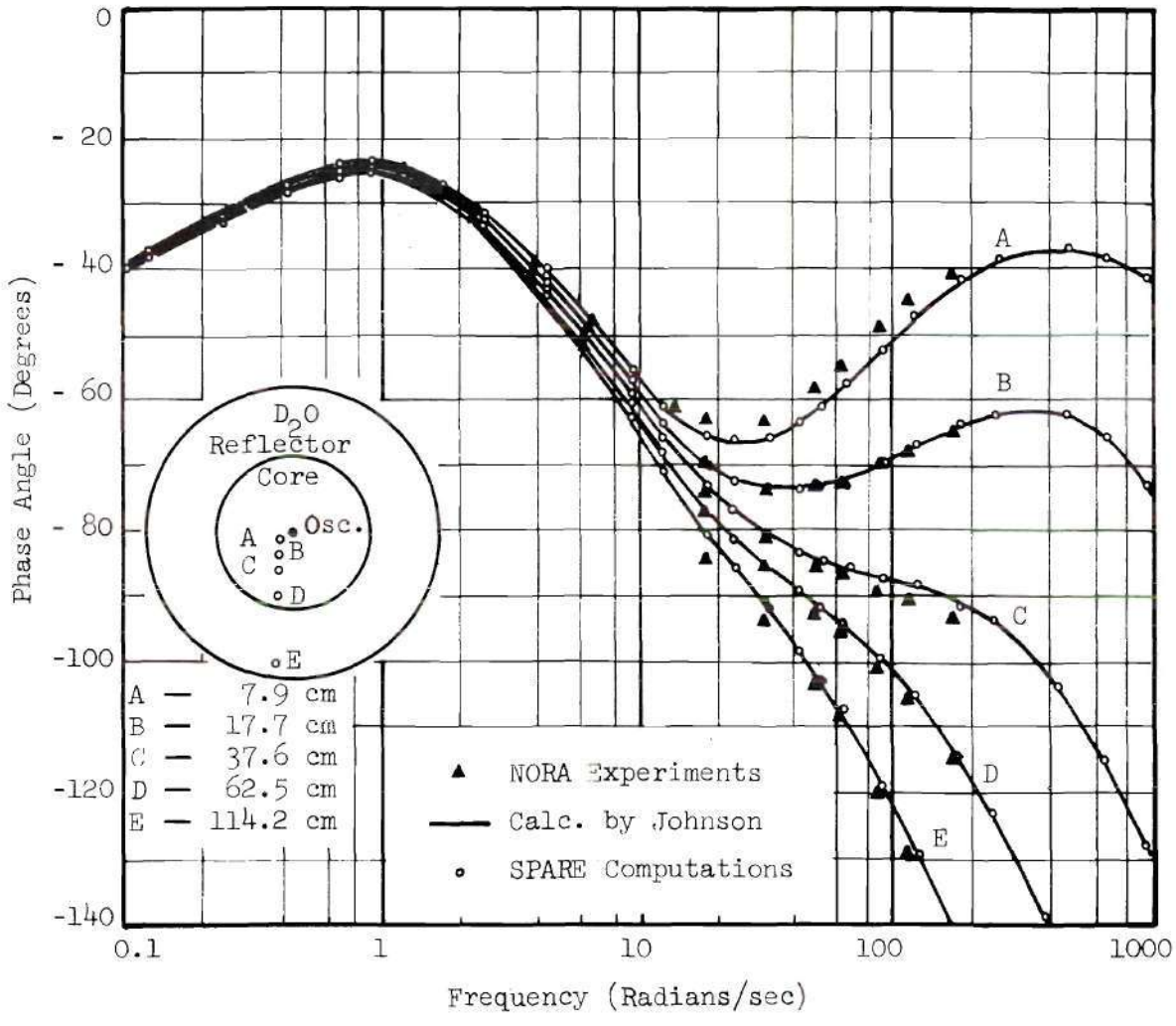

Figure 6. Experimental Phase Angle Results Compared with Prior Digital Computations and with SPARE Computations for the NORA Reactor

CHAPTER IV

INSTRUMENTATION AND EQUIPMENT

The Georgia Tech Research Reactor

The experimental phase of this investigation was performed on the Georgia Tech Research Reactor (referred to as the GTRR). The fuel used in this heterogeneous, heavy water-moderated and cooled reactor consists of highly enriched (greater than 93 percent U-235) plates of an aluminum-uranium alloy which are aluminum clad.[71] Figure 7 is a cutaway view of a typical fuel element. Each plate is approximately 2.8 inches wide and 0.06 inch thick and has an active fuel region 23.5 inches long.

The reactor core configuration consists of fuel elements standing vertically in the plenum of the core tank and arranged on a six-inch triangular pitch. A fully loaded core with 19 elements has an approximate radius of 13.5 inches, with a core height of 23.5 inches. The fuel is centrally located in a six-foot diameter aluminum reactor vessel which contains the heavy water. This configuration provides a radial D_2O reflector thickness of 24 inches and a top reflector thickness of 29 inches.

A vertical section through the reactor is shown in Figure 8. This figure provides a view of the fuel elements, the semaphore control blades, and the beam-tube entry to the reactor core. Figure 9, a horizontal section of the GTRR, illustrates the fuel element triangular pitched positions within the D_2O reflector. A two-foot thick graphite reflector cup surrounds the core tank. A concrete biological shield completely encloses

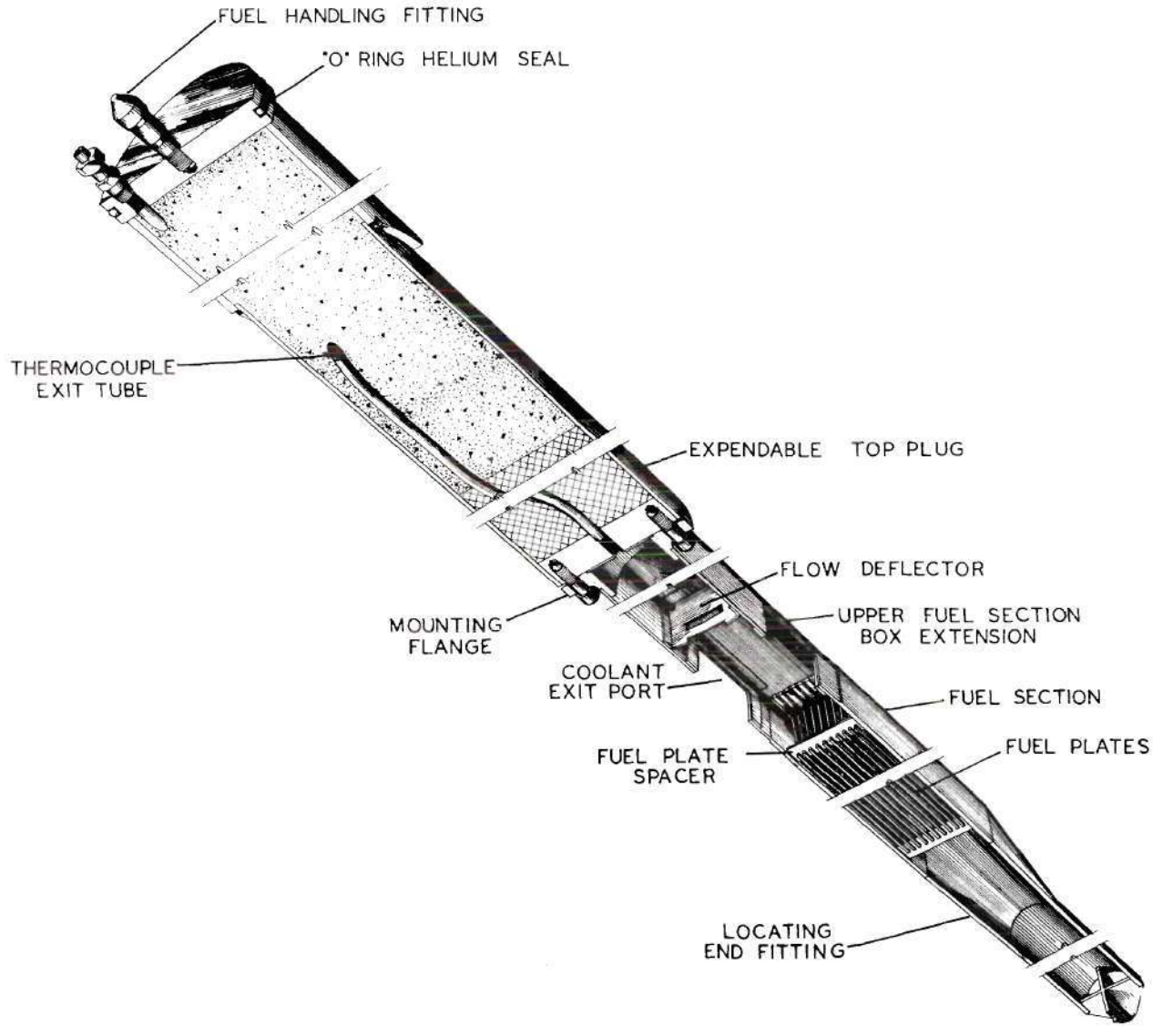

Figure 7. Georgia Tech Research Reactor -- Fuel Element Cutaway View

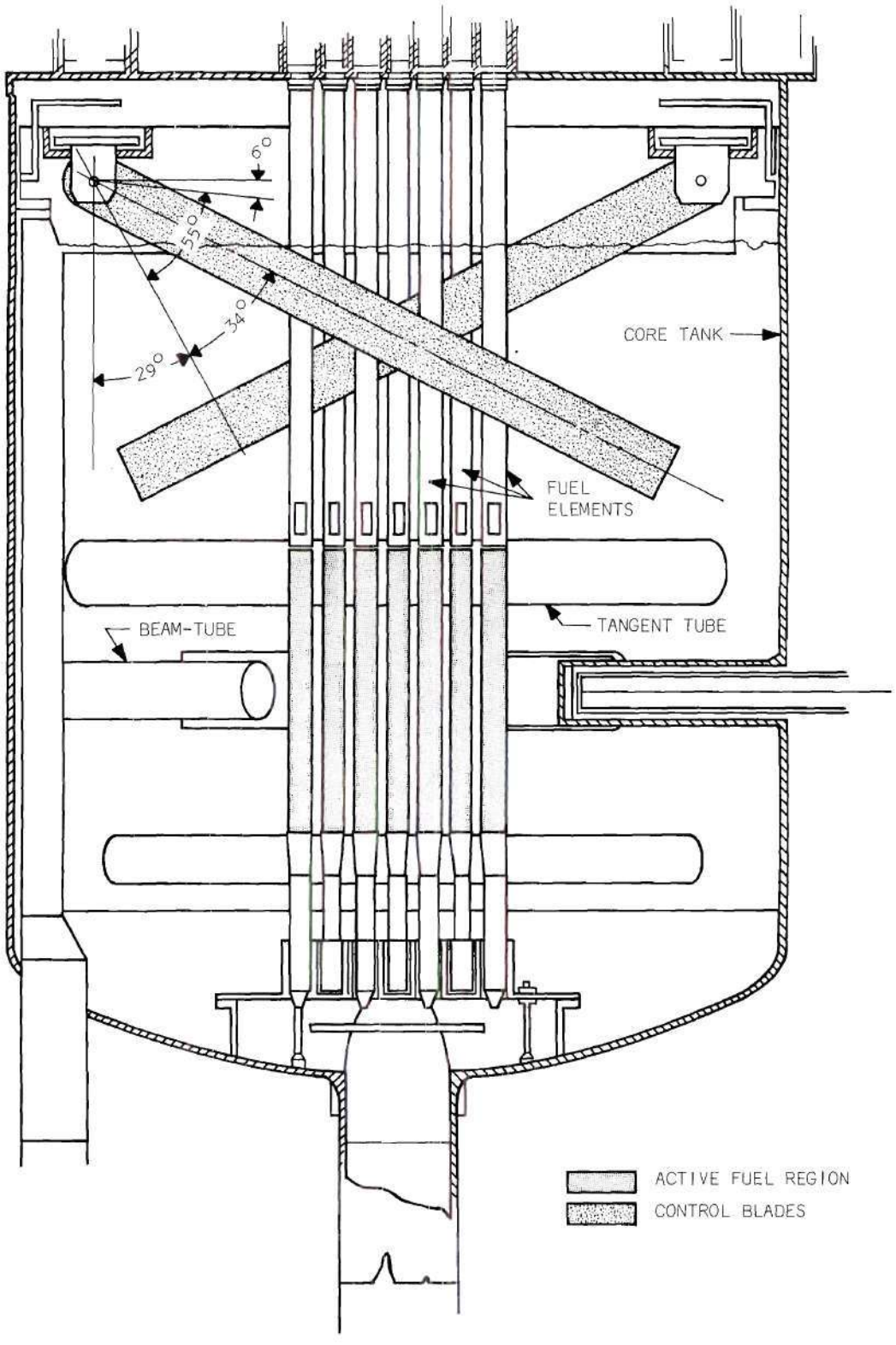

Figure 8. Vertical Section Through GTRR Core Tank Showing Critical Control Blade Configuration

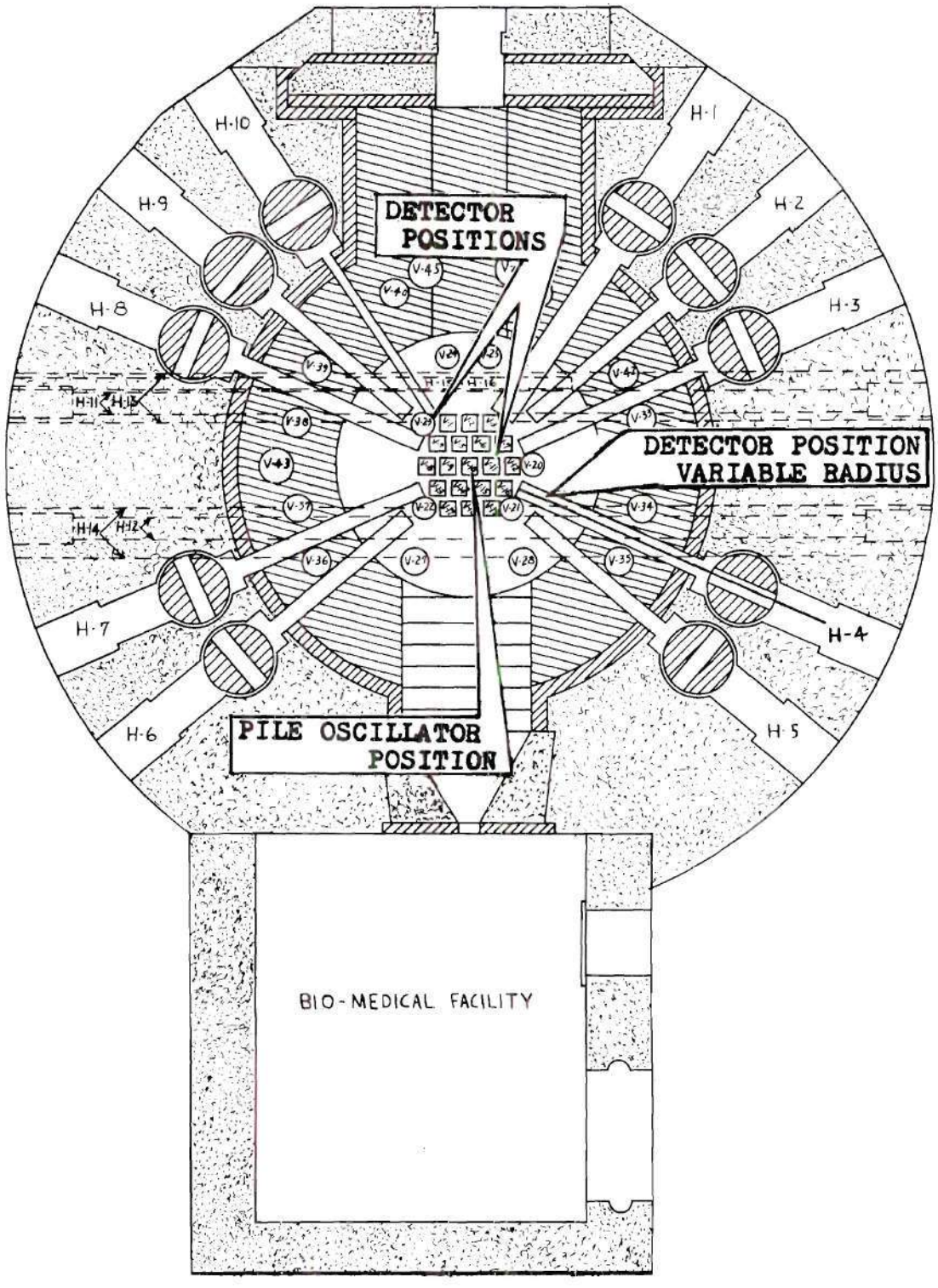

Figure 9. Georgia Tech Research Reactor--Horizontal Section at the Core Midplane Showing the Oscillator and In-Core Detector Positions

the reflector system. The configuration of the horizontal beam tubes, H-1 through H-10, which are all centered on the core mid-plane, is also shown in Figure 9. To indicate the relationship of the radial beam ports, reflector regions, fuel elements, and control blades, a cutaway perspective view of the reactor is provided in Figure 10.

Pile Oscillator

The experimental aspect of this investigation was primarily concerned with the measurement of the source transfer function; therefore, a periodically varying source was utilized. Specifically, the source effect was introduced by varying the degree of neutron absorption with the selective movement of cadmium within the reactor. The use of this approach assumes that small changes in the configuration of the reactor, e.g. varying absorption, produce the same kinetic behavior in the reactor as a varying external source. The selective movement of cadmium is done in accordance with a method of frequency response testing known as the pseudo-random binary sequence. A discussion of the pseudo-random binary sequence is presented in Appendix B.

The device constructed for this task was a pile oscillator which was the major piece of equipment for the experiment. The pile oscillator was designed for and operated in the active core region in a fuel element position. The fuel element position used was V-10 which is at the geometrical center of the reactor. This selection was made for reasons of symmetry. This experimental arrangement allowed comparison between measurements and theoretical results attained from a one-dimensional analysis with the perturbing source at the center. The flux response was

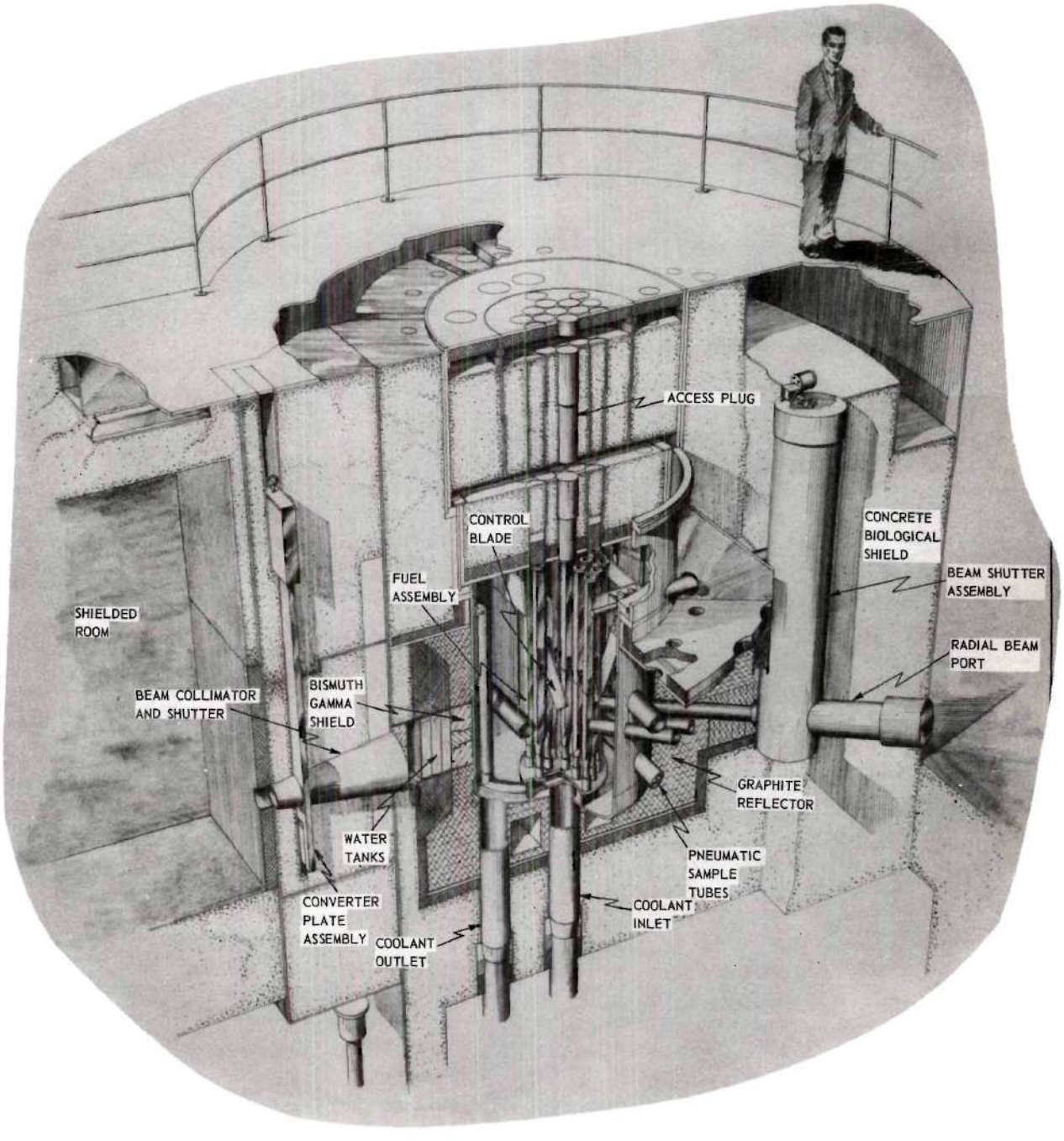

Figure 10. Cutaway View of Georgia Tech Research Reactor

measured and computed at various known radial positions in the reactor from the pile oscillator.

The basic design of the pile oscillator used the cadmium shading principle. Cadmium sheets that are 20 mils thick or greater absorb practically all thermal neutrons impinging on the sheet. Thus, if two cadmium sheets are placed in such a manner as to shadow each other, the net result is that the same amount of absorption occurs as if only one sheet were present. However, if the two sheets of cadmium do not shadow each other, then the two sheets give a greater absorption than the single sheet. It follows then that the amount of absorption is proportional to the exposed surface area rather than the total volume or weight of cadmium. This technique was implemented by a telescopic movement. Two rings of cadmium, three-eighths inch wide by three-fourths inch outside diameter were mounted around a three-fourths inch tube inside an aluminum housing. Two other rings, one-fourth inch wide by five-eighths inch diameter, were mounted inside the three-fourths inch tubing on a movable shaft. The shaft was then designed for a linear movement of one-eighth inch. One position of the movable shaft was in a completely shaded position, i.e. the small cadmium rings inside the larger rings. The other position occurred with the small rings projecting one-eighth inch beyond the large cadmium rings thereby exposing a larger cadmium area. The effect of the cadmium movement is shown in a radiograph of the oscillator in Figure 11. The small cadmium rings mounted on the movable shaft constituted the rotor assembly and the large rings attached to the structural housing constituted the stator assembly.

The oscillator is shown in Figure 12 suspended in the reactor

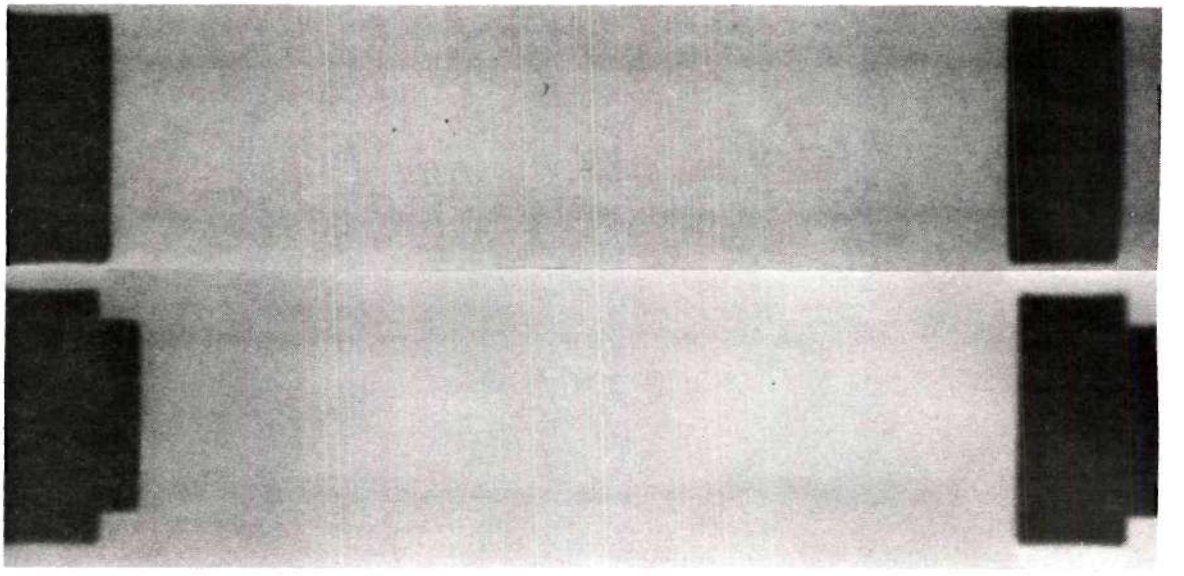

Figure 11. Radiograph of the Pile Oscillator Rotor in Both the Shadowed (Upper) and Unshadowed (Lower) Positions

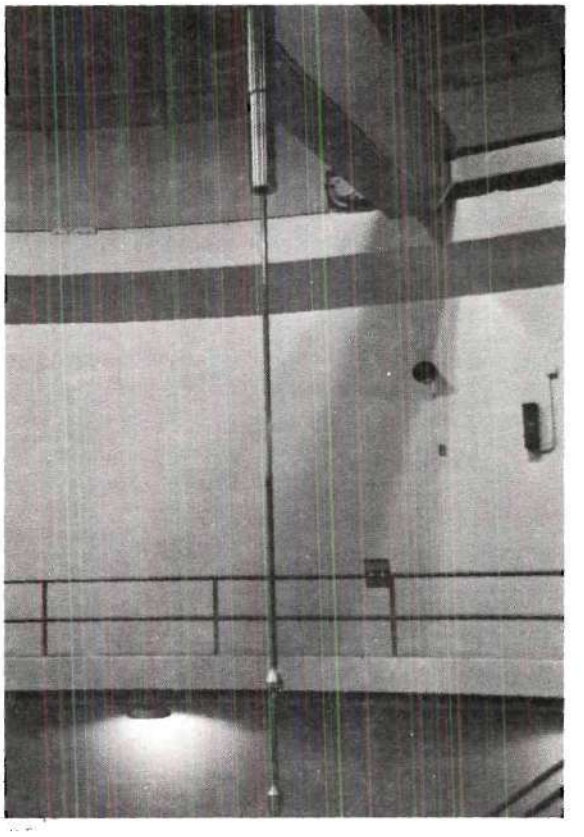

Figure 12. Pile Oscillator

containment building. The top end of the assembly houses the driving units in the upper portion of a modified lower shield plug. The oscillator rotor is housed in a seven-eighths inch aluminum tube which extends from the top of the shield plug to the plenum opening at the bottom of the reactor vessel, a distance of approximately 10 feet. The rotor cadmium is shaded with the stator cadmium at the center of the reactor core at approximately 12 inches from the flexible joint in the housing unit. This arrangement is shown in the schematic drawing of the pile oscillator in Figure 13. More detailed photographs of the pile oscillator are shown in Figures 14 and 15. The drive unit for the oscillator consists of two solenoids which are alternately operated depending upon the binary position desired. Upon a signal from the computer one solenoid holding a given position was deactivated and the second solenoid activated to provide the driving and holding force for the second position. A schematic drawing of the power system for driving the solenoids is shown in Figure 16. A voltage pulse from the computer was used to drive a flip-flop circuit which in turn provided the voltage level for activating one of the solenoids through a solenoid driver or power card. Activation of solenoid one drives the oscillator to the "one" position or the higher power level position and activation of solenoid zero drives the oscillator to the "zero" position or the lower power level position. These two positions, one and zero, correspond to the two positions spelled out and used in the pseudo-random binary sequence. The time of movement between the two positions was approximately 40 milliseconds. The solenoid driver or power card was housed in the computer interface section. A schematic drawing of the solenoid driver is shown in Appendix D.

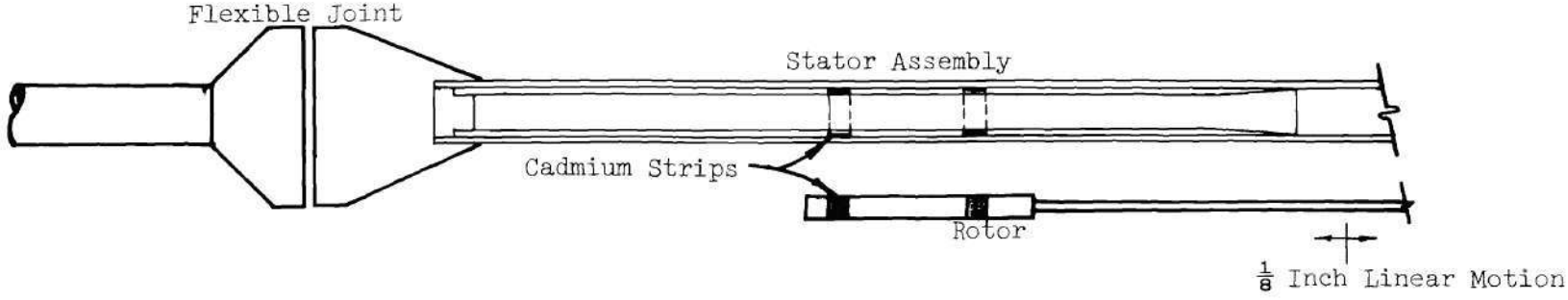

Detail of Rotor and Stator Assembly

Rotor Schematic

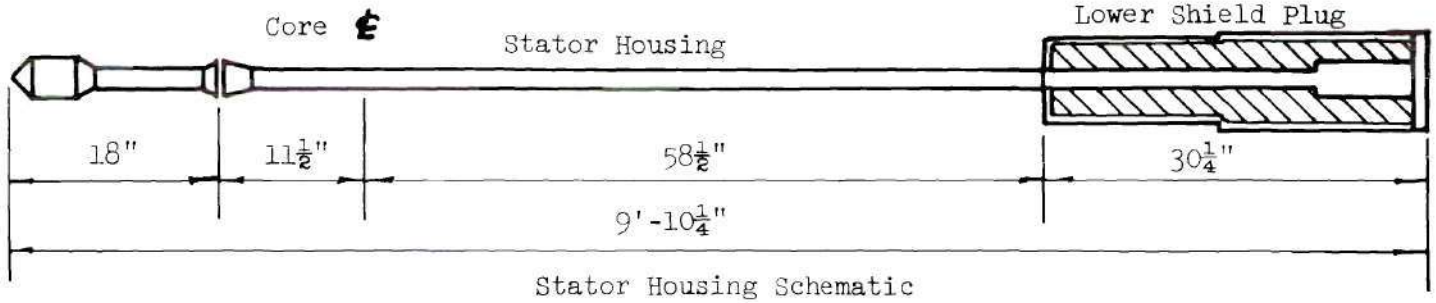

Stator Housing Schematic

Figure 13. Schematic Diagram of Pile Oscillator

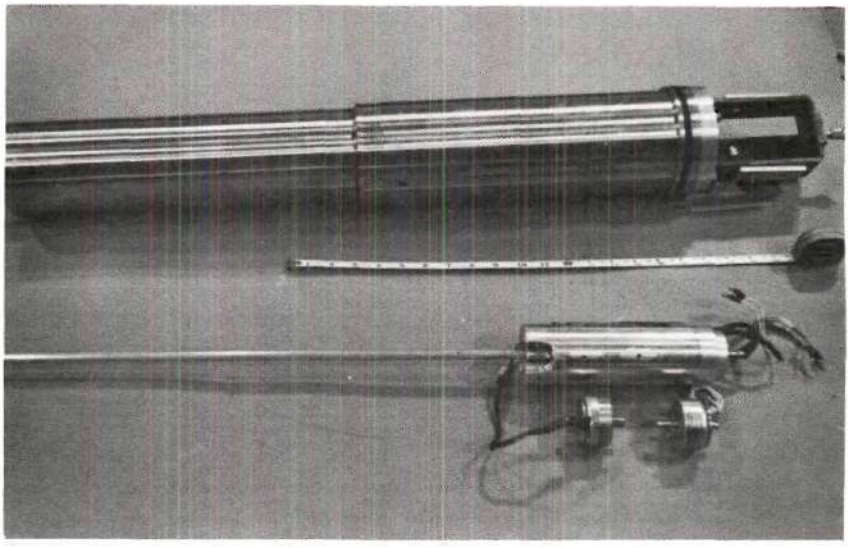

Figure 14. The Upper End of the Oscillator Showing the Lower Shield Plug, the Rotor Housing Unit, and the Drive Solenoids

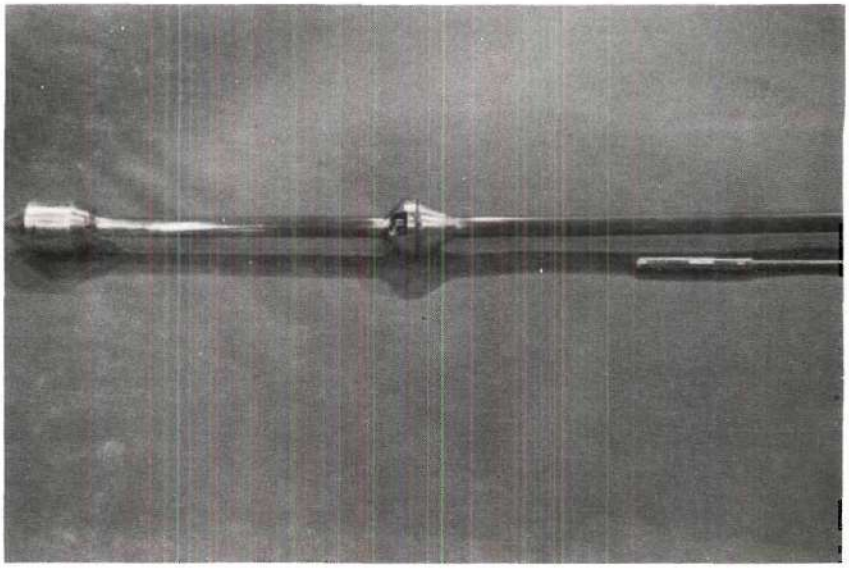

Figure 15. The Lower End of the Oscillator Showing the Flexible Joint and the Rotor

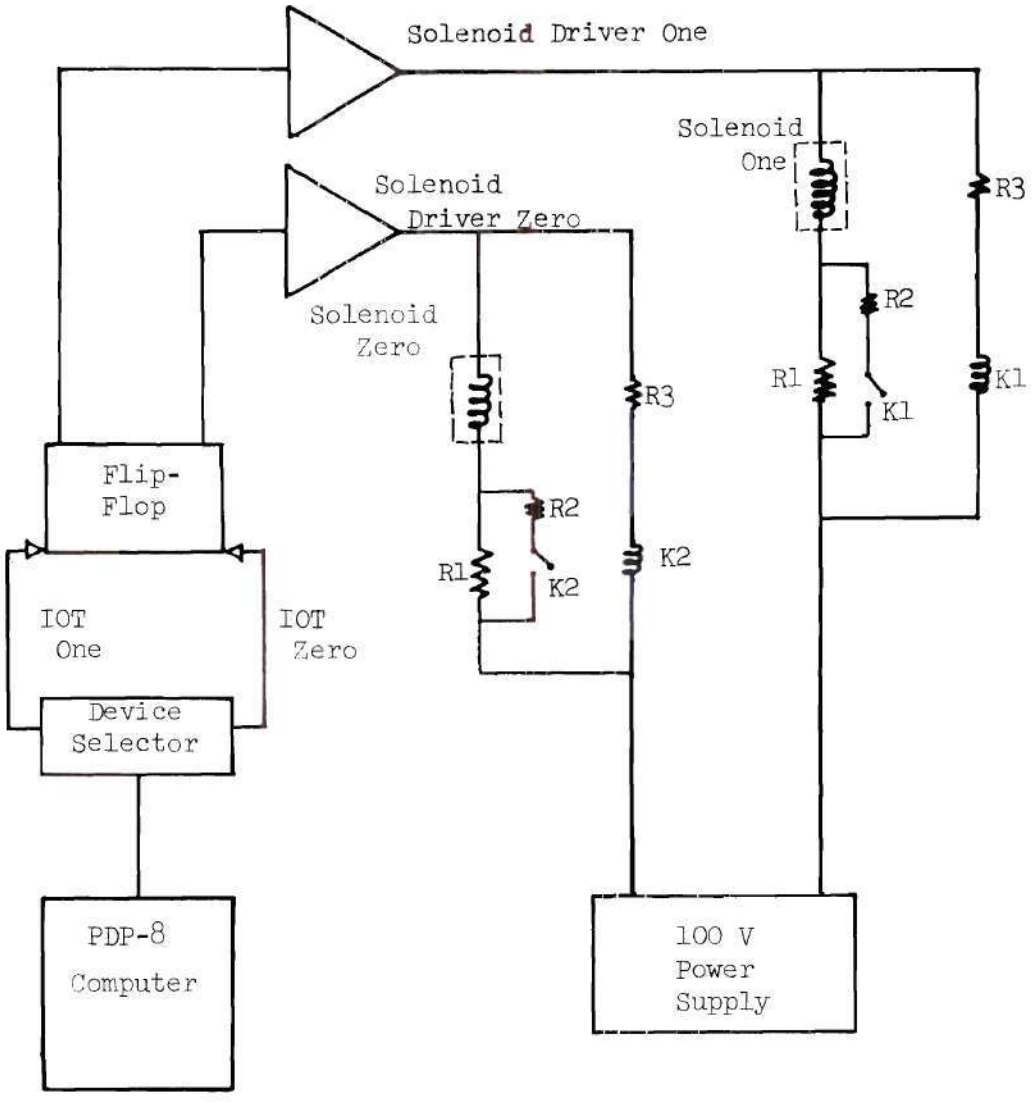

Solenoids	Size 5 (Model 129415-029) Ledex Company	
Resistors	R1	150 Ω 38 W
	R2	50 Ω 15 W
	R3	2 K Ω 1 W
Relays	K1 and K2	
	Model SJ 26043 C. P. Clare Company	
	Contacts	4 amps 150 W
	Coil	40 V 2.5 K Ω

Figure 16. Schematic Diagram of System for Driving the Pile Oscillator Solenoids

The drive units were housed in the upper end of the shield plug. The lower end of the shield plug was filled with lead (balls) to protect the drive unit from the high radiation levels of the reactor. Since the experiment was run with the reactor at full power, the unshielded gamma radiation could cause significant damage to the solenoid circuitry. Earlier models of the pile oscillator with the drive unit located at the bottom of the shield plug were somewhat less reliable in operation. This was due to a combination of factors which included among others such problems as gamma radiation damage, gamma heating, and excessively high neutron activation of the drive assembly.

The cadmium rings used for the oscillatory effect were mounted in the center of the reactor core which is approximately 58½ inches below the bottom of the lower shield plug. Below the core center a flexible coupling was located in the aluminum housing member. The flexible joint was necessary to permit seating of the assembly in the fuel element plenum opening, since the remaining portion above the joint was attached rigidly to the lower shield plug.

Detection and Data Recording System

Detectors

The neutron detectors used for this investigation were U-235 lined fission chambers. Fission chambers were necessary since a great deal of the experimental measurements were made in the active core region with the reactor at full power where fluxes as high as 2×10^{13} $n/cm^2/sec$ were encountered. In order to conduct the experiment with an adequate number of detectors it was necessary to use two different types of detectors.

Although two different types of commercial fission chambers were used, the physical and electrical characteristics of the two were quite similar. One type used was the Reuter-Stokes Electronic Components, Inc. In-Core Flux Probe, designated RSN-186S-M2. This model had a miniature stainless steel chamber one-fourth inch by two inches long, with a sensitive length of one inch and an integral 16 foot-long one-eighth inch diameter stainless steel cable. The Reuter-Stokes fission chamber was filled with helium gas and lined with 3.1 mg of U-235.

The second type of fission chamber used was the Reactor Controls, Inc. RC-2810 Series Neutron Sensitive In-Core Ionization chamber unit. The RC-2810 ionization chambers were designed for practically the same conditions of high temperature and neutron flux as the Reuter-Stokes Model. The RC-2810 fission chamber had a miniature stainless steel chamber three-sixteenths inch diameter by two inches long, with a sensitive length of one and one-half inches and an integral 20 foot-long one-sixteenth inch diameter stainless steel cable. The Reactor Controls fission chamber was lined with 5.0 mg of U-235.

A typical neutron detector used in this experiment is shown in Figure 17. The neutron detectors were mounted in small aluminum tubes 12 feet long for handling and positioning in the various fuel element and beam hole locations.

Both types of detectors were operated at 100 V and exhibited similar output characteristics for reactor operation between zero power and full power of one megawatt.

Current Electrometer

The electrometer system and accompanying power supply used in the

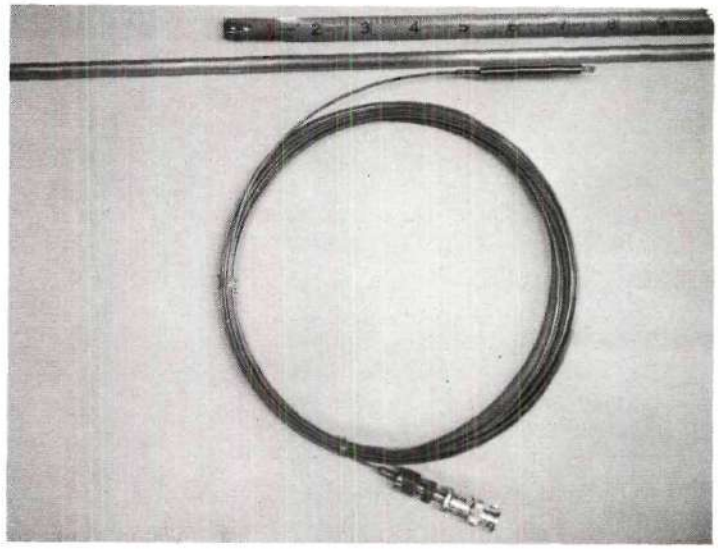

Figure 17. In-Core Neutron Detector with Integral Cable and Aluminum Tube Detector Mount

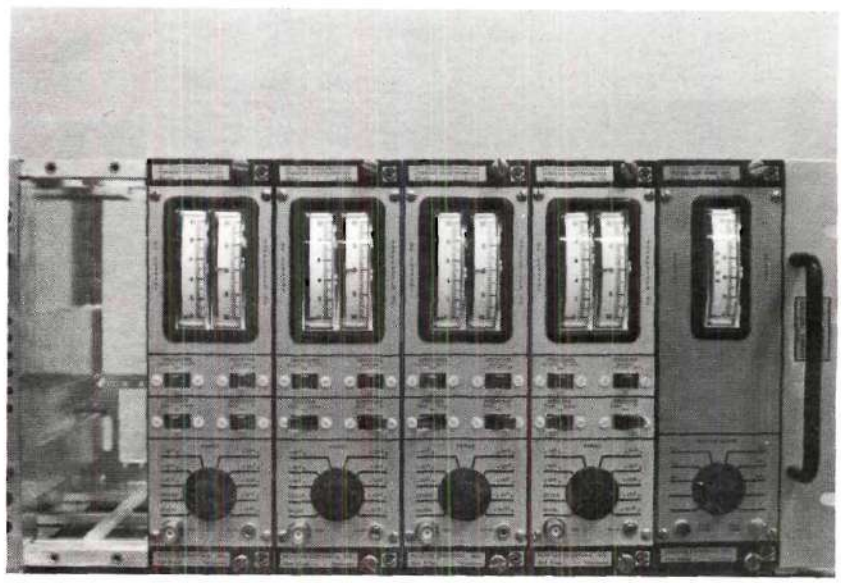

Figure 18. The Electrometer and Electrometer Power Supply Mounted in the NIM Bin

experiment was a special instrument package designed by Reactor Controls, Inc. and designated In-Core Instrumentation Current Electrometer Model E-908. The system was built to accommodate a wide range of reactor kinetic experiments based on specifications submitted by several experimenters at Georgia Tech.

The nuclear instrument module (hereafter referred to as NIM) current amplifiers were designed to operate in two basic modes. One mode, the more conventional use, was the so called current mode. In the current mode the electrometer received a current input from a detector and output a voltage signal proportional to the ratio of current reading to the current full scale. This electrometer output signal varied from 0 to +10 volts. The input to the electrometer could vary from 10^{-10} to 10^{-4} amps depending on the range setting. The voltage output from the electrometer was transmitted to the PDP-8 computer-interfaced sample-and-hold device.

The suppressed mode was the mode designed to accommodate noise analysis and other frequency domain experiments. The suppressed mode was the mode selected for use in this experimental work. The distinguishing feature of the suppressed mode is the manner in which it filters the signal from a detector. The range of current for the suppressed mode is the same range mentioned earlier. The first part of the filtering operation is the removal of the mean value (DC) portion of the current. Hence, a fluctuating signal from the detector results in an output from the amplifier indicative of the current fluctuation about some mean value. Since the suppressed mode was planned for frequency regime experiments, this mode also had the characteristic of filtering undesired frequencies. The electrometer had built-in high-pass and low-pass filters. This feature

had the obvious advantage of removing frequencies outside the range of interest and preventing interference with the analysis such as might be introduced by "aliasing" effects. The high-pass filters had time constants ranging from 10^{4} seconds (10^{-4} radians/sec) to one second (1 radian/sec) and low-pass filters with time constants ranging from 10^{-3} seconds (1000 radians/sec) to 10 seconds (10^{-1} radians/sec). Any combination of band widths could be obtained by a switch selection. The output of the fluctuating signal was also a voltage signal. However, the output varied from -10 V to +10 V full scale which also served as a signal to the sample-and-hold device. The sample-and-hold device had biasing and gain adjustments for conditioning the signal such that the output after a necessary inversion was from 0 to -10 V. The electrometers also had calibration circuits for checking out the equipment before use.

Four electrometers were available providing the capacity for an equal number of different detectors per experiment. The electrometers were mounted in a separate NIM bin along with a single power supply designated the Reactor Controls, Inc. Voltage and Power Unit Model E-908. A view of the electrometers and the bin is shown in Figure 18 (page 71). A schematic drawing of the electrometer circuitry is presented in Appendix D.

Sample-and-Hold Device

The sample-and-hold circuit was used to convert the voltage signals from the detector electrometers to conditioned signals for an analog to digital operation by the PDP-8 computer at given time intervals. Sample-and-hold circuitry is normally used when it is necessary to convert one or more rapidly changing signals at discrete time intervals. Upon receiving

a signal from a sample command pulse at preset time intervals the sample-and-hold unit holds the analog voltage present on its input until the converter has completed its operation. The sample-and-hold is basically an operational amplifier which charges a capacitor during the track or sample mode and retains the value of the charge on the capacitor during the hold mode. The sample-and-hold unit had adjustable gain and bias levels for the input signals which removed the stringent requirement for an input signal of 0 to +10 volts. The sample-and-hold device inverted the input signal such that, after bias and gain adjustments, the output signal ranged from 0 to -10 V. The latter voltage range was required by the PDP-8 computer for the analog to digital signal conversion (referred to as an ADC).

The sample-and-hold unit used in this investigation was designed and constructed at Georgia Tech by members of the Nuclear Engineering Staff. For this experimental work the gain of the sample-and-hold amplifier was usually close to one although the available range of the gain varied from approximately one tenth to ten.

PDP-8 Computer and Peripheral Equipment

The computer used for the data handling and complete control and operation of the experiment was one of a series of small general purpose computers manufactured by the Digital Equipment Corporation.[76] This particular model, PDP-8 (Programmed Data Processor), had the standard 12-bit word length with a 4096 word core memory and buffered input-output control for peripheral devices.

The peripheral devices used in the experiment included a teletype, an interface tie-in with a sample-and-hold device, and a teletype link to

another small computer, the PDP-8/I.

The teletype used with the PDP-8 was a standard model 33 ASR (Automatic send-receive) and was used for the programatic input of information via the keyboard or paper tape reader and special output via the teleprinter. The teletype transmitted and received at a rate of 10 characters per second in an 8-bit ASCII (American Standard Code for Information Interchange).

The sample-and-hold device is in effect a standard I/O device for the PDP-8 computer and has been described previously. The sample-and-hold provides up to an input of four simultaneously sampled signal voltages for analog to digital conversion by the computer. This was done in the experiment at regular intervals by programmatic control of an interface timer.

A teletype link to the PDP-8/I computer was used for the transfer of data stored in the PDP-8 memory to the PDP-8/I where the data were in turn stored in a PDP-8/I memory buffer for subsequent transferral to magnetic tape. The process seems to be a bit cumbersome, but this was necessary since the magnetic tape unit was physically near and interfaced to the PDP-8/I computer. The PDP-8 and other data recording system components are shown in Figure 19.

The teletype communications link between the two computers is called a PT08 line and since this type of line was similar to the teletype line the logic elements were identical. This meant that the capability for transmission was 8 bits per transmission. Data were taken by the ADC operation and stored as a 12-bit word. Therefore, more than one transmission was required per data word transmitted. This, of course, was under

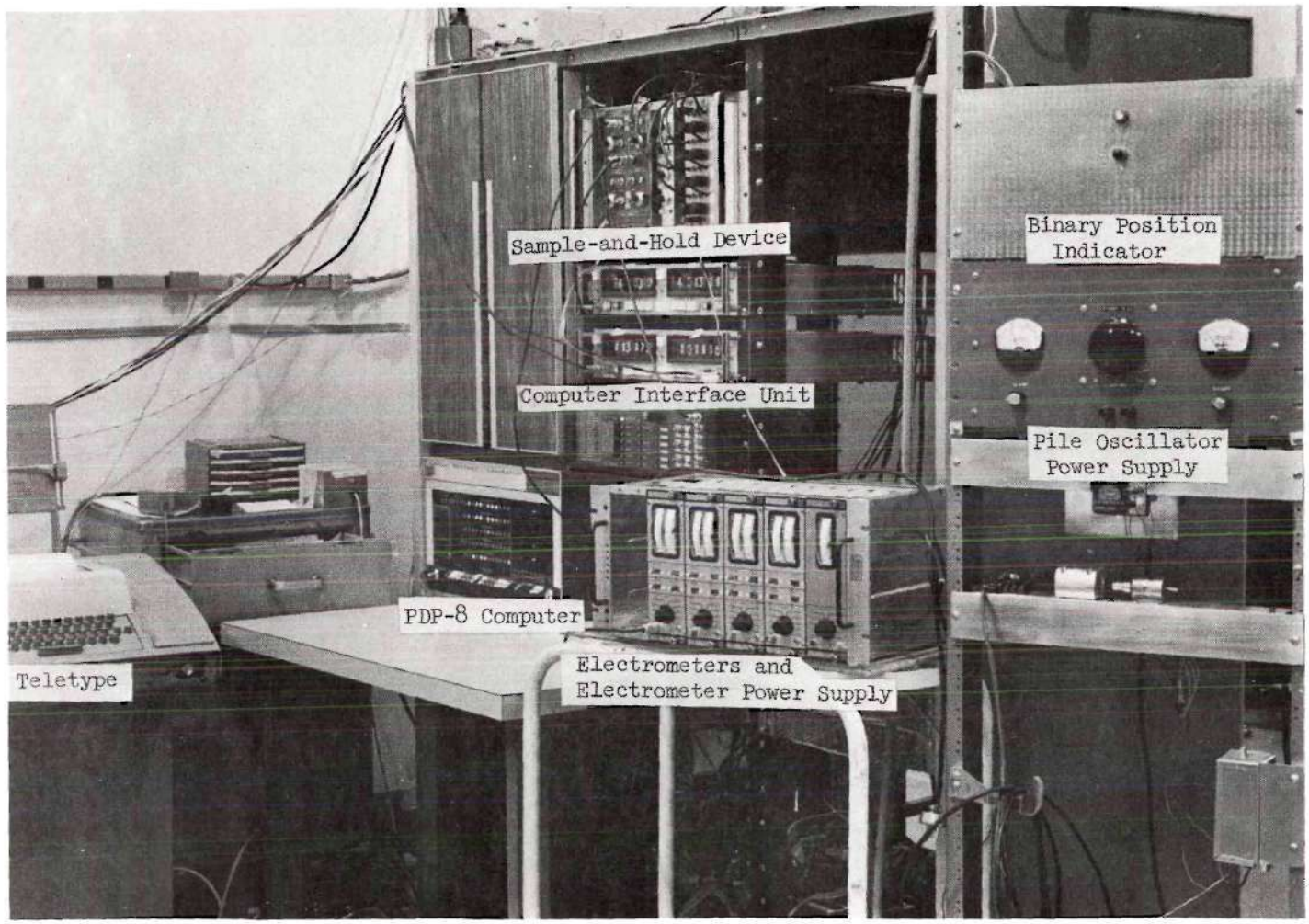

Figure 19. PDP-8 Computer with Detection and Data Recording System Equipment and Power Supplies

programmatic control and in this particular experimental program a single (12-bit) data word was broken down into two separate six-bit words and reconstructed at the PDP-8/I as a 12-bit data word from the two six-bit transmissions.

The PDP-8 computer has the capability for a number of different symbolic language programs such as PAL (program assembly language), FORTRAN, FOCAL, etc. The symbolic language used in this experiment was the PAL language. This particular language is very basic and quite similar to direct binary coding. As a result, this type of programming permits operation of the PDP-8 computer at maximum speed and efficiency. The PDP-8/I had a disc loaded PAL Assembler for translation of the PAL symbolic programs to binary coded programs.

CHAPTER V

EXPERIMENTAL PROCEDURES AND RESULTS

Theoretical Basis for the Experimental Approach

The experimental approach often taken for transfer function measurements with a pile oscillator is limited by realistic considerations and these limitations in many cases lead to a modified approach for the transfer function measurements. The most basic approach is the measurement of the system response with a known input sinusoid. When this approach is applied to a real situation the resultant response is often not a true sinusoid. The reason for the deviations from the ideal performance is that practically all physical phenomena are to some degree statistical in nature or subject to small perturbations due to unpredictable environmental changes. For example, the fission process varies statistically in a reactor.

The net effect of these inherent or externally stimulated statistical fluctuations on oscillation tests performed on reactors is that either the input reactivity amplitude may be required to be large enough so that the power oscillations have an amplitude much larger than the statistical fluctuations or the power oscillations must be Fourier-analyzed, in order to extract the fundamental frequency component and reduce the contribution from the inherent fluctuation.[38]

Increasing the amplitude is undesirable on two counts. First, the output is distorted because the system no longer behaves as a linear system. One then tends to measure the describing function rather than the

transfer function. Second, it may be unsafe or mechanically difficult to use large amplitude reactivity inputs.

Fourier analysis of the power oscillations is in a sense a cross-correlation of the output with a sinusoid. Consequently, if cross-correlation is to be used in order to reduce the errors due to statistical fluctuations, it is not necessary to excite the reactor by a pure sinusoid input reactivity. Any small amplitude periodic reactivity will accomplish the same purpose. The reason is that any periodic waveform (square wave, saw-tooth, etc.) may be considered as a sum of pure sinusoids. Each sinusoid results in its own contribution to the steady-state response of the output power. Thus by comparing respective input and response frequency components, it is possible to measure the transfer function.[38]

The presence of statistical fluctuations in the reactor system indicates the need for Fourier analysis of the power oscillations and, in turn, suggests that it may be more appropriate to excite the reactor with an input reactivity that contains a broad band of frequencies with nearly equal amplitudes and to cross-correlate this input with the corresponding output. The result of this operation is again the measurement of the dynamic characteristic of the reactor system, the transfer function. In addition, this suggests a more expedient approach for the transfer function measurements since a broad band of frequencies can be investigated in a single experimental run rather than a single frequency value per run.

One such periodic signal for introducing a band of frequency inputs is that of the pseudo-random binary sequence. For this investigation a pseudo-random binary sequence was chosen as the technique for introducing the input signal. A description of the binary sequence as a method of

frequency response testing is presented in Appendix B.

Considering that the input signal and the output signal have been either measured or are known, this section will now be concerned with deriving a method for evaluating the transfer function using a conventional correlation approach.

A few definitions will be presented first and then the necessary intermediate steps taken for arriving at the final equations. The equations and definitions as presented will be peculiar to a periodic signal since the pseudo-random binary sequence is periodic. For non-periodic signals the same general definitions apply with the limit taken as the period, T, approaches infinity.

Consider a system with an input signal $x(t)$ and an output signal, $y(t)$, for a stationary process. The autocorrelation function at time delay, τ, for a periodic signal of period, T, is defined[77] as

$$\Phi_{xx}(\tau) = E[x(t)\cdot x(t+\tau)] = \frac{1}{T}\int_{-T/2}^{+T/2} x(t)x(t+\tau)dt \qquad (65)$$

The cross-correlation function for a time delay, τ, where T is the period is defined as

$$\Phi_{xy}(\tau) = E[x(t)y(t+\tau)] = \frac{1}{T}\int_{-T/2}^{+T/2} x(t)y(t+\tau)dt. \qquad (66)$$

Definitions also of interest are the covariance functions which are special cases of the correlation functions. The autocovariance function[79] is defined as

$$C_{xx}(\tau) = E[x(t)\cdot x(t+\tau)] - \mu_x^2 = \Phi_{xx}(\tau) - \mu_x^2 \qquad (67)$$

where μ_x is the mean value of x(t).

The cross-covariance function is defined as

$$C_{xy}(\tau) = E[x(t)\cdot y(t+\tau)] - \mu_x\mu_y = \Phi_{xy}(\tau) - \mu_x\mu_y \qquad (68)$$

where μ_x and μ_y are the mean values of x(t) and y(t), respectively.

For a case where either of the terms μ_x or μ_y is zero then the correlation and covariance functions are identical. For the purposes of this discussion all values of μ_x and μ_y will be assumed zero. This is the case in our experimental situation since these averages are normally removed by either the detector electrometers or by the FFT analysis program. This essentially removes the DC component of the signal since DC represents a frequency component equal to zero.

The above definitions can be considered in the frequency regime by the application of Wiener's theorem.[78] This results in the following definitions.[79]

$$\text{spectral density:} \quad P_{xx}(\omega) = \int_{-T/2}^{+T/2} \Phi_{xx}(\tau)\, e^{-j\omega\tau} d\tau \qquad (69)$$

and

$$\text{cross-spectral density:} \quad P_{xy}(\omega) = \int_{-T/2}^{+T/2} \Phi_{xy}(\tau)\, e^{-j\omega\tau} d\tau \qquad (70)$$

Let us consider a linear system having an impulse response h(t) and an input x(t). The output of the system y(t) is given by the convolution integral[80] to be

$$y(t) = \int_{-T/2}^{+T/2} h(\lambda)x(t-\lambda)d\lambda \qquad (71)$$

The cross-spectral density is then given by

$$P_{xy}(\omega) = \int_{-T/2}^{+T/2} \Phi_{xy}(\tau)\ e^{-j\omega\tau} d\tau = \int_{-T/2}^{+T/2}\int_{-T/2}^{+T/2} x(t)y(t+\tau)\ e^{-j\omega\tau} dt d\tau/T \quad (72)$$

with the substitution for $\Phi_{xy}(\tau)$ introduced.

Substituting the value for $y(t)$ in the cross-spectral density term results in the following identity.

$$P_{xy}(\omega) = \frac{1}{T} \int_{-T/2}^{+T/2}\int_{-T/2}^{+T/2}\int_{-T/2}^{+T/2} x(t)h(\lambda)x(t+\tau-\lambda)\ e^{-j\omega\tau} d\lambda d\tau dt \quad (73)$$

By introducing the definition, $\xi = \tau-\lambda$ the cross-spectral density $P_{xy}(\omega)$ then becomes

$$P_{xy}(\omega) = \frac{1}{T} \int_{-T/2}^{+T/2}\int_{-T/2}^{+T/2}\int_{-T/2}^{+T/2} h(\lambda)x(t)x(t+\xi)\ e^{-j\omega\xi}\ e^{-j\omega\lambda} d\lambda d\xi dt \quad (74)$$

By further reduction with the use of the above equations the cross-spectral density $P_{xy}(\omega)$ reduces in the following manner.

$$P_{xy}(\omega) = \int_{\lambda=-T/2}^{+T/2} h(\lambda)\ e^{-j\omega\lambda} d\lambda \int_{\xi=-T/2}^{+T/2} \Phi_{xx}(\xi)\ e^{-j\omega\xi} d\xi \quad (75)$$

therefore $$P_{xy}(\omega) = H(\omega)\ P_{xx}(\omega) \quad (76)$$

and $$H(\omega) = \frac{P_{xy}(\omega)}{P_{xx}(\omega)} \quad (77)$$

The result is that the impulse response term in the time realm is the transfer function in the frequency regime and that the transfer func-

tion, $H(\omega)$, for a given linear system is equal to the ratio of the cross-spectral density between the input and the output signals to the spectral density for the input signal for a given frequency. Since the spectral density terms can be determined from noise analysis procedures it can be easily seen that this technique provides a straightforward method for determining the transfer function for a given system.

The derivation provided above applies to an ideal system where the transfer function, $H(\omega)$, is ideal and is not concerned with such practical problems as electronic noise, data system transfer functions, etc. Consider now a more practical approach where electronic noise and electronic transfer functions are included. The output signal then consists of the input signal operated upon by the system transfer function and the electronic channel transfer function, in addition to an electronic noise component. The correlation process between the input and output signals is then carried out in a manner just described. The terms involving the correlation of the input signal and the electronic noise are assumed to be zero since there shcuild be no correlation between the two signals.

It then is straightforward to arrive at the following equation for experimentally measuring the system transfer function for a given frequency, ω

$$H_S(\omega) = \frac{P_{XY}(\omega)}{P_{XY}(\omega)\, H_E(\omega)} \tag{78}$$

where

$H_S(\omega)$ is the system transfer function

$P_{XY}(\omega)$ is the cross-spectral density between the input signal, $X(t)$, and the output signal, $Y(t)$

$P_{XX}(\omega)$ is the auto spectral density for the input signal, X(t)

$H_E(\omega)$ is the electronic channel transfer function.

This results in a direct method for computing the transfer function from the spectral power measurements and the known characteristics of the electronic channel.

Range of Frequency Selection and Binary Sequence

The frequency range of interest for this investigation was the temperature effects region which has been shown by Schultz[63] to be generally from 10^{-3} Hz to 10^{-1} Hz. Point model studies (see Appendix E) and studies of the spatial model for the GTRR indicated that indeed the frequency range of interest was from 5×10^{-4} Hz to 2×10^{-2} Hz.

Based on the theoretical prediction it was decided to investigate the frequency range from 5×10^{-4} Hz to 10 Hz. This broad range permitted study of the region affected by feedback effects and, in addition, a large portion that would probably be unaffected by temperature feedback effects.

The pseudo-random binary sequence, hereafter referred to as the PRB sequence, was chosen, as noted earlier, as the method for frequency response testing. The use of the PRB sequence permitted the investigation of a broad range of frequencies for a given sequence depending on bit selection and the length of the period. One has the choice of investigating a few numbers of frequencies with a great deal of spectral power per frequency interval by selecting a small value of Z, the number of sequence bits, or a much larger number of frequencies with a smaller amount of spectral power per frequency interval with a large value of Z.

The subject of PRB sequence frequency spectrums is discussed in Appendix B along with a theoretical development for predicting the frequency spectrum for a given sequence.

Once the PRB sequence was determined, the spectrum shape was selected, i.e. the spectral power was distributed in a known manner. The next selection necessary is the time interval per bit which results in the PRB sequence period and the first harmonic frequency. This time interval selection was based on the frequency of interest. It was then necessary to select the sampling interval or the number of samples per bit which determines the Nyquist frequency (1/2* sampling interval). The Nyquist frequency, f_N, is the maximum frequency at which frequencies are detected in the Fourier analysis. In the event frequencies above f_N are actually present in the continuous signal, a phenomenon known as "aliasing" takes place. An intrinsic consequence of Fourier analysis of digital data is to give spectral answers for frequencies only up to f_N. Frequencies above the Nyquist frequency appear as frequencies below the Nyquist frequency in a "foldback" pattern which accounts for the term "aliasing." This phenomenon is discussed at great detail in Blackman and Tukey.[79]

Since the frequency range of interest varied over four orders of magnitude it was felt that a single sequence would be inadequate to span this expanse with sufficient spectral power per frequency interval. Theoretically, this would be possible, but, one would have the practical problem of collecting enough data points over several periods to make the investigation statistically sound. It was, therefore, decided to investigate the frequency range with two PRB sequences, each covering

slightly over two orders of magnitude.

The first low-frequency range PRB sequence chosen had the following characteristics

Z = number of bits = 511

sampling interval = 600 milliseconds

bit time = 9.6 seconds

T = period = 4906 seconds

number of data points/period = 8176

This sequence contained the large majority of the spectral power in the first 500 harmonics, although there was a finite spectral power in the harmonics as high as the $10{,}000^{th}$ and higher. With the sampling interval of 600 milliseconds the Nyquist frequency occurred at the 4088^{th} harmonic. This PRB sequence was used for the investigation of the first 400 harmonics; therefore, the error due to the foldback phenomenon was negligible for this frequency band. The spectral power of the 400^{th} harmonic is approximately six percent of the spectral power of the fundamental harmonic. The spectral power density continues to decrease with increasing frequencies. This effect can be seen from the spectrum for Z = 511 shown in Figure 20. It is interesting to note that 89.4 percent of the total spectral power for this PRB sequence is in the first 400 harmonics and that 98.7 percent of the total spectral power is in the first 4088 harmonics. This sequence permitted the thorough investigation of the frequency range from 2×10^{-3} Hz to 8×10^{-2} Hz. This range, however, proved to be inadequate for measurements of the lowest desired frequencies and was subsequently replaced by a different PRB sequence. Nevertheless, for this first experimental run, two cycles of the PRB sequence were chosen with

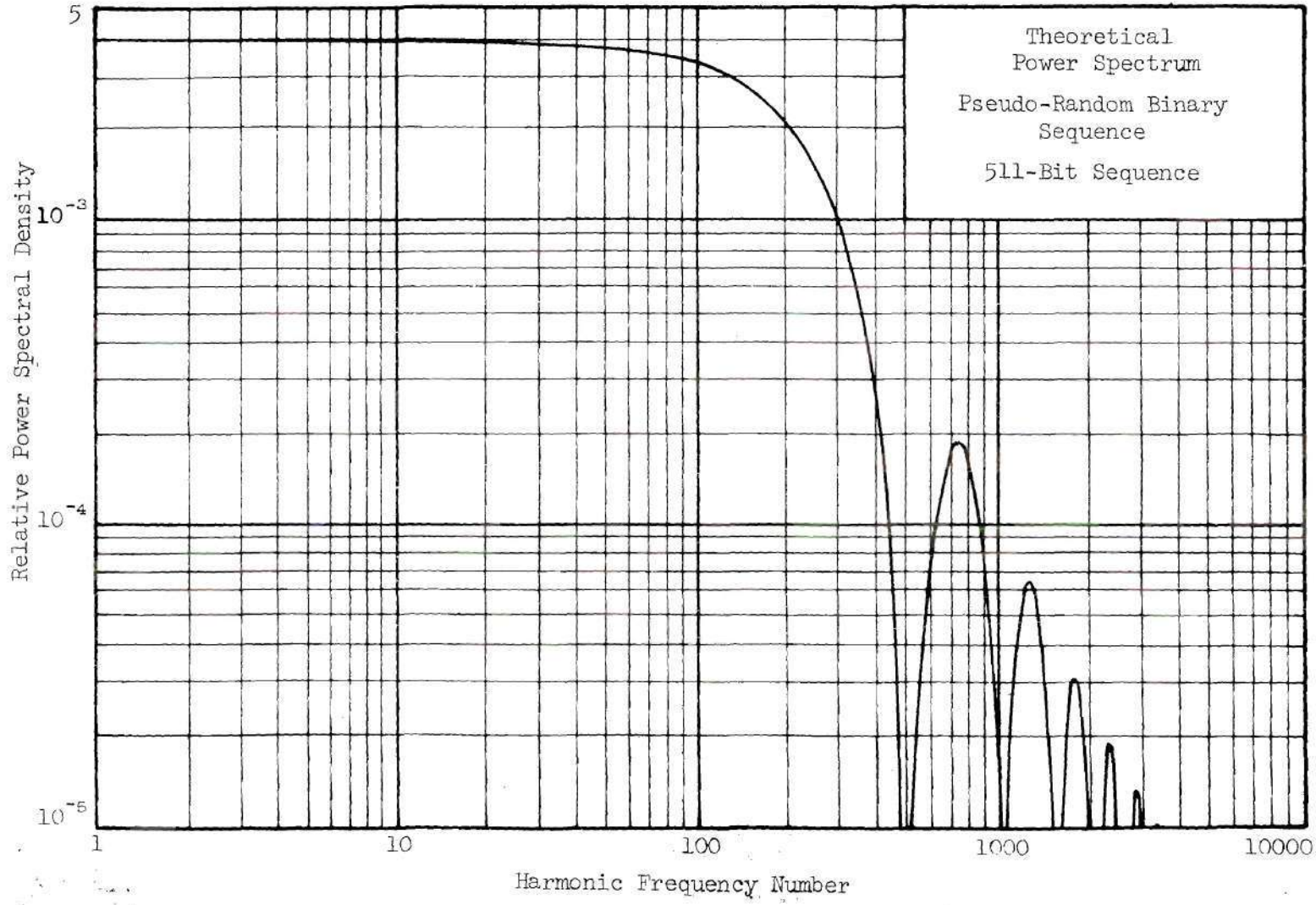

Figure 20. Power Spectrum for 511-Bit Pseudo-Random Binary Sequence

a total run time of two hours and forty-five minutes and a collection of 16,384 data points per detector.

The second low-frequency PRB sequence was chosen with a bit number of 127 in an effort to concentrate more spectral power in the lower frequencies and permit more thorough investigation in this range. A typical sequence used then had the following characteristics

Z = number of bits = 127

Δt = sampling interval = 700 milliseconds

bit time = 89.6 seconds

T = period = 11,379 seconds = 3.16 hours

number of data points/period = 16,384

This sequence essentially has the same features for the first 100 harmonics that the previously described sequence had for the first 400 harmonics, i.e. 89.4 percent of the total spectral power in the first 100 harmonics and the ratio of the spectral power in the 100^{th} harmonic to the first harmonic approximately six percent. This reduced PRB sequence permits a more thorough investigation of the lower harmonics since the harmonic frequencies are both lower in magnitude and, in addition, have an increased spectral power per harmonic. A diagram of the spectral power distribution for this PRB sequence is shown in Figure 21. The use of this PRB sequence permitted measurements for frequencies as low as 4×10^{-4} Hz which then proved to be adequate.

Measurements in the original high-frequency PRB sequence chosen proved to be adequate. The high-frequency range PRB sequence had the following characteristics

Z = number of bits = 511

Δt = sampling interval = 30 milliseconds

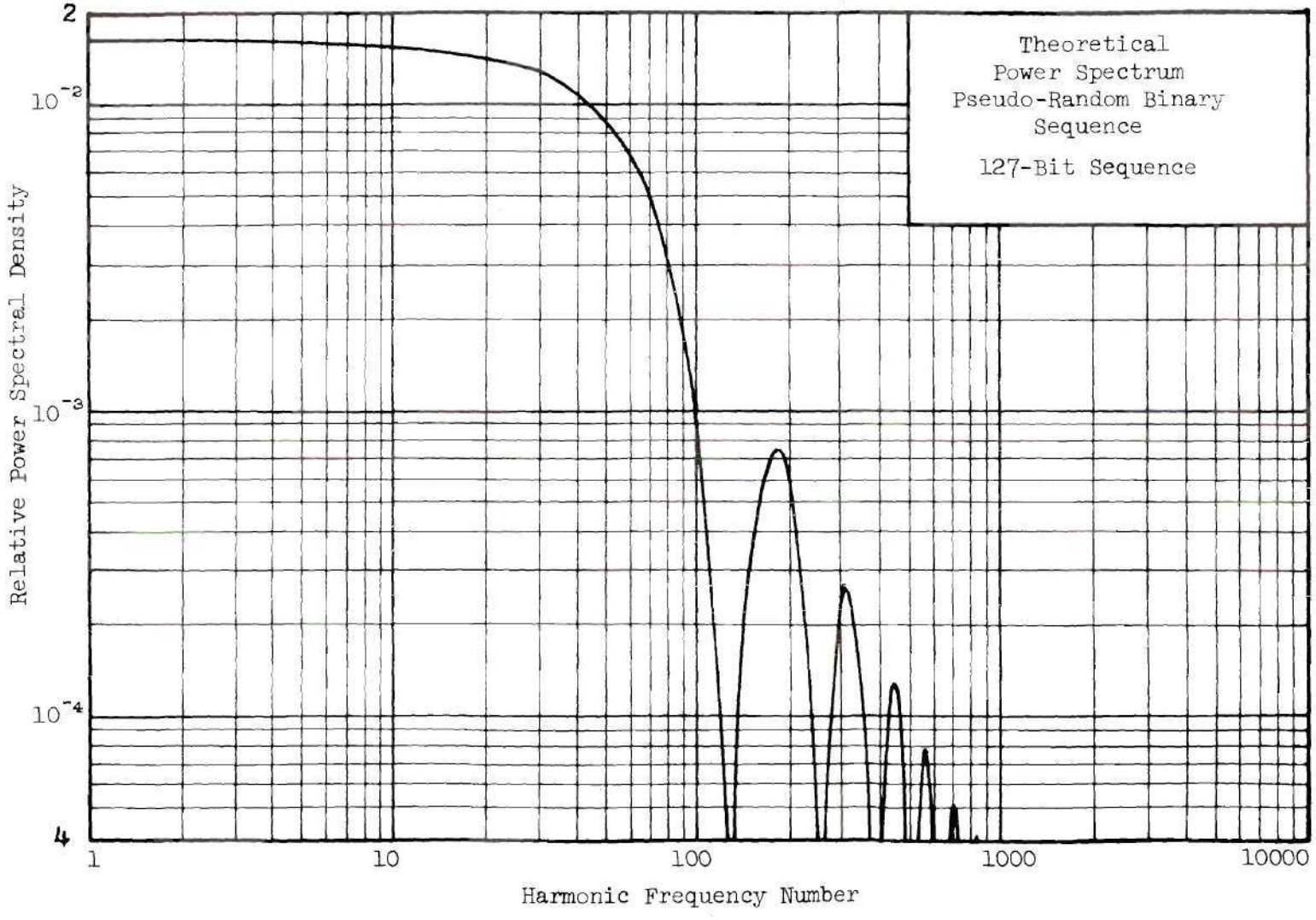

Figure 21. Power Spectrum for 127-Bit Pseudo-Random Binary Sequence

bit time = 240 milliseconds

T = period = 122.6 seconds

For this experimental run the Nyquist frequency occurred at the 2044^{th} harmonic frequency. Again the first 400 harmonics were used in the analysis. The "aliasing" problem was a bit more prominent in this sequence with the error due to the foldback phenomenon being approximately two percent at the 400^{th} harmonic and completely negligible for the 300^{th} harmonic and below. This sequence permitted the investigation of the range from 1.6×10^{-2} Hz to 5.5 Hz. The sampling time could have been reduced to remove the foldback problem but this would have required a great deal more data points in the analysis and provided no additional information in the lower end of the frequency scale. These additional data were not added, but rather more cycles of the PRB sequence taken. Likewise, the bit time could have been reduced but mechanical considerations dictated that the rotor not be driven at bit times of less than the 200 milliseconds. The oscillator could be driven at bit times of as low as 40 milliseconds; however, this results in an astonishing amount of wear and tear in the system which in turn, leads to frequent mechanical breakdowns. For this portion of the experiment four cycles of the PRB sequence were run with a total run time of approximately eight minutes and a collection of 16,384 data points per detector.

Reactor Configuration for the Experiments

For reasons of symmetry the pile oscillator was placed in the center of the GTRR in fuel element position V-10. This configuration permitted the development of a one-dimensional theoretical model for comparison with

the experimental results. As pointed out in the description of the GTRR, there are 19 fuel element positions available. The fuel loading for this experimental work was done with both 17- and 18-element cores. The 17-element core measurements required the insertion of a dummy fuel element in the lattice position in which an in-core detector was placed, in addition to the pile oscillator in the center element position. The dummy for positioning the detector was located in position V-11.

In addition to the detector placement in the fuel element location, measurements were also made with detectors in a vertical thimble located adjacent to the core position (V-23), and in the horizontal beam H-4. The positioning of the detectors in the vertical thimble required a detector holder very similar to the specially constructed dummy fuel element for holding in-core detectors. A photograph of the fuel element dummy is presented in Figure 22. Likewise, the horizontal beam measurements required a special horizontal beam plug with an offset tubular opening extending from the reactor core to the outside of the reactor shielding. A view of a detector inserted in beam H-4 is shown in Figure 23.

The core fuel loading in its state of fuel burnup and the experimental equipment arrangement proved ideal with regard to possible flux distortion from the semaphore control blades. In all experiments the control blades were very close to full out, thereby not imposing the unusual flux distortions caused by the blades when they are down in the active core region. The 17-element core loading was quite noteworthy since the elements had reached such a degree of fuel burnup that the reactor configuration would not maintain criticality with the moderator temperature above 85°F. At xenon equilibrium all four shim blades were in the full

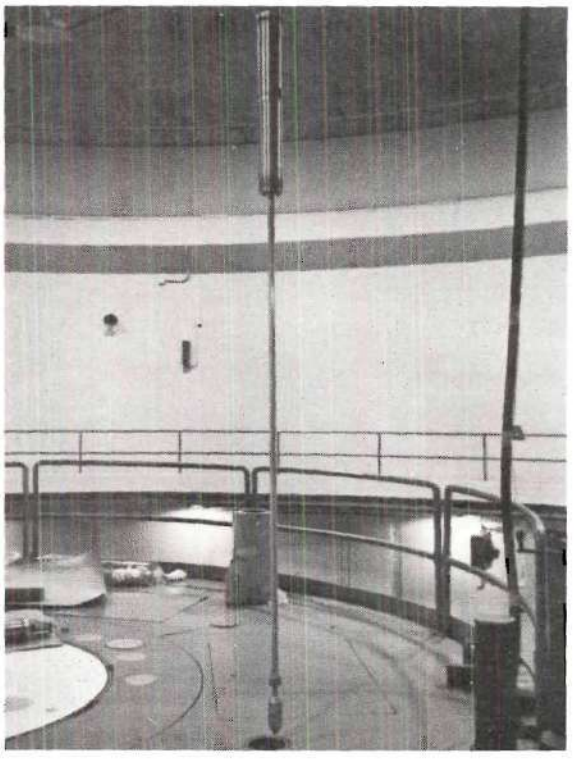

Figure 22. Dummy Fuel Element for Positioning the Detector Used in Core Position V-11

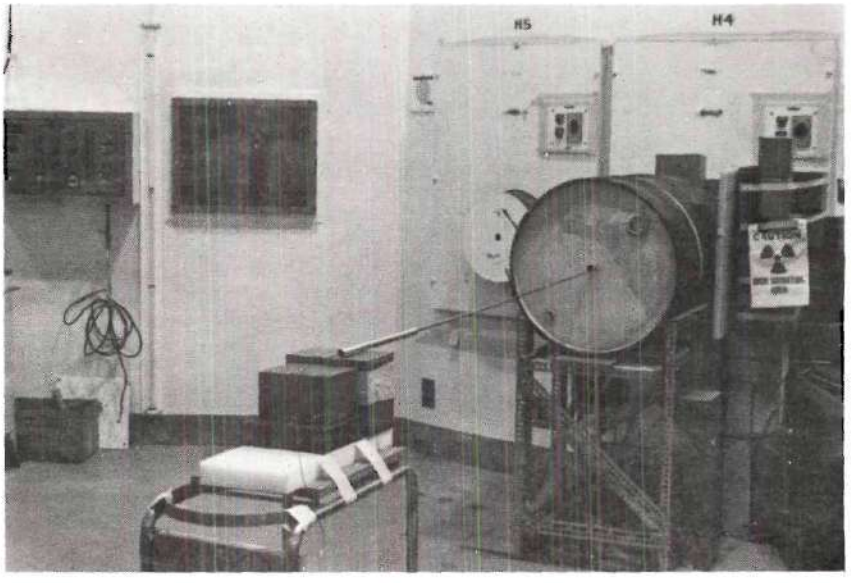

Figure 23. Detector Inserted through External Shielding to Beam H-4 for In-Core Measurements

out position (55°) with the regulating rod at nine inches and the D_2O temperature ranging from 77°F on the cold leg to 82°F on the hot leg. As a result the 17-element core configuration experiments were run at this reduced temperature.

The 18-element core loading was somewhat more flexible. Equilibrium configuration consisted of the shim blades at 30° with moderator temperature varying from 100°F to 105°F. This higher temperature was used for the 18-element core configuration experiment since temperature feedback effects are slightly more pronounced at the higher temperatures. This increased temperature coefficient is primary due to the increased coefficient of expansion of the heavy water with increasing temperature in this temperature range.

The shim blade positions for the latter experiment were also very good. A review of the shim blade calibration curves[71] indicates that the individual blade worths between 30° (experiment position) and the full out position of 55° is practically negligible (approximately 0.6 percent $\Delta k/k$). In a full out position the distortion of the reactor flux by the control blades is not significant. This provides the decided advantage of making the experimental configuration more nearly approximate the theoretical model configuration.

The pile oscillator contains two strips of cadmium in the stator and two strips in the rotor. The stator mounted strips are three-fourths inch outer diameter by three-eighths inch long and mounted three inches apart at the reactor core center. The rotor cadmium strips are five-eighths inch in diameter by one-fourth inch long and the rotor effectively shades and unshades an effective length of one-eighth inch. The entire

oscillator worth was approximately 0.54 percent $\Delta k/k$ and the movable reactivity about 0.02 percent $\Delta k/k$.

The reactivity worth of the dummy fuel element and the dummy vertical thimble for positioning the detectors was approximately 0.10 percent $\Delta k/k$, depending on the exact location. Overall, the total experimental worth was approximately 0.65 percent $\Delta k/k$. This was considerably below the upper limit of 1.5 percent $\Delta k/k$ approved by the Atomic Energy Commission for pile oscillator experiments of this type in the GTRR.

Detector locations were positioned in such a manner as to make experimental measurements from very close to the core center to radii well out into the graphite reflector at the outer limits of the reactor.

Throughout this entire experimental program a great deal of effort was expended on problems of a radiation hazards nature. The concept of an at-power experiment requires such special considerations from the outset, since this involves full-power activation of the assembly and all adjacent mechanical and electrical components, activation of detector equipment, and radiation streaming from the reactor core by the introduction of these devices to the core. In the area of neutron activation of the experimental equipment, a number of rather basic ideas were implemented in order to reduce the radiation hazard from this source. These ideas in the equipment design stage included minimizing the amount of material introduced into the active region of the reactor, locating experimental components as far as possible from the active core and shielded from both the gamma and thermal neutron radiation, and the use of materials in the equipment such as aluminum with small neutron cross sections and short half-lives. In the experimental procedure the radiation exposure from

the neutron activation was reduced by allowing a three day "cooling" period after each experiment before relocating the apparatus from the reactor. This time period permitted sufficient decay of the induced radioactivity to insure relatively low exposure levels for the removal operations. The problem of radiation streaming from the reactor core at the entry points of the oscillator and the neutron detectors to the reactor required a number of special shielding measures. These special shielding measures included the construction of special horizontal and vertical shield plugs with the entry holes offset one diameter over the length of the shield plug to remove direct radiation streaming. In addition, this shielding work included the construction of special beam catchers such as the one shown in Figure 23, and the use of special stacked temporary shielding around the openings.

This brief discussion was included to point out the magnitude of the radiation hazards considerations for an experimental program such as this.

Data Collection and Procedure

The equipment used for data collection and storage has been described in the chapter on Instrumentation and Equipment. A block diagram of the equipment used in the experimental system is shown in Figure 24 which shows the relationship between the various components. The objective of this section is to describe in some detail the techniques and procedures used during an experiment.

Since these experiments were designed to observe temperature effects, it was necessary to conduct the experiments at both zero power and full power. The full-power experiments were conducted such that the

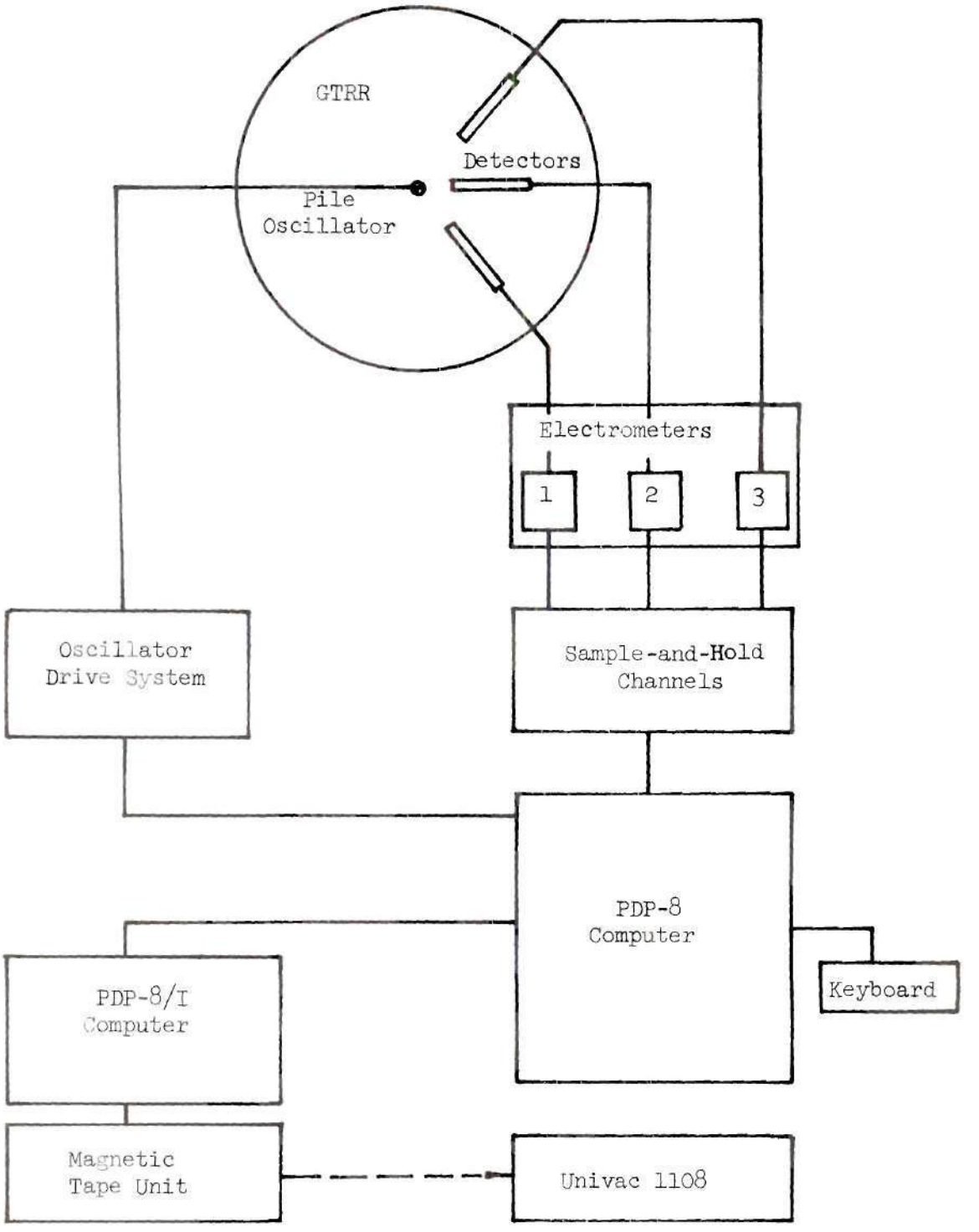

Figure 24. Schematic Diagram of Experimental Arrangement

maximum power attained was 1000 kW, which is the maximum power authorized under the GTRR license. Since the power fluctuated about some steady state level and went as high as 1000 kW at the maximum level, this resulted in the mean power level of from 900 kW to 950 kW.

In preparing for a full-power experiment it was first necessary to operate the reactor under near xenon equilibrium conditions. In order to conduct the experiment the reactor was necessarily on manual control and unless the xenon was at or very near equilibrium, the build-up of xenon to the equilibrium value tended to shut the reactor down. From a practical aspect it was necessary to operate approximately 32 to 35 consecutive hours prior to the experimental runs. This operating time established the xenon concentration at a value in excess of 95 percent of the equilibrium value. Changes in the xenon concentration then varied only slightly during the remaining experimental time in the attaining of the equilibrium value. The best experimental runs were made, however, when the reactor had operated in excess of 40 continuous hours.

At the start of an experimental run the reactor was under manual control and essentially self stabilized. The experiment was controlled and operated from the PDP-8 computer under keyboard control from the computer teletype. The first part of the computer program controlling the experiment requested input parameters such as the experiment identification number, the data sampling interval, the number of detectors to be used, the number of data points, and the characteristics that describe the PRB sequence. This input was done through the use of the teletype. This approach was taken for two primary reasons. One was that this method permitted the experimenter the most flexible use of such a program since

the input parameters could vary with each run. The second was that the use of the teletype provided documentation in the form of a typewritten sheet which identified the run by identification number and listed all the input parameters along with appropriate comments. After this input information was supplied the program was ready to start the pile oscillator.

Upon a keyboard signal the pile oscillator started operation of the PRB sequence as defined by the input information. This was continued for a variable period of time controlled by the experimenter prior to actual data collection. This initial period of operation was necessary to set up and stabilize the reactor power level about some median level and make desired switch and range settings on all the electronic apparatus (which consisted primarily of the electrometers and the sample-and-hold channels). Upon signal from the experimenter the computer then, in addition to driving the pile oscillator in the desired manner, started taking data using previously established parameters.

It is interesting to note that, for the full-power runs, the reactor system was completely driven and run by the pile oscillator. The reactor was on manual control and the pile oscillator moving in the binary sequence drove the reactor power up and down for periods in excess of three hours without intervention by the operator. This required a great deal of skill by the operators in establishing the power level during the stabilization time such that subsequent action by the oscillator did not tend to put the reactor on a short period or, on the other hand, drive the reactor power to zero. This, needless to say, required several trial and failure operations.

Once established correctly, the power tended to fluctuate between

two levels with feedback occurring at both levels to stabilize the system.

A typical run showing the manner in which the flux was driven by the oscillator is shown in Figure 25. This curve is from the reactor power chart recorder. The scale is linear and the value of 80 on the power chart represents a power of one megawatt. The example shown in the figure is an experiment with a bit time of 83.20 seconds. Notice how the feedback tends to oppose the oscillator-driven power change. In several cases the feedback not only stops the rise of power, but it tends to drive the power back down before the oscillator drives the power further down with a downward movement. The next figure (Figure 26) shows the hot and cold leg temperature response of the heavy water during a typical experiment. The temperature variation in the hot leg is rather slight but definitely present. The cold leg is more nearly constant in temperature.

The general remarks concerning feedback and self stabilization of course are obviously not applicable to the zero-power runs. The zero-power runs were generally accomplished at one kW and likewise had to be stabilized during the initial experimental phase. However, in many cases for the extremely low frequency runs the pile oscillator would be positioned in, for example, a positive position (shaded cadmium position causing a power rise) for a long period of time as is characteristic of low frequency runs. The power level would begin to rise beyond the limits of acceptability; therefore, the reactor operator would of necessity drive the power down slightly with the regulating rod. This power reduction normally required only a "flick" of the regulating rod and had to be done at fairly infrequent intervals during the low-power low-frequency runs. This intervention, however, introduced an element of feedback into the

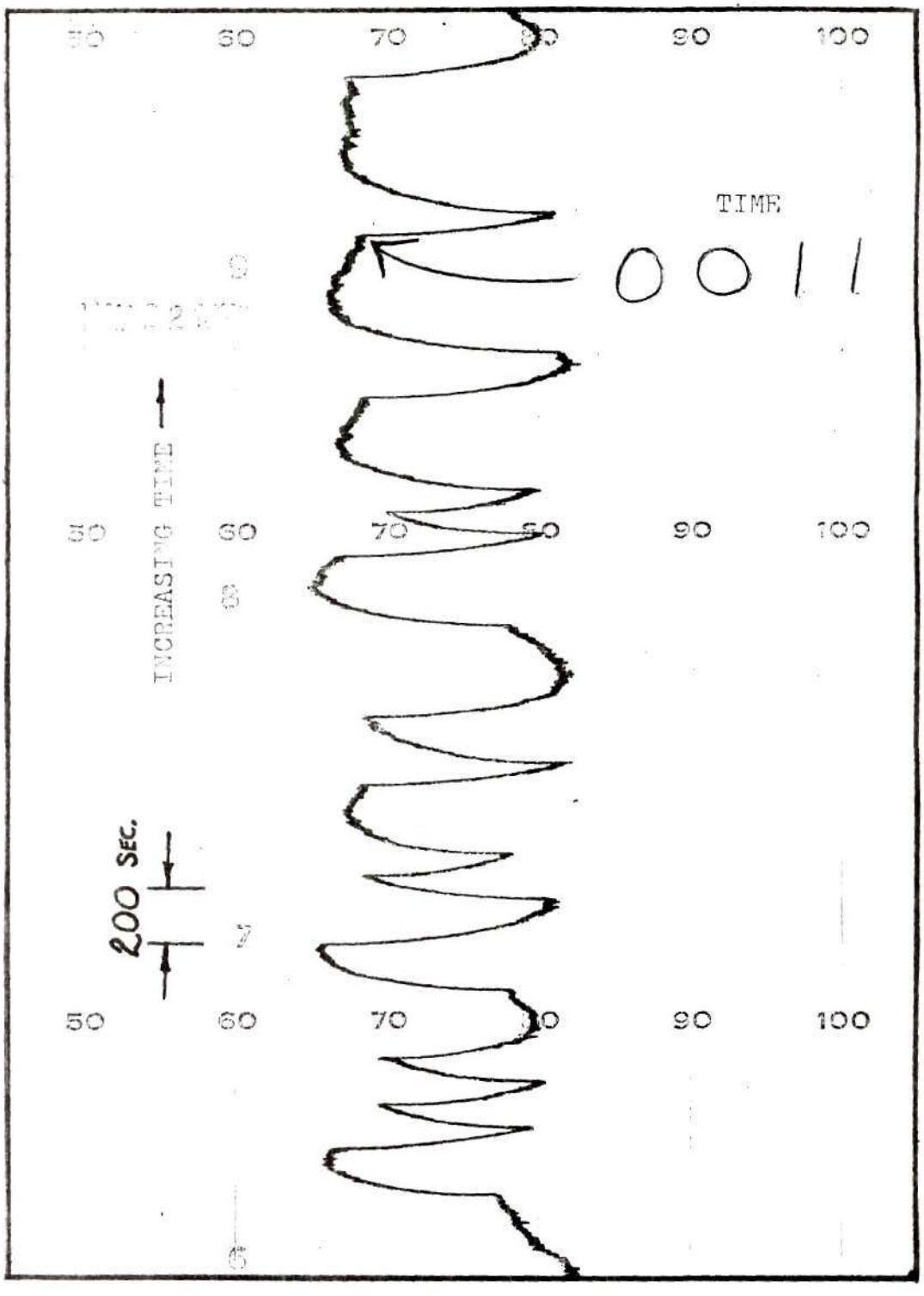

Figure 25. Power Trace of the GTRR with the Pile Oscillator Driven with a PRB Sequence

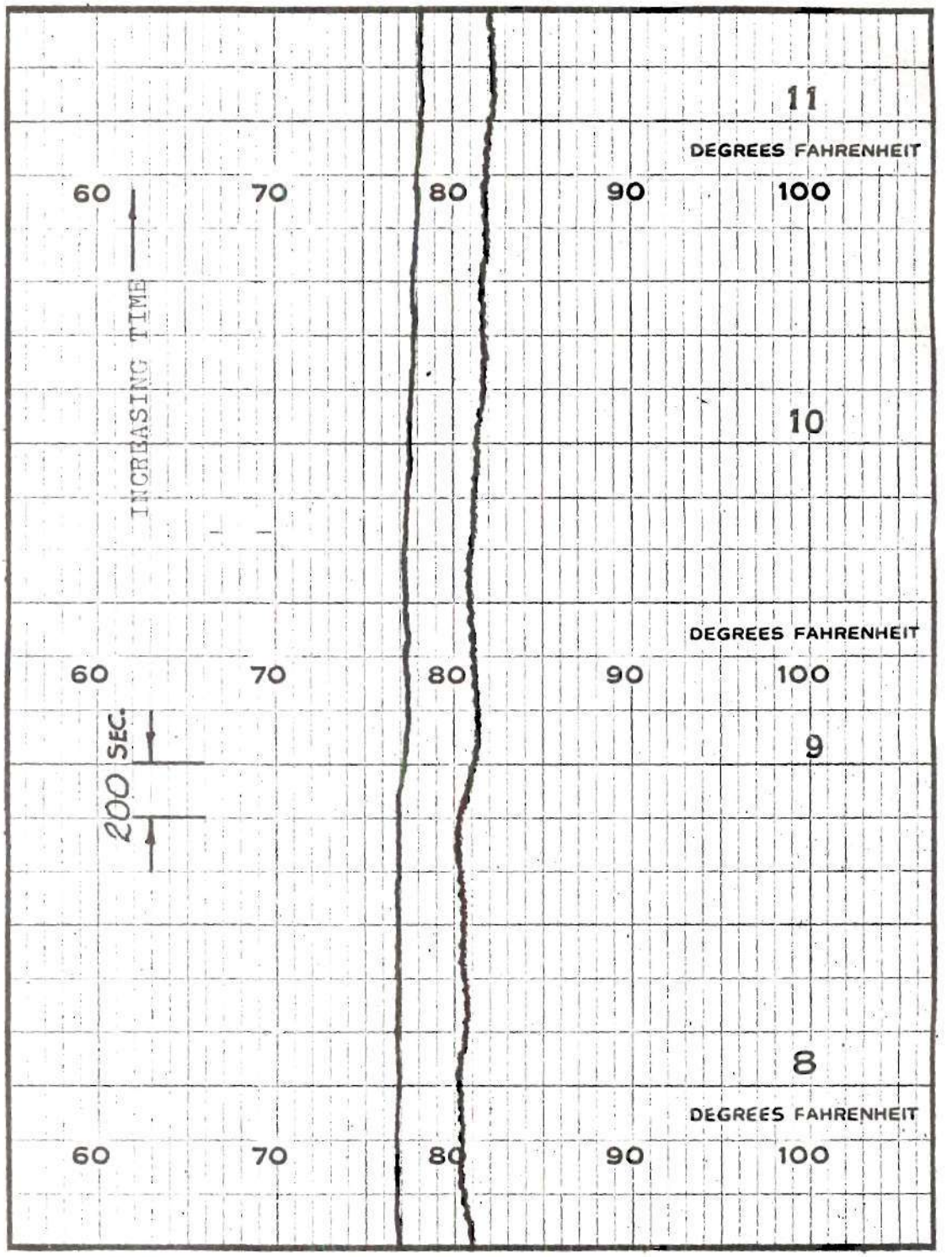

Figure 26. Hot and Cold Leg Temperatures of D_2O During Pile Oscillator Experiment Using a PRB Sequence

system. This procedure was required simply because the oscillator approach is really not very acceptable for very low-frequency low-power runs. The experimental results in the zero-power low frequency range should be judged in light of this intervention and accepted as an approximation only.

For this investigation a total of four neutron detection channels were used. Three of these incorporated procured in-core detectors. The fourth detector was obtained from a picoammeter channel and was located in the graphite which is a part of the normal reactor instrumentation.

Upon command from the PDP-8 at a given sampling interval the sample-and-hold channel sampled the four input channels simultaneously for a period of one millisecond. This analog signal, from the detector through the electrometer to the sample-and-hold channel, was inverted by the sample-and-hold unit and the output signal sampled and held. With the appropriate electrometer and sample-and-hold electronic settings this signal varied between the limits of 0 to -10 volts. On computer instruction the analog sampled value was then converted to a digital value by the computer through the medium of an analog to digital conversion operation, hereafter referred to as an ADC, for each of the four channels. Upon completing this aspect of the program the PDP-8 sent the ADC value for each of the four channels to another computer, the PDP-8/I, over a communications line known technically as a PT08 line. The PDP-8/I then stored the input data in a buffer or table within the computer core, which was of such a length as to be a single record length on the magnetic data tape. On receipt of enough data to fill a buffer the collection of data was written on magnetic tape and another table started for the receipt of additional data from the PDP-8. For these experiments the number of data

points usually consisted of either 16,384 values or 32,768 values per channel. The Fast Fourier Transform used in the digital analysis of these data had the capability of transforming 2^n number of points with n varying from 12 (4096 points) to 15 (32,768 points).

The data collection system outlined broadly above consisted of two main programs. The program in the PDP-8 computer which was located on the reactor floor near the bio-medical facility was named ACQUIRE and the program in the PDP-8/I for receiving the data and writing on magnetic tape was named HANDLE. The ACQUIRE and HANDLE programs were written in program assembly language (PAL) which is unique to the Digital Equipment Corporation's small computers. The flow diagrams for these two programs are presented in Appendix F.

One significant feature of ACQUIRE will be discussed presently. This is the matter of sending data from the PDP-8 to the PDP-8/I. The number of 12-bit data word transmissions for each sampling interval was made inflexible and this value was set at nine. This was done for reasons to be discussed later but primarily because of different word lengths between the PDP-8/I and the Univac 1108 which was used in the FFT analysis. The number of input channels was variable and could have been as large as eight. The ninth transmission was always the status bit of the PRB sequence. The PRB status bit was always either zero or one, and depending on the value of this number the cadmium of the pile oscillator rotor was either unshaded or shaded. For this experiment the status bit of zero was used for maximum or unshaded cadmium and a data transmission of 0 was made since this value of zero would result from the ADC operation on a 0 volt analog signal or the minimum level of the two levels in the PRB sequence.

The status bit of one was used for minimum or shaded cadmium and a data transmission of 7777_8 was made since this value would result from the ADC operation on a +10 volt input signal to the sample-and-hold channel (assuming a gain of one) which then represented the maximum level in the PRB sequence. When the number of input data channels was less than eight, the remaining transmissions consisted of sending zeros.

The data were handled in this way for the purpose of having actual data in the first eight words transmitted and then having the theoretical value sent ninth in the sending of nine data words. This approach facilitates subsequent data shuffling in the analysis which is discussed in the next section. In the analysis the actual data were correlated against the theoretical values of the status bit data. Having taken this approach it was then necessary to do experiments comparing theoretical performance to actual performance in the rotor movement. This consisted of another transfer function measurement with the PRB status bit as the input, the solenoid drive system as the system, and the actual performance of rotor movement as the output signal. This work was done in addition to routine frequency response measurements on the electrometers and the sample-and-hold unit. The discussion and results from this work are presented in Appendix G. This aspect was not overly important in the measurement of feedback effects since the feedback becomes significant in the 10^{-3} to 10^{-2} Hz range whereas the actual performance to theoretical movement transfer function is essentially one for frequencies up to one Hz.

Although the speed of data collection was unimportant because this happened to be a low frequency experiment, it is interesting to note that this data collection system had a capability in excess of 2000 total data

points per second.

The teletype at the PDP-8 computer was used for keyboard control in addition to the input of experimental parameters to the program ACQUIRE. This keyboard control was useful in other areas such as interrupting or aborting the experiment, controlling the magnetic tape unit both before and after an experiment in writing end-of-files or rewinding, and typing appropriate messages. In addition to documenting the experiment the teletype typed out messages indicating such items as program completion, instructions for restarting the experiment, instructions for the magnetic tape operations, and the program interrupt message if the keyboard was used to stop the experiment. This approach proved to be an invaluable aid in minimizing human operator errors during the experimental runs.

Data Reduction and Analysis

The experimental data taken and stored on magnetic tape were analyzed at the Rich Electronic Computer Center on the Univac 1108. The digital analysis was done using a Fourier Transform program[56] developed at Georgia Tech.

This Fourier Transform program was based primarily on the particularly efficient method reported by Cooley and Tukey[81] for computing the discrete Fourier transform of a series of data samples. This method is known as the Fast Fourier Transform and referred to as the FFT. The FFT program used had a capability for transforming up to 32,768 data points. In addition to the transform calculations this FFT package had a number of other interesting features. Among them was the capability of inputing two different time series of data samples. The FFT package computed auto-

and cross-power spectrums for the two data records and calculated the transfer function in a manner described earlier. In addition, this FFT package did an error analysis on the input data and was programmed to compute certain confidence levels. The statistical calculations for the transfer function determinations were based on a formalism developed by Goodman.[82] This approach implies that for a series of transfer function measurements at a given frequency there will be some average value for the transfer function Fourier coefficients and these values will be distributed about the mean value in an approximately normal distribution. Gaussian statistics then apply and this provides an interpretation of the data in a probabilistic sense. For example, the chance that an average value measurement differs from the true mean value by more than the standard deviation is 0.317 for the normal distribution.[83] In a similar manner, limits can be established about the measured value such that the true value lies within these limits with a given probability. For the FFT program this probability was established at 0.80 and the limits were referred to as the 80 percent confidence limits. The 80 percent confidence limits were calculated and printed out on all transfer function amplitude and phase angle determinations using the FFT program.

In order to use the FFT program it was necessary to write a program that would interface the PDP-8/I data tape with the FFT program on the Univac 1108. One of the main reasons for this was the incompatibility between the word length of PDP-8/I words which consist of 12 bits and the Univac words which consist of 36 bits. The first task completed by the interface program SPCTRM was to read the nine PDP-8/I data words from the data tape by the Univac, which interpreted this as three words. The next

task then consisted of breaking the three Univac words into nine Univac words by the use of the FORTRAN field (FLD) functions. This data manipulation was continued until all the data words from the PDP-8/I were converted to an equivalent number of Univac words. Upon completion of this, a number of two-dimensional arrays were created which consisted of the status bit data word and the detector input data word. The number of such arrays, of course, depended on the number of input detector channels, which for this experiment was usually four.

This set of operations then prepared the collected data in the correct format for the subsequent analyzing program which related the theoretical input (status bit data word) to the detector response for each of the input detector signals. Most data records for the experimental runs had either 16,384 or 32,768 data words.

The FFT program did the calculations and output the transfer function amplitude and phase angle information as a function of frequency. This information provided the spatial response of the reactor flux to the input perturbations for the frequency bands investigated.

Experimental Results

The purpose of this experimental program was to measure the GTRR source transfer function over a wide range of frequencies with emphasis in the low frequency range. These measurements were to observe spatial and temperature feedback effects and to be compared with theoretical values from a model developed for this purpose.

The experimental program was conducted in three phases and in all cases the measurements were made with the pile oscillator in the center

of the GTRR. The first phase consisted of measurements on the 18-element core with the moderator at a relatively high temperature (100° to 105°F), the second phase was characterized by the 17-element core with the relatively cool moderator (77° to 82°F), and the third phase consisted of the zero-power (1 kW) measurements. Discussion will then follow in that manner.

The measurements on the 18-element core were made at seven spatial locations with the radius from the center of the core to the detector varying from 40 cm to 150 cm. The experimental results for four of these spatial positions are presented in the following figures. Figure 27 displays a comparison between the experimental values for detector position V-23 (R=40 cm) and the SPARE calculations for R = 40 cm with the transfer function amplitudes normalized at 1×10^{-2} Hz. The experimental data in Figure 27 and all subsequent graphs are plotted with the 80 percent confidence limits which were discussed in the previous section on Data Reduction and Analysis. The confidence limits are not necessarily symmetrical about the data point since the amplitude and phase angle confidence limits are derived from the error analysis on the Fourier coefficients from the FFT program.

The SPARE computations are remarkably close to the experimentally determined values. The transfer function measurements indicate definitely the effect of temperature feedback with the characteristic downward break in the amplitude curve with decreasing frequency at approximately 2×10^{-3} Hz. This is contrasted to the ever increasing amplitude curve with decreasing frequency for the zero-power condition. The phase angle measurements also show the temperature feedback effect with an upward break in

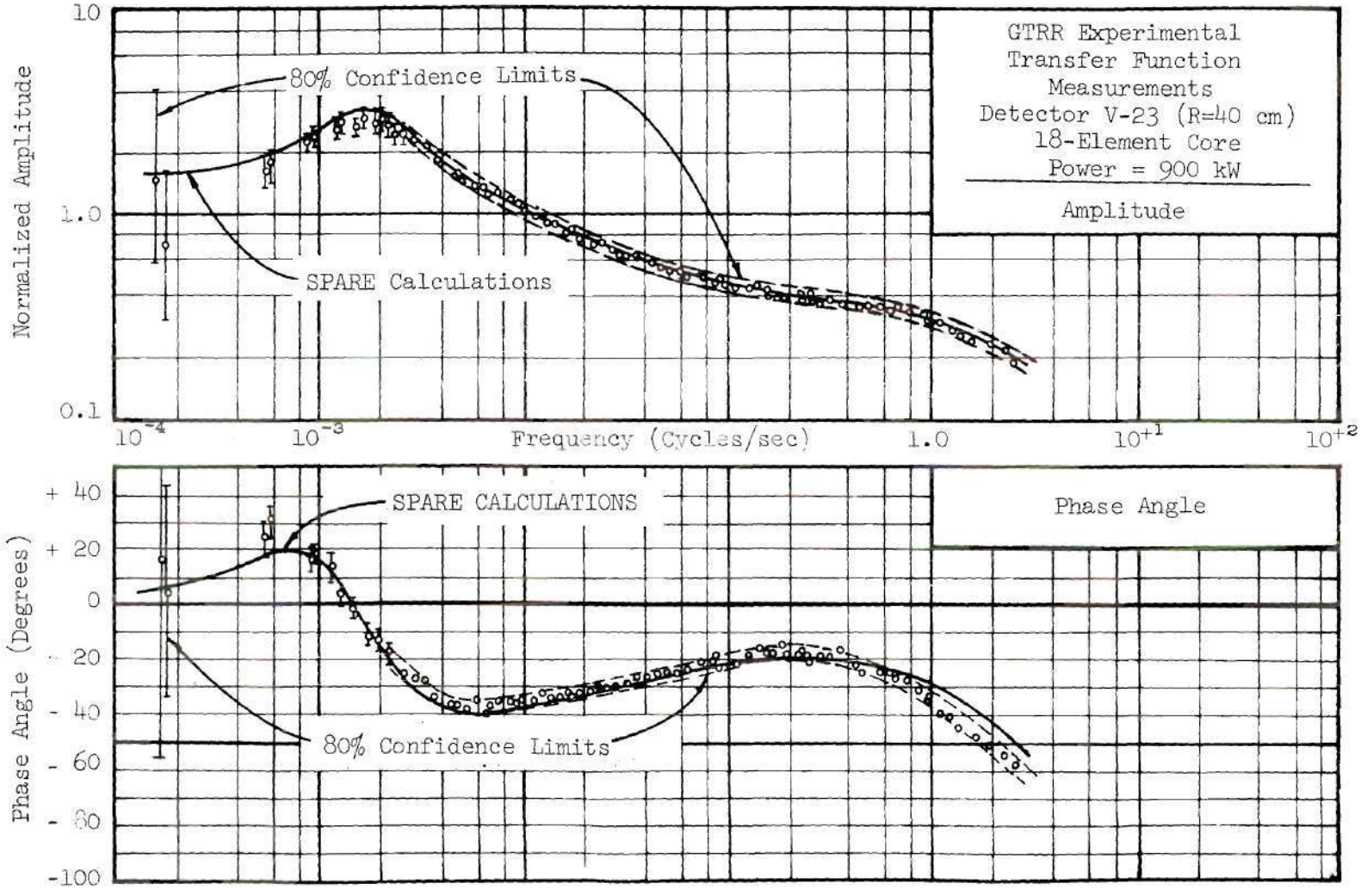

Figure 27. Transfer Function Measurements versus SPARE Computations at Detector Position V-23 with GTRR (18-Element Core) Power of 900 kW

Page missing from thesis

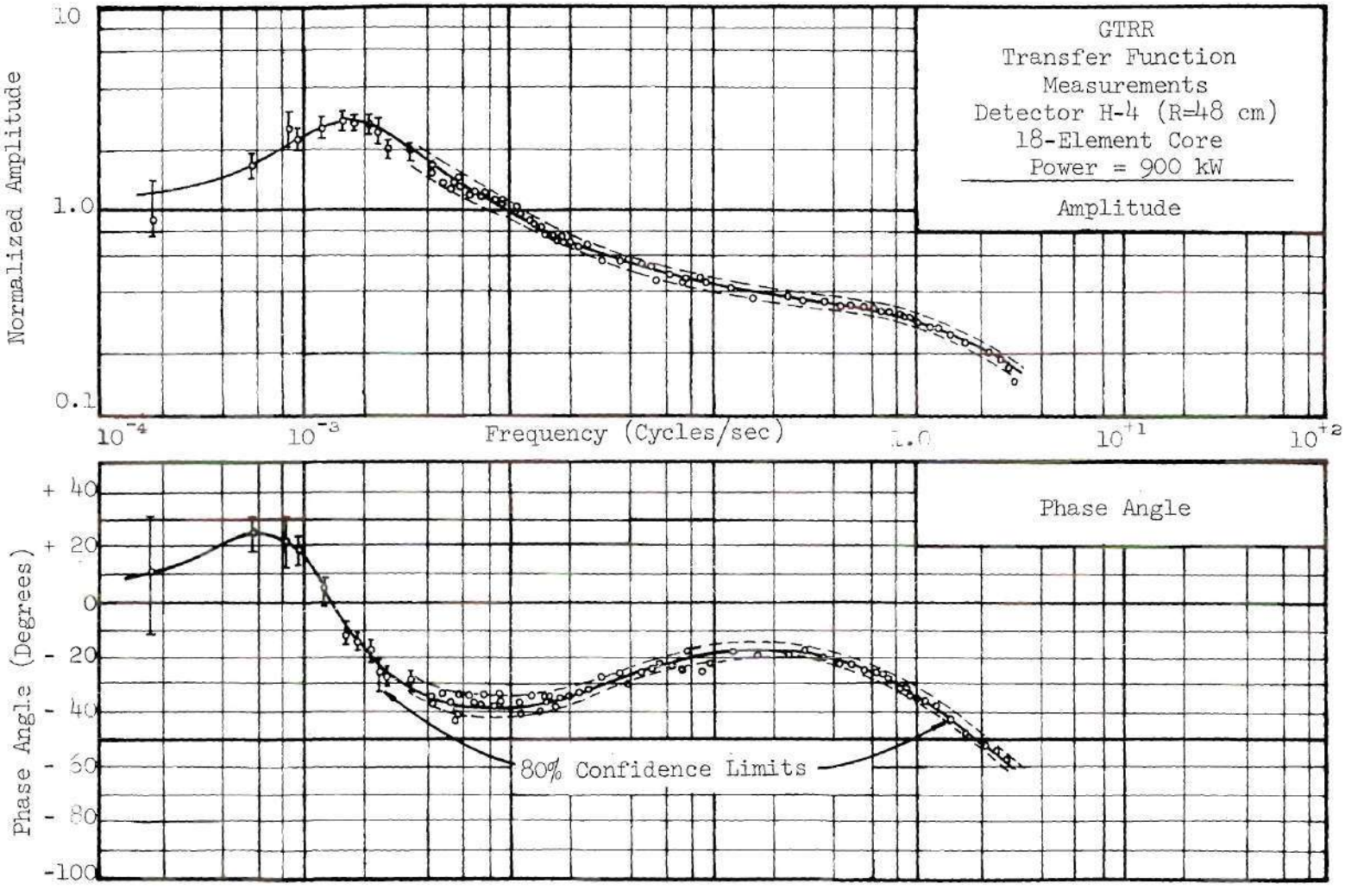

Figure 28. Transfer Function Measurements at Detector Position H-4 (R=48 cm) with GTRR (18-Element Core) Power of 900 kW

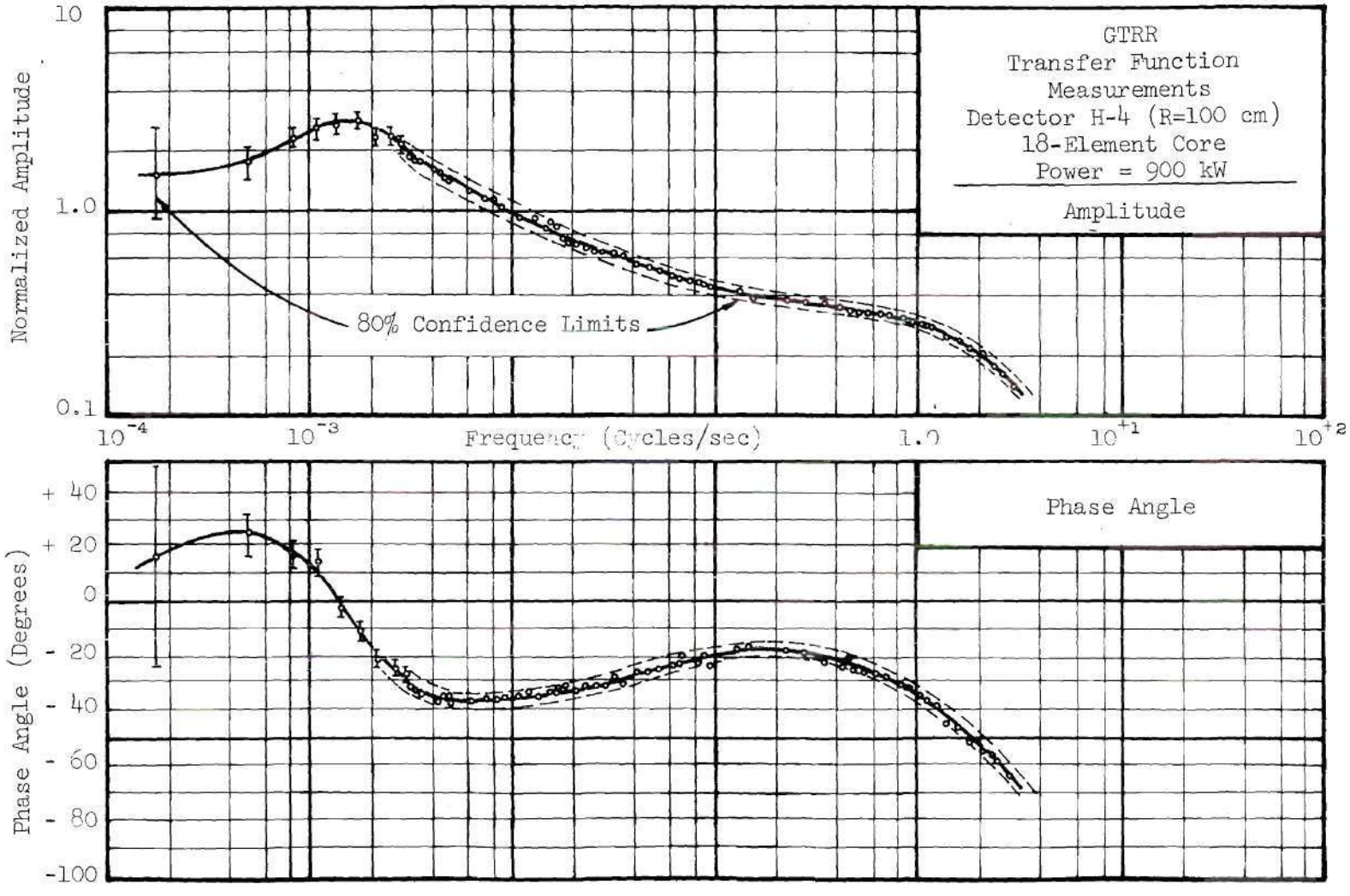

Figure 29. Transfer Function Measurements at Detector Position H-4 (R=100 cm) with GTRR (18-Element Core) Power at 900 kW

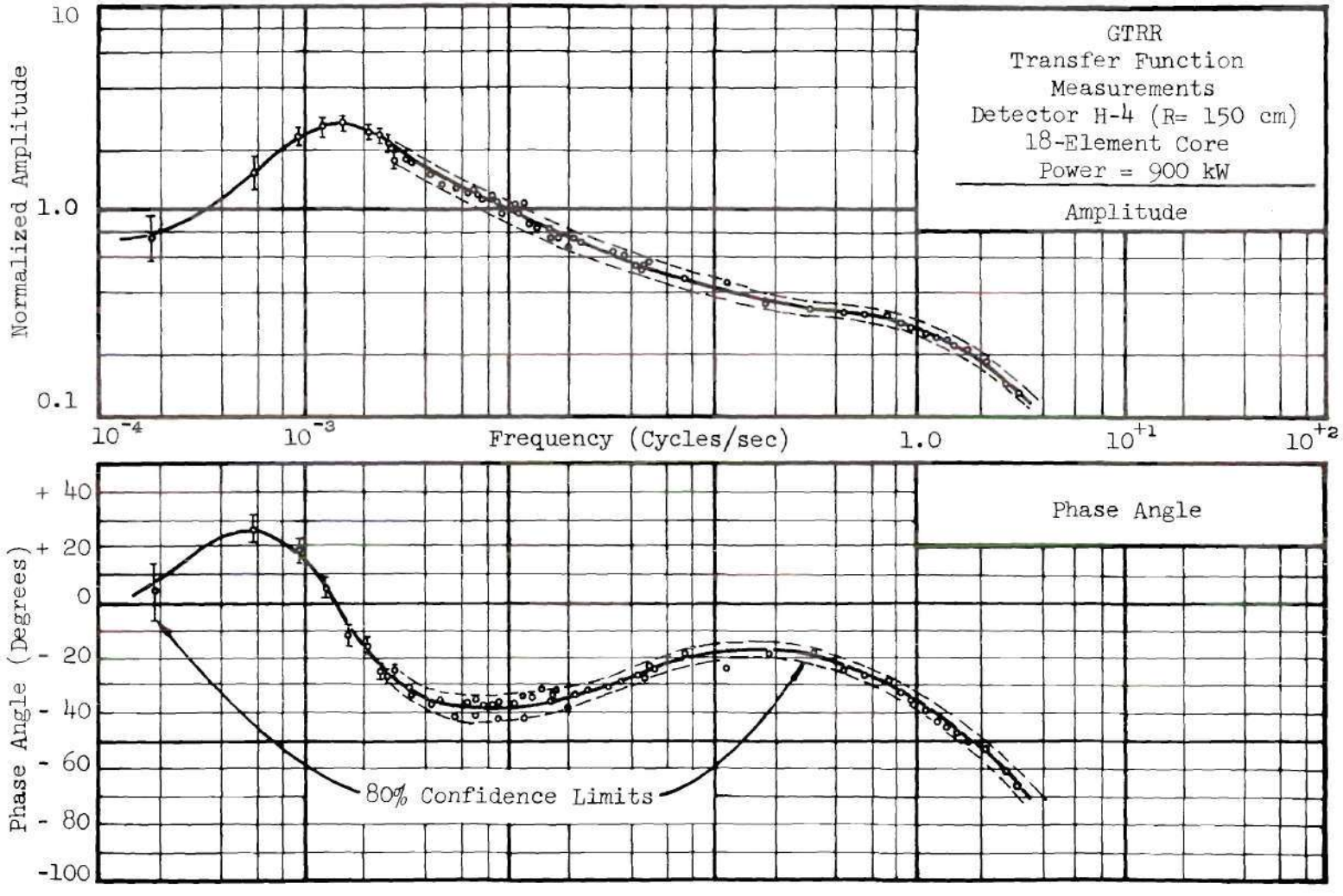

Figure 30. Transfer Function Measurements at Detector Position H-4 (R=150 cm) with GTRR (18-Element Core) Power of 900 kW

from three other locations, R = 60 cm, R = 75 cm, and the reactor pico-ammeter. From an analysis of these data it is concluded that the GTRR spatial response degenerates to that of a point model for frequencies of less than one Hz. This phenomenon is predicted by the analytical program SPARE. Calculations from SPARE indicate no spatial effects at all for the transfer function amplitude for frequencies of one Hz and smaller, and only slight phase angle differences over the limits of the reactor for these lower frequencies. The phase angle variations as calculated by SPARE range from less than one degree at 1×10^{-3} Hz and increase to approximately six degrees at one Hz. At the frequency of one Hz over four degrees of the six degree phase angle variation was calculated to occur between the oscillator and the first spatial location investigated (R=40 cm). The phase angle variations at one Hz were not considered sufficiently large to be significant. For this reason the calculations and the experiments were considered to be consistent with each other within the experimental error. Spatial effects were observed experimentally for frequencies above one Hz.

The second phase of the experimental program was conducted on the 17-element core with the 18^{th} fuel element position used to position a detector. The fuel element position vacated for the neutron detector afforded an opportunity for a true in-core measurement. Four spatial measurements were made during this aspect of the investigation at positions V-11 (R=15 cm), V-23 (R=40 cm), H-4 (R=100 cm), and H-4 (R=150 cm). The next three figures, Figures 31, 32, and 33, display the results of the 17-element core transfer function measurements for positions V-11 (R=15 cm), V-23 (R=40 cm), and H-4 (R=150 cm), respectively. Curves

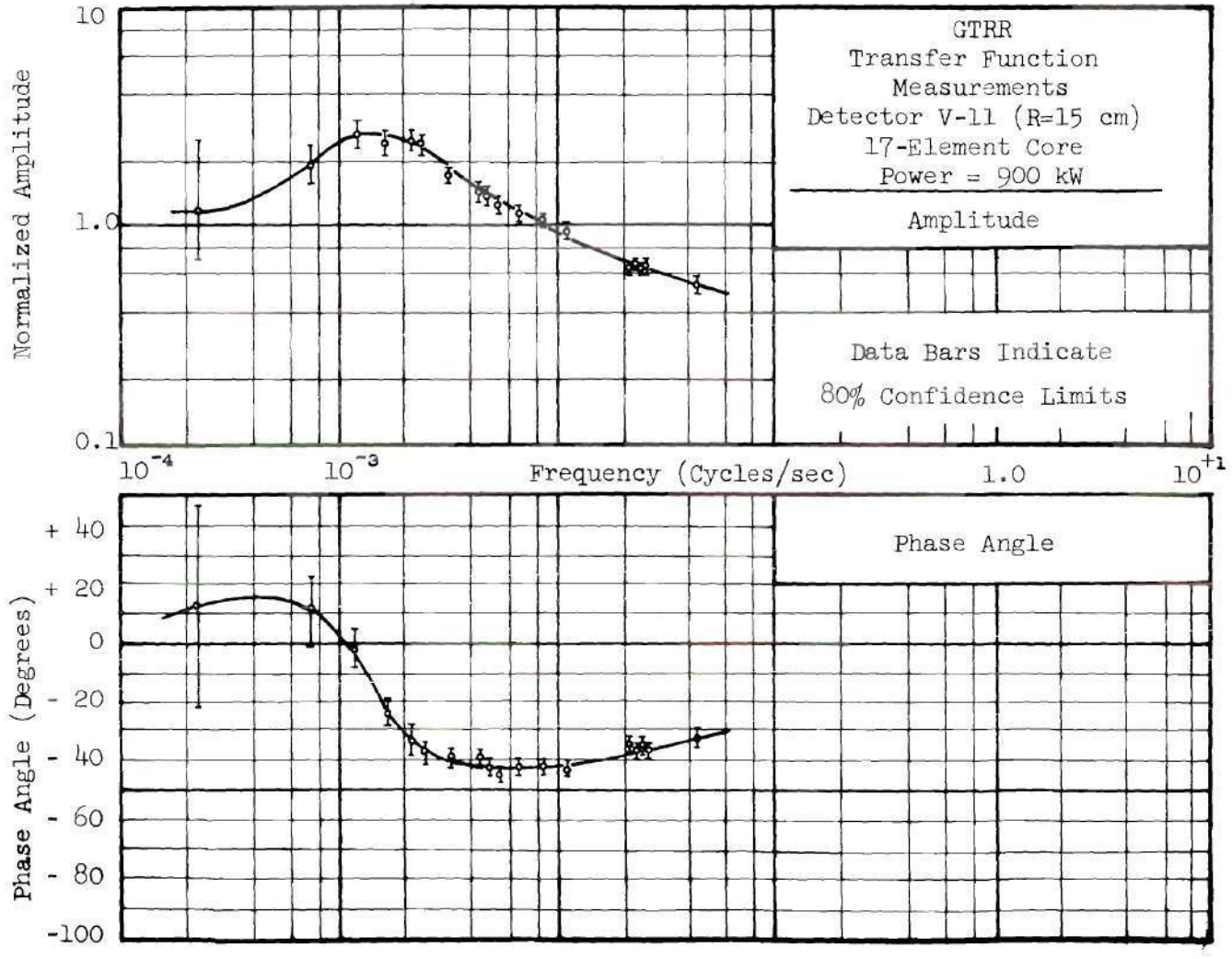

Figure 31. Transfer Function Measurements at Detector Position V-11 (R=15 cm) with GTRR (17-Element Core) Power of 900 kW

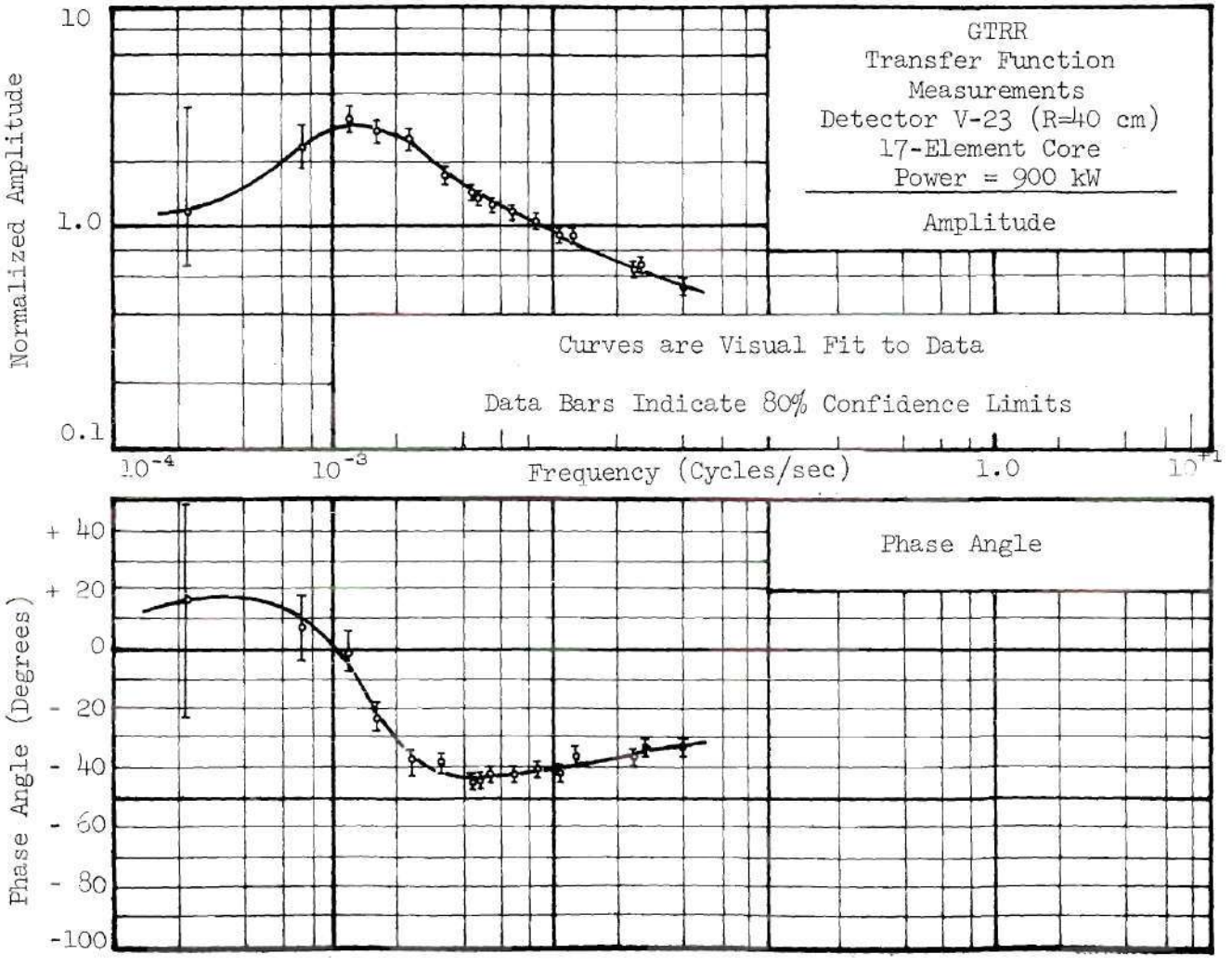

Figure 32. Transfer Function Measurements at Detector Position V-23 (R=40 cm) with GTRR (17-Element Core) Power of 900 kW

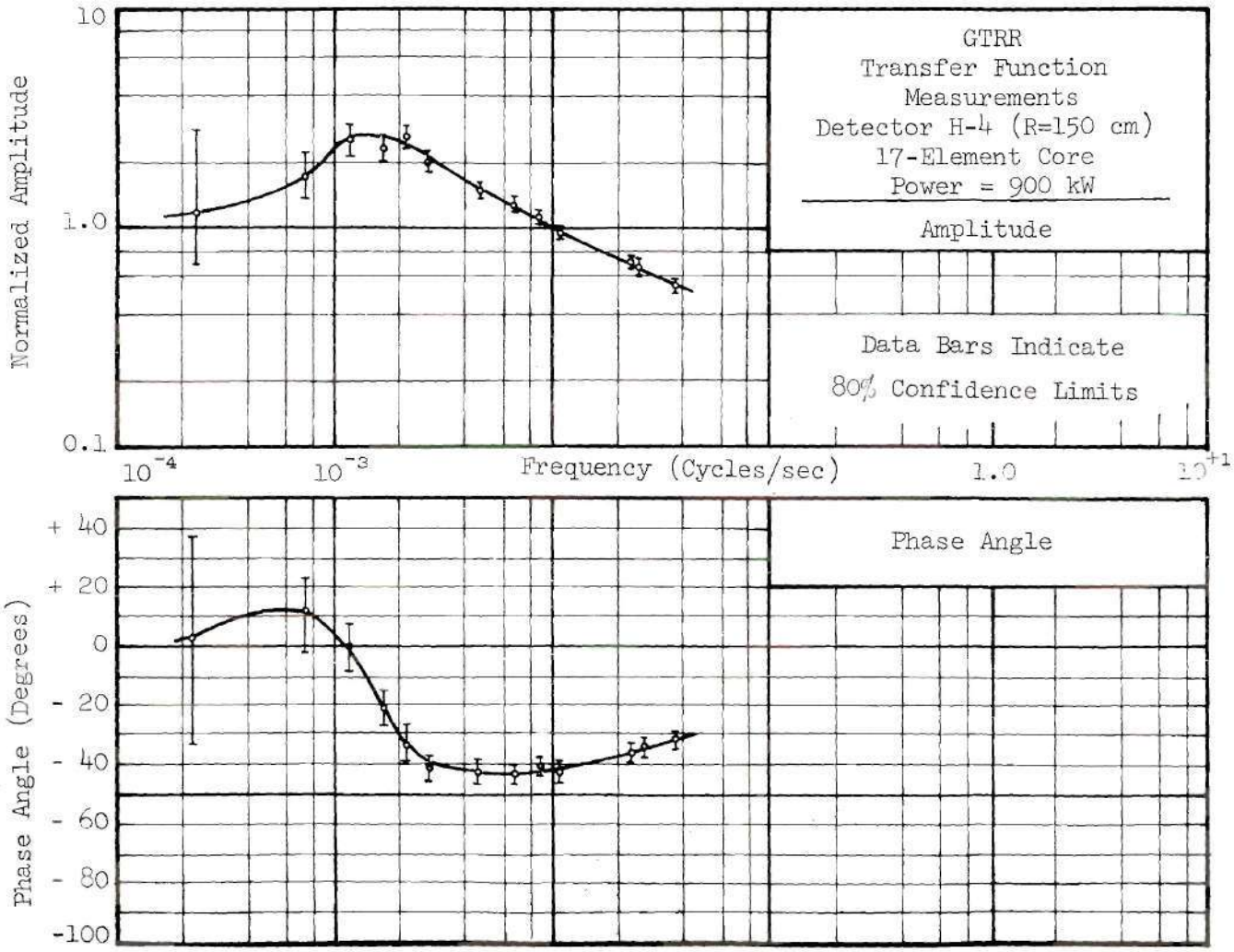

Figure 33. Transfer Function Measurements at Detector Position H-4 (R=150 cm) with GTRR (17-Element Core) Power of 900 kW

in these figures are visual fits to the data. The data from the H-4 (R=100 cm) position were not significantly different from the data at the other three spatial positions.

No significant additional information is available from the 17-element core data. This is true both for this experimental phase in general and for the measurements from the in-core detector (V-11), in particular.

The discussion of the 17-element core data is, therefore, essentially the same as for the 18-element case. One interesting feature does exist, however. It was noted earlier that the 17-element core experiments were run with the relatively cool moderator temperature 77°F to 82°F. The cooler moderator temperatures offer less feedback effect and this is borne out by comparison of the two sets of curves. The experiments with the cooler temperatures indicate both the features of amplitude curve "peaking" and the phase angle curve intersection with the zero degree axis are shifted to a lower frequency. This effect is an indicator of less feedback. The frequency at the intersection with the zero degree axis shifts from 1.5×10^{-3} Hz to 1.1×10^{-3} Hz. This is the general effect one would predict since the temperature feedback coefficient increases with increasing temperature. This effect is primarily due to increased coefficient of expansion of D_2O with increased temperature in this temperature range. The increased-temperature-coefficient effect as a function of increasing temperature has been observed experimentally in the GTRR during temperature coefficient measurements.[73]

The last phase of the experimental investigation involved the zero-power measurements. For practical reasons stemming from the sensitivity

of the neutron detectors it was necessary to conduct the zero-power measurements at one kilowatt. The results from these measurements are shown in Figures 34, 35, and 36 for detector locations V-11 (R=15 cm), V-23 (R=40 cm), and H-4 (R=150 cm), respectively. There is an obvious difference between the zero-power and the at-power experimental runs. The zero-power amplitude measurements characteristically increase with the decrease in frequency as would be expected. The phase angle measurements, however, do indicate some feedback effect with the upward break in the phase angle curve at approximately 4×10^{-3} Hz. This effect was not observed in the amplitude measurements because feedback effects are reflected in the phase angle values before the amplitude values are affected. That is to say, feedback effects can be observed at a higher frequency with the measurement of phase angle response rather than amplitude response. If the experiment had been designed to observe lower frequencies the amplitude would indicate feedback also with the characteristic downward break as the frequency further decreased. The phase angle in this case indicates a small amount of feedback that can be attributed to the external perturbation on the experiment by the reactor operators in the regulating rod movements. It was noted earlier that for zero-power experiments external control was required by regulation rod movement at irregular intervals to maintain the zero-power (one kilowatt) experiments within certain power limits. In the frequency range above 4×10^{-3} Hz where the external perturbation had no significant effect the zero-power data fit the calculated zero-power amplitude and phase angle curves by SPARE. From a comparison of the at-power data displayed in Figures 27 through 30 and the zero-power data displayed in Figures 34 through 36,

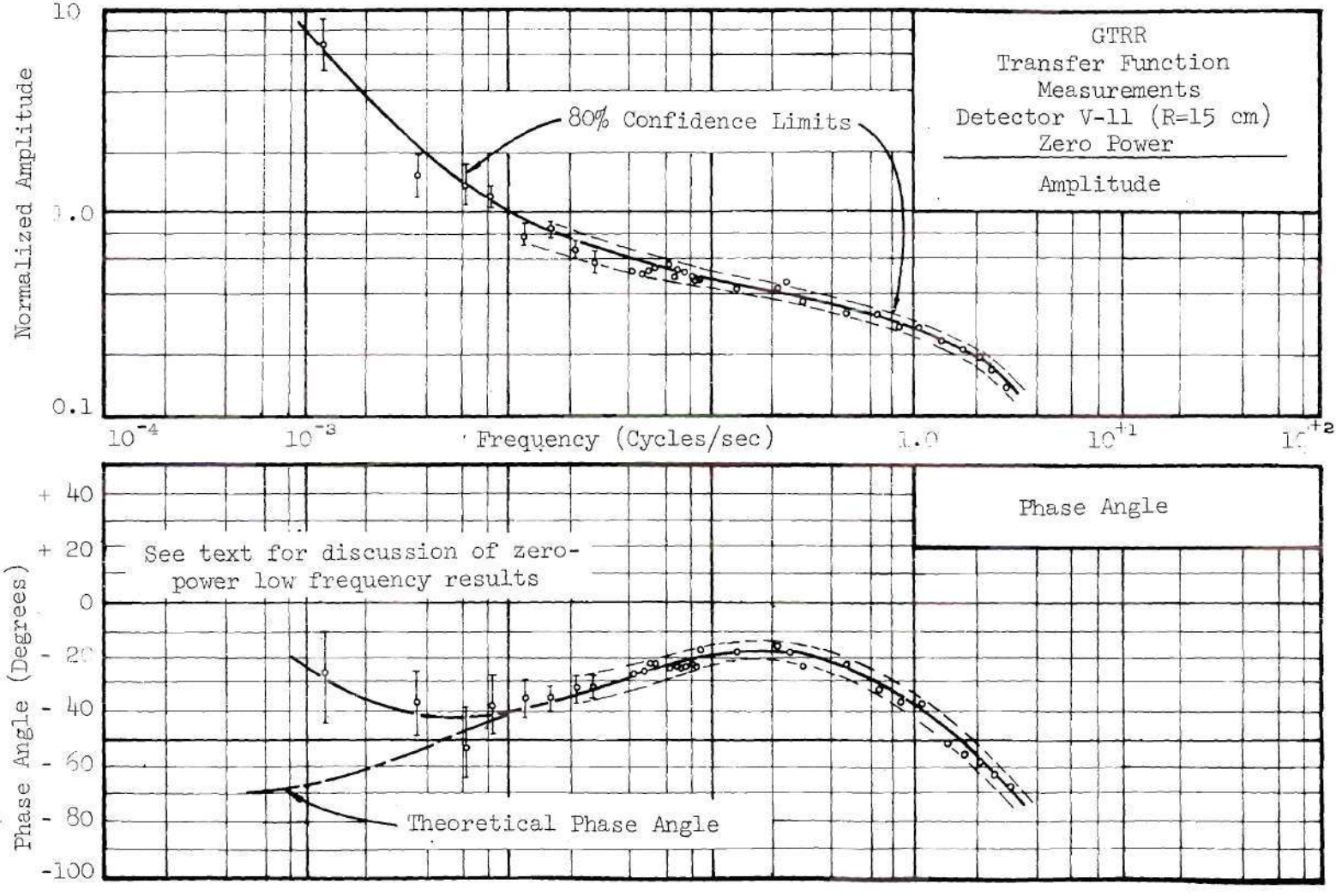

Figure 34. GTRR Zero-Power Transfer Function Measurements at Detector Position V-11 (R=15 cm)

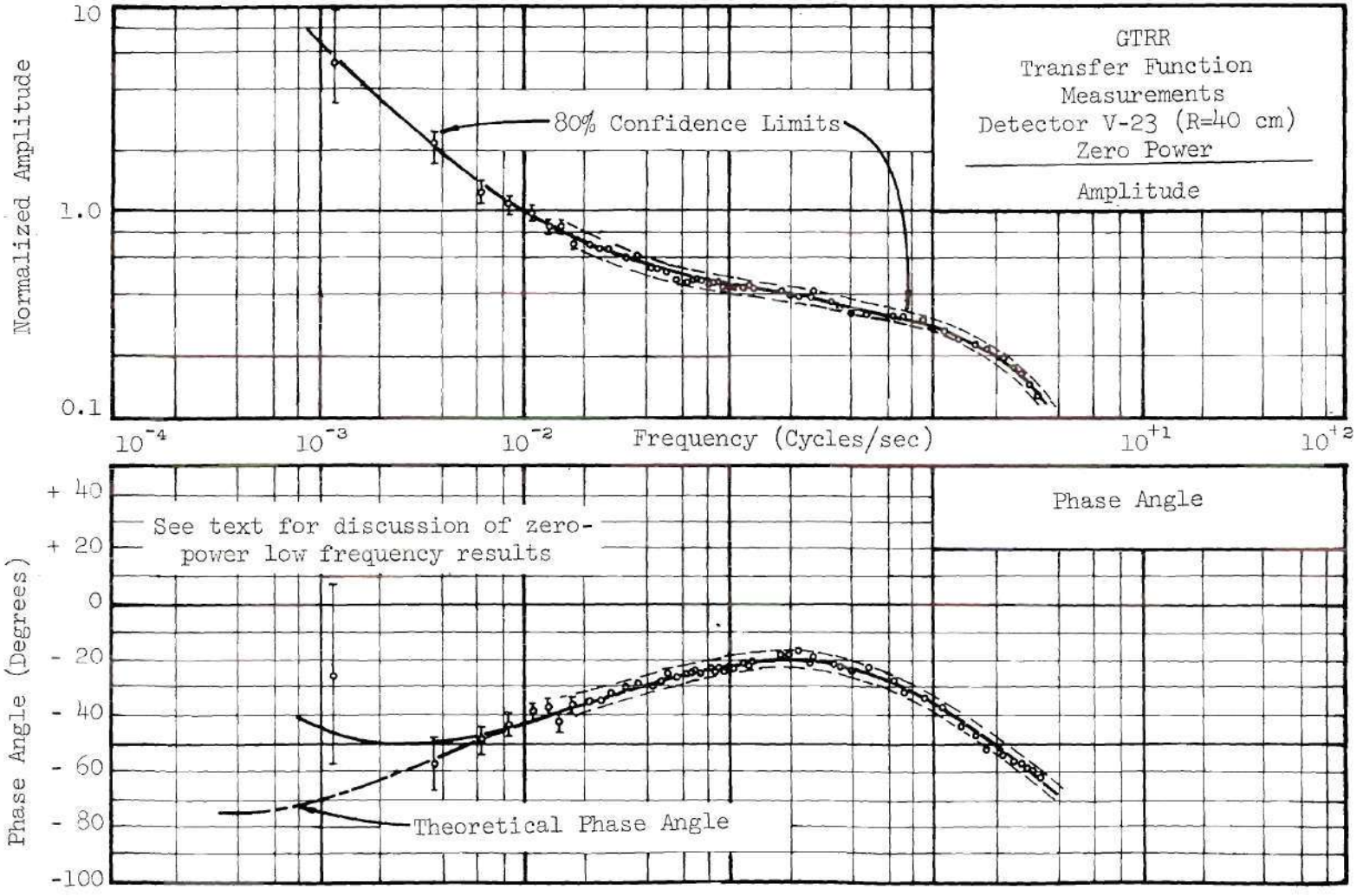

Figure 35. GTRR Zero-Power Transfer Function Measurements at Detector Position V-23 (R=40 cm)

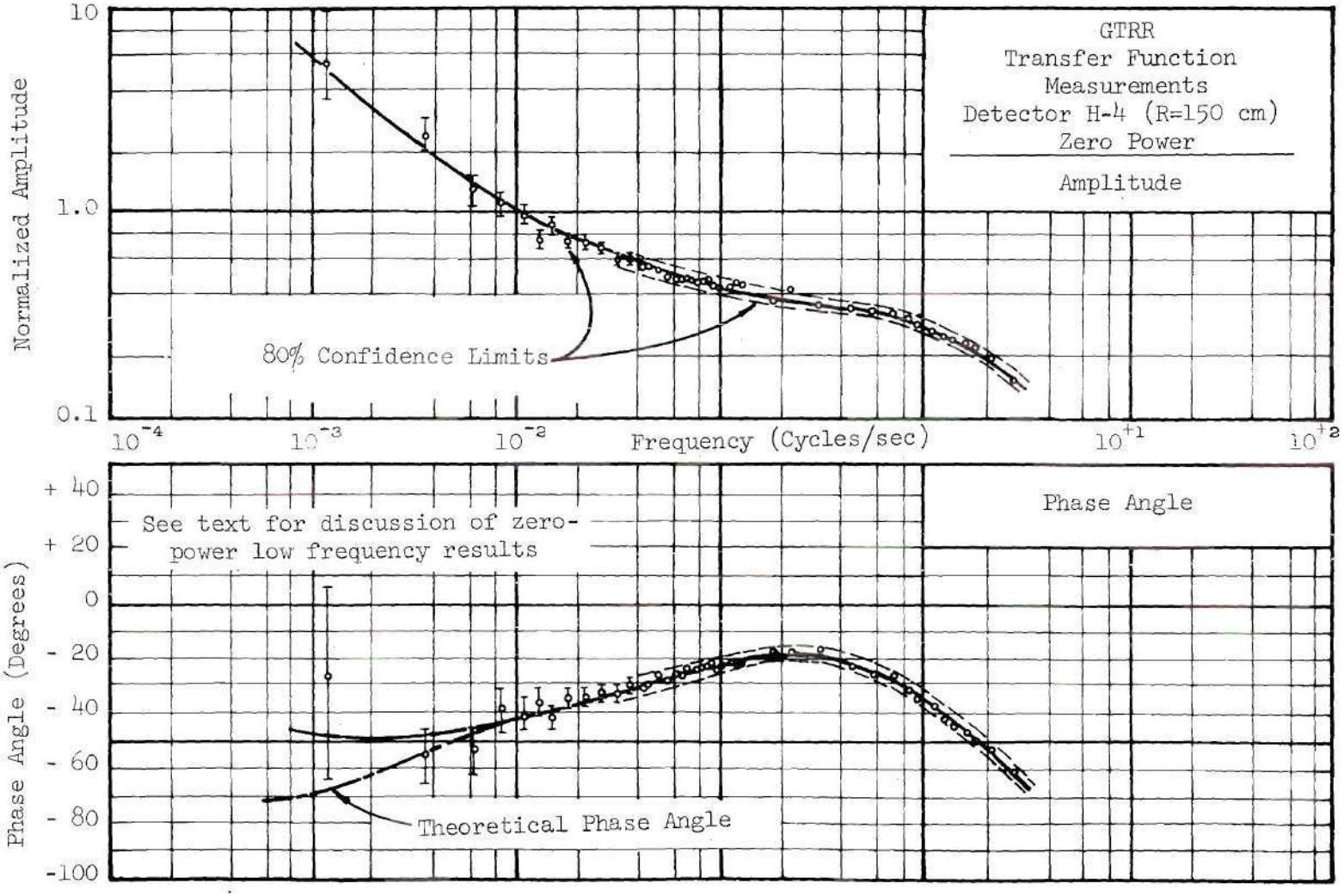

Figure 36. GTRR Zero-Power Transfer Function Measurements at Detector Position H-4 (R=150 cm)

it can be seen that temperature feedback first became significant at 2×10^{-2} Hz with the deviations between the zero-power and at-power phase angle measurements. As frequency was further reduced the temperature feedback effects became much more significant in both the transfer function amplitude and phase angle curves. At a frequency of 1×10^{-3} Hz the difference between the zero-power and at-power curves is quite pronounced. The zero-power data also indicate no spatial effects for frequencies less than one Hz.

From the experimental data it was ascertained that, for the GTRR, temperature feedback effects are significant only at frequencies of 2×10^{-2} Hz and below. At frequencies in this range and even frequencies as high as one Hz there are essentially no spatial effects present. The transfer function amplitudes in the low frequency range, of course, are the single exception since the amplitude of the transfer function is proportional to the thermal flux level at a given location. This effect was both predicted by SPARE and experimentally observed.

During this investigation experiments were run with data taken for frequencies as high as 8.5 Hz. Spatial effects were observed in this frequency region, but, as noted earlier, temperature feedback effects were not significant in this range.

The transfer function measurements for the higher frequencies are shown in Figures 37 and 38. The curves in these two figures are visual fits to the data. Figure 37 involves two spatial positions, V-23 (R=40 cm) and H-4 (R=100 cm). No spatial effects are observed in the gain which is normalized to 1.0 at one Hz; however, at four Hz and above there is a phase angle lag between the two positions which is indicative of spatial

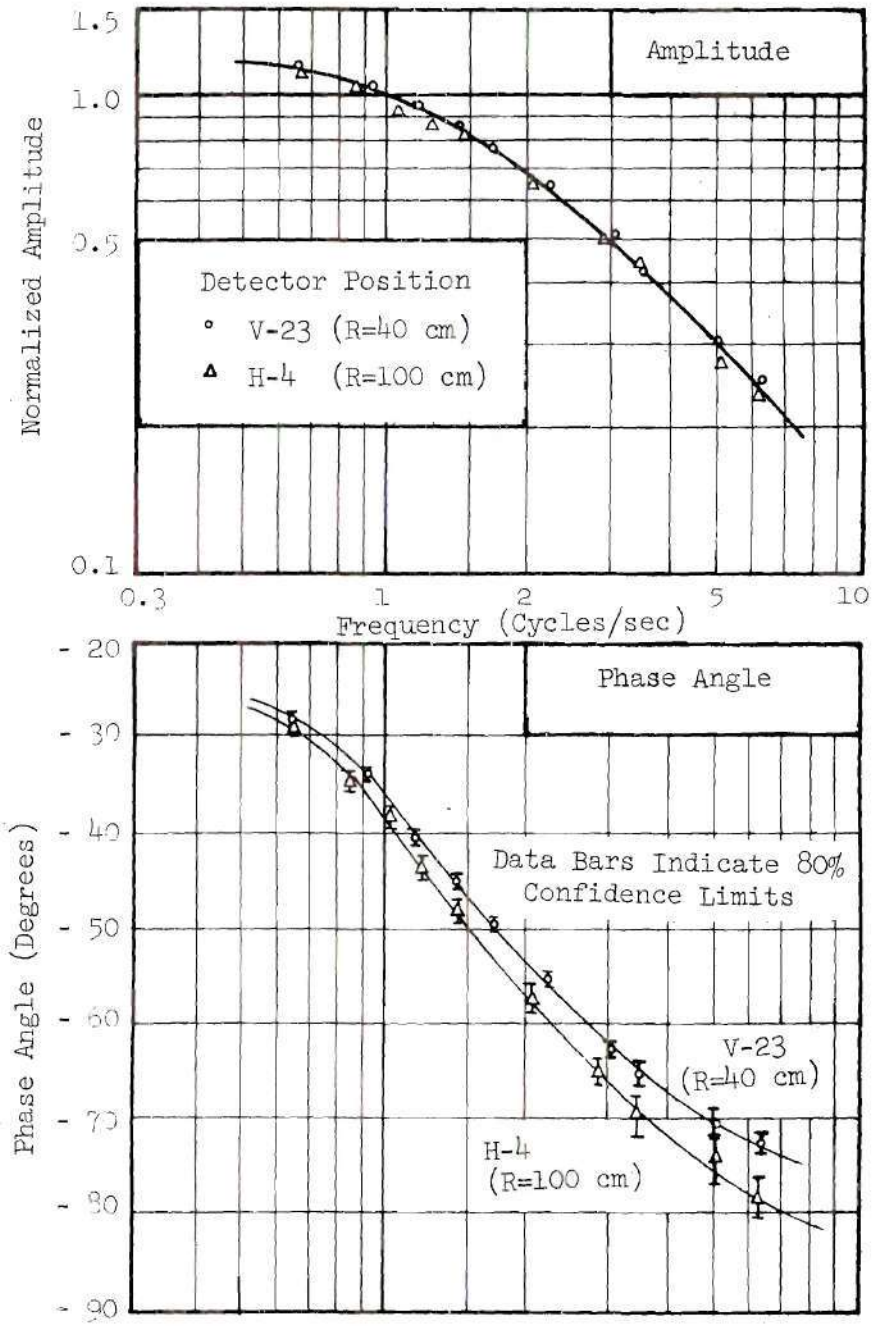

Figure 37. GTRR Transfer Function Measurements at Detector Positions V-23 (R=40 cm) and H-4 (R=100 cm)

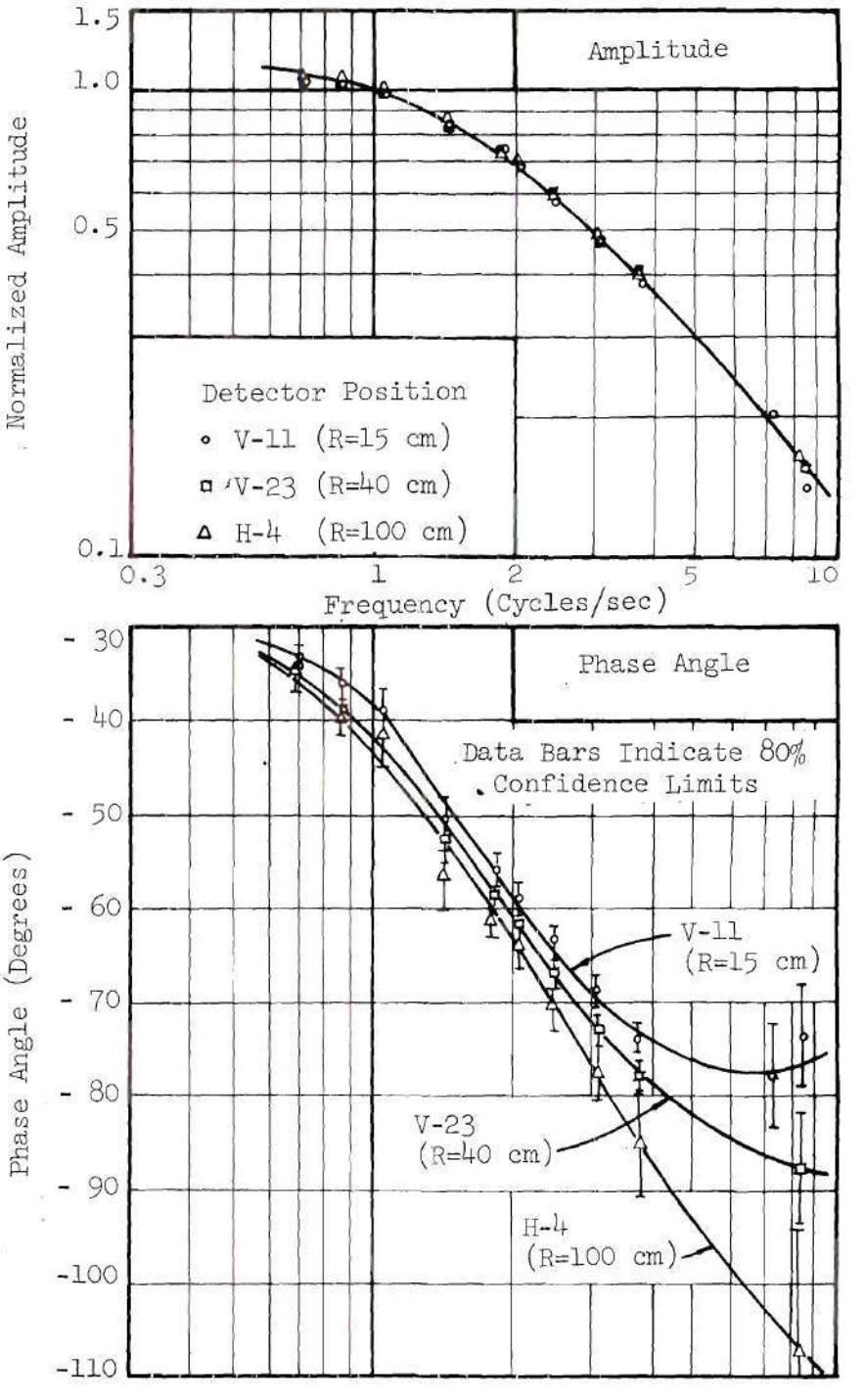

Figure 38. GTRR Transfer Function Measurements at Detector Positions V-11 (R=15 cm), V-23 (R=40 cm), and H-4 (R=100 cm)

effects due to the physical distance between the two points. The curves in Figure 37 were run in several experiments and the data confirmed more than once. The curves in Figure 38 were run in a single experiment which also was the experiment with the highest frequency component of 8.5 Hz. The confidence limits in Figure 38 are quite large, however, there is a definite spatial effect noted. As pointed out earlier, the spatial effect observed occurs only in the phase angle.

CHAPTER VI

CONCLUSIONS

The purpose of this investigation was to study theoretically and experimentally the reactor source transfer function both at zero power and full power. Particular emphasis was placed on temperature feedback and spatial effects in the calculations and measurements of the spatial source transfer function.

An existing theoretical model, known as the complex source method[34] and capable of predicting the neutron flux response to a small periodic disturbance, was extended to include temperature feedback effects. In addition, the general equations derived were applied to a one-dimensional model of the GTRR and a computer program, SPARE, was developed for computing the source transfer function as a function of power level. In support of this analytical code a one-dimensional two-energy group diffusion code was developed for the GTRR and served as a source of power level input for SPARE. The validity of SPARE transfer function calculations was checked over the frequency range from 1×10^{-4} Hz to 1×10^{2} Hz for both zero-power and high-power (1 MW) conditions. These computational checks included comparisons with independent prior calculations[33] using a different approach and with experimental results[26] from the NORA reactor. Further, at very low frequencies (e.g. 1×10^{-3} Hz) where the SPARE calculations indicated practically no spatial response, results from SPARE calculations were compared with point model calculations for zero

and high-power levels for the GTRR. The results from all of these computational checks were very good and served to establish the validity of the SPARE calculations.

An experimental program was undertaken to measure the source transfer function in the GTRR using an in-core pile oscillator. The pile oscillator, employing a pseudo-random binary sequence to introduce the desired frequency components, was used to measure the source transfer function over a frequency range of four orders of magnitude from 4×10^{-4} Hz to 8.5 Hz. Experimental data were taken for several spatial detector positions for zero-power and at-power (900 kW) conditions.

The results from the GTRR at-power and zero-power experiments verified the calculations by SPARE as to the extent of temperature feedback between the two power conditions. At-power measurements to frequencies as low as 4×10^{-4} Hz indicated significant temperature feedback effects. Zero-power measurements were made for frequencies as low as 1×10^{-3} Hz; however, reliable results were obtained in the zero-power condition only for frequencies of 4×10^{-3} Hz and higher. This result was related to the practical restrictions of conducting low-frequency, low-power pile oscillator experiments. Comparisons between the zero-power and at-power data indicated that temperature effects first became significant in the low frequency range at a frequency of 2×10^{-2} Hz. As the frequency further decreased the temperature feedback effects became increasingly more pronounced.

The GTRR experiments also reflected a change in the temperature feedback coefficient when measurements were made with the reactor at two different temperatures. A reduced temperature effect shifted the amplitude

and phase angle curves in a definite manner indicating less temperature feedback.

The results from the GTRR experiments were also very close to the predicted values by SPARE with regard to spatial effects. The SPARE calculations and the experiments indicated no spatial effects in the shape of the transfer function amplitude curve for frequencies below one Hz for both at-power and zero-power conditions. The experiments also indicated a spatially independent phase angle response for frequencies below one Hz for both at-power and zero-power conditions. The SPARE calculations indicated slight phase angle variations over the spatial limits of the reactor but these phase angle variations were not significant for frequencies less than one Hz. Experimental results indicating no phase angle variation for the detector positions measured were consistent within experimental error. In this sense the experiments verified the phase angle calculations.

Experiments in the frequency range from one Hz to 8.5 Hz indicated spatial variations in the phase angle measurements but with no significant variation in the amplitude measurements. No further work was done at higher frequencies since this frequency region was outside the range of interest for temperature feedback effects. In addition, spatial effects had been observed in the GTRR for this frequency range by Johnson.[33]

From this investigation the following summarizing conclusions can be drawn. A theoretical model was developed and programmed as the program SPARE to predict the power-dependent spatial source transfer function. The results from the analytical program SPARE were compared to both experimental results and other digital calculations and found to yield

correct results over a frequency range of six orders of magnitude for both zero-power and at-power conditions. Experiments were conducted on the GTRR over a frequency range of four orders of magnitude for zero-power and at-power conditions. Temperature feedback effects were found to be significant in the GTRR at 900 kW in the low frequency region, and the extent of the temperature feedback predicted by SPARE was confirmed by the experimental results. Experiments at two different temperatures with different temperature feedback coefficients yielded experimental results which reflected this change in conditions. At very low frequencies the SPARE calculations for the spatial response indicated a degeneration of the spatial model to that of a point model for both at-power and zero-power conditions. The experimental results served to confirm the SPARE calculations in this respect also. The higher frequency experiments indicated spatial effects in the frequency range above one Hz.

This approach has been shown to be valid for predicting spatial source transfer functions with temperature feedback in the GTRR. This technique should also be useful for predicting at-power spatial transfer functions for larger reactor system stability studies where temperature feedback and spatial effects are a great deal more pronounced than in the GTRR. Further, this approach should be useful in dynamic studies for predicting at-power response to reactivity fluctuations. In general, this technique should find application in the study of space and energy effects in the general area of reactor system dynamics.

CHAPTER VII

RECOMMENDATIONS

The results of the investigation in this area have demonstrated the validity of introducing feedback in the analytical model for calculating the spatial source transfer function. However, it is felt that this feedback model still needs further development and improvement in two areas. The first of these is in the area of spatial feedback. In this development the feedback effect was considered on a unit cell basis with feedback considered in this case from the "average" unit cell. A more descriptive model would relate the fuel and moderator transfer functions as a function of spatial position much in the same way as the neutron flux is described spatially. The second area in need of improvement relates to the regions which contribute to feedback. The model as it was presented herein accounts for feedback only from the homogenized fuel region. Admittedly this region contributes primarily to the feedback effect, but surrounding moderator and reflector regions should also be considered to more fully describe the physical phenomenon. This latter suggestion would probably not improve significantly the application of this technique to large power reactors since these reactors consist of a large number of unit cells and and are not affected by slight temperature changes in the reflector and moderator surrounding the entire group of assemblies.

The extension of this one-dimensional model to a two-dimensional

analysis with feedback would be a task worthy of accomplishment. In addition to being much more descriptive as a two-dimensional model is, this two-dimensional extension would permit analytical checks on experimental results obtained with a pile oscillator in positions other than at the center of the reactor core. Such a two-dimensional model would permit the use of beam holes for pile oscillator experiments which would not offer the penalty of the loss of a fuel element.

Another area of fruitful research would be the investigation of feedback mechanisms other than those of temperature. These mechanisms include among others void formation and vibrational effects. These effects would be interesting since the frequency range of interest for these effects would be the same frequency range in which spatial effects are pronounced. An experiment involving void formation in the GTRR could be simulated by the external introduction of helium bubbles.

A number of other topics in closely related areas would assist greatly in the further understanding of spatial kinetic effects. Among these are source transfer function studies in higher frequency regions using several different reactor core configurations in which the resultant spatial effects are studied. Also of interest would be long range studies of the at-power reactor noise for the determination of reactor characteristics. Another area of practical application would be studies in nonlinear reactor system response. Such measurements would be similar to the transfer function measurements but would be describing function measurements instead.

In future pile oscillator experiments there may be some advantage to using other methods of introducing desired frequency components rather

than by the use of sinusoidal signals or PRB sequences. One such technique is that of ternary sequences[86] where the driven signal has three levels rather than two levels as in the PRB sequences. The selection of the method of frequency response testing should, however, be governed by the requirements of the experiment.

APPENDICES

APPENDIX A

FUEL AND MODERATOR TEMPERATURE FEEDBACK TRANSFER FUNCTIONS

Temperature feedback effects can, in general, be expected from both the fuel and moderator. A change in fuel temperature results in both a change in the fuel density and a change in the U-238 resonance cross sections due to "Doppler broadening." A change in moderator temperature changes the thermal neutron energy spectrum, in addition to the moderator density. This, in turn, affects both the absorption cross sections and the neutron leakage.

Feedback can then be assumed to occur through two feedback paths, through that of the fuel and that of the moderator. The reactor power originates in the fuel element in the form of heat from the fissioning process. Then as the element heats up the thermal energy is transferred to the moderator. Meanwhile the fuel is presumed to have a temperature coefficient of its own, α_F, thus changing reactivity quite quickly. It should be noted that the fuel then has a short time constant for the temperature feedback effect. The moderator also is assumed to have a separate temperature coefficient, α_M, which results in a reactivity change only after the heat is deposited in the moderator. This reactivity effect occurs much later than the immediate fuel reactivity effect. The moderator has a longer time constant than that of the fuel, and the moderator feedback effect will lag behind that of the fuel. This lag is related to the time required for the heat to flow from the fuel to the moderator.

Any resistance to the heat flow serves to increase the time constant.

The fuel and moderator temperature feedback transfer functions are developed for the GTRR model in this appendix. Consider the schematic diagram of the GTRR cooling system shown in Figure 39. The heat transfer is described in eight different equations from the generation of the heat in the fuel element to the dissipation of the heat in the cooling tower. The representation presented here assumes lumped fuel element-cladding thermal characteristics with no time delay existing between the fuel temperature and cladding temperature. This is clearly a good approximation for a metallic-alloy, bonded cladding fuel element.

For this model the heat transfer equations have been handled in the conventional manner for the unit cell, i.e. heat generation in the fuel with subsequent heat flow to the moderator. This heat transfer model assumes also that the fuel and moderator are homogenized in the same manner that the neutronic properties are homogenized. This approach has the advantage of conforming to the neutronic model and further provides an approach for conforming to the simplified heat transfer equations. The power generated at each spatial point is removed by the moderator at that spatial point with no heat flow between adjacent spatial points. This assumption implies that the fuel and moderator temperatures at a given location in the reactor core are a function of the power density at that point and vary only when that power density varies.

The first two equations describe the flow of heat from the reactor fuel which is assumed to be the sole source of heat to the moderator.

$$M_f(\bar{x}) \frac{dT_f(\bar{x},t)}{dt} = P(\bar{x},t) - H(\bar{x})(T_f(\bar{x},t) - T_m(\bar{x},t)) \qquad (79)$$

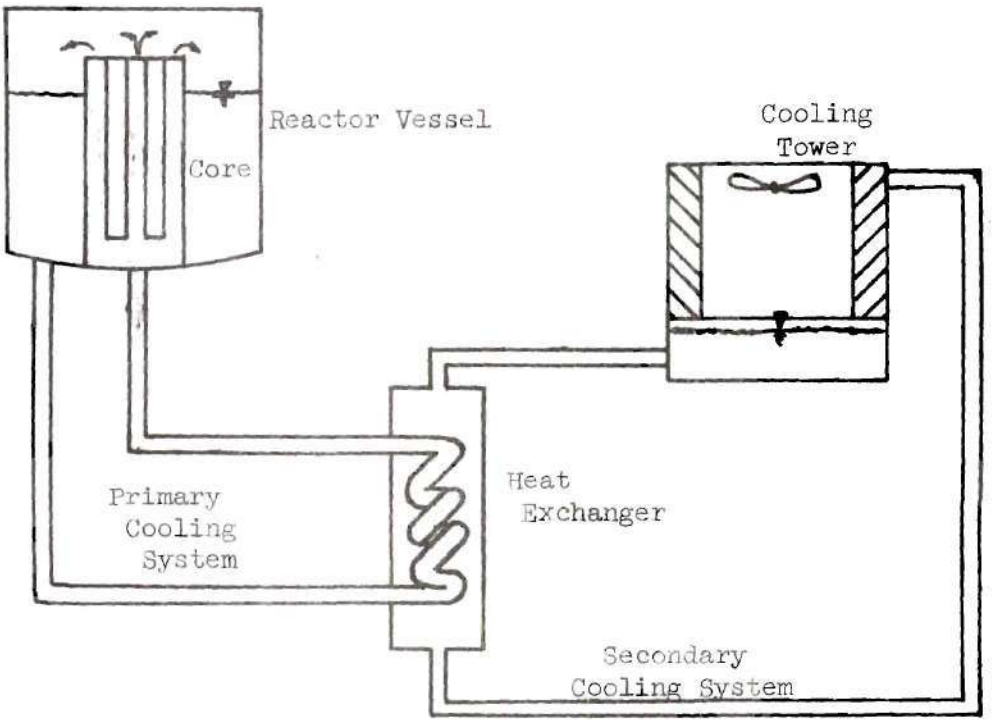

Figure 39. Schematic Diagram of GTRR Cooling System

$$T_m(\bar{x},t) = (T_{m_i}(\bar{x},t) + T_{m_o}(\bar{x},t))/2 \tag{80}$$

where

$P(\bar{x},t)$ is the power density in the fuel region (kW/cm^3)

$M_f(\bar{x})$ is the fuel heat capacity (mass of fuel-aluminum matrix* specific heat of the matrix)($kW\ sec/°C\ cm^3$)

$T_f(\bar{x},t)$ is the reactor fuel temperature (°C)

$T_m(\bar{x},t)$ is the average moderator temperature in the fuel cell (°C)

$T_{m_i}(\bar{x},t)$ is the moderator inlet temperature (°C)

$T_{m_o}(\bar{x},t)$ is the moderator outlet temperature (°C)

$H(\bar{x})$ is a lumped parameter coefficient which is a product of the heat transfer coefficient and the area of heat flow divided by the volume of the homogenized fuel region ($kW/°C\ cm^3$).

The third equation describes the heat balance within the fuel cell moderator.

$$M_m(\bar{x}) \frac{dT_m(\bar{x},t)}{dt} = H(\bar{x})\ (T_f(\bar{x},t) - T_m(\bar{x},t)) \tag{81}$$

$$- F(\bar{x})\ C_m(T_{m_o}(\bar{x},t) - T_{m_i}(\bar{x},t))$$

where

$M_m(\bar{x})$ is the moderator heat capacity ($kW\ sec/°C\ cm^3$)

$F(\bar{x})$ is the moderator flow rate ($gm/sec\ cm^3$)

C_m is the moderator specific heat ($kW\ sec/gm\ °C$).

The next equation describes the mixing delay as the moderator leaves the fuel cell and mixes in large bulk volume of moderator in the reactor vessel proper.

$$M_B(\bar{x}) \frac{dT_B(\bar{x},t)}{dt} = F(\bar{x})\ C_m(T_{m_o}(\bar{x},t) - T_B(\bar{x},t)) \tag{82}$$

where

$M_B(\bar{x})$ is heat capacity of the bulk moderator (kW sec/°C cm^3)

$T_B(\bar{x},t)$ is the temperature of the bulk moderator (°C)

$T_{m_o}(\bar{x},t)$ is the outlet temperature from the fuel cell (°C).

The next two equations describe heat flow from the moderator in the heat exchanger to the secondary cooling water

$$M_X \frac{dT_X(t)}{dt} = FC_m(T_B(t) - T_{m_i}(t)) - H_X(T_X(t) - T_W(t)) \tag{83}$$

$$T_X(t) = \left(\frac{T_B(t) + T_{m_i}(t)}{2}\right) \tag{84}$$

where

M_X is the heat capacity of the moderator in the heat exchanger and associated piping (kW sec/°C)

F is the moderator flow rate (gm/sec)

$T_B(t)$ is the average temperature of the bulk moderator (°C)

$T_X(t)$ is the average temperature of the moderator in the heat exchanger (°C)

$T_{m_i}(t)$ is the average inlet temperature of the moderator to the fuel cell (°C)

$T_W(t)$ is the average temperature of the secondary water on the shell side of the heat exchanger (°C)

H_X is the product of the heat transfer coefficient and the area of heat flow from the primary cooling water to the secondary cooling water (kW/°C).

The last two equations describe the heat flow from the secondary coolant in the heat excharger to the cooling tower.

$$M_W \frac{dT_W(t)}{dt} = H_X(T_X(t) - T_W(t)) - F_W C_W(T_{W_o}(t) - T_{W_i}(t)) \tag{85}$$

$$T_W(t) = (T_{W_o}(t) + T_{W_i}(t))/2 \tag{86}$$

where

M_W is the heat capacity of the secondary coolant in the heat exchanger (kW sec/°C)

F_W is the flow rate of the secondary coolant (gm/sec)

C_W is the specific heat of the secondary coolant (cal/gm °C)

$T_{W_o}(t)$ is the outlet temperature of the secondary coolant leaving the heat exchanger (°C)

$T_{W_i}(t)$ is the inlet temperature of the secondary coolant entering the heat exchanger (°C).

With these eight equations to describe the system transient response a small perturbation will be introduced in the power density in a manner similar to the perturbation in Chapter II. The response of the various temperatures in the system will vary about some steady state value and can be expressed in the following manner.

$$T_f(\bar{x},t) = T_{f_o}(\bar{x}) + \delta T_f(\bar{x},t) \tag{87}$$

$$T_M(\bar{x},t) = (T_m(\bar{x}))_o + \delta T_m(\bar{x},t) \tag{88}$$

$$T_B(\bar{x},t) = T_{B_o}(\bar{x}) + \delta T_B(\bar{x},t) \tag{89}$$

$$T_W(\bar{x},t) = (T_W(\bar{x}))_o + \delta T_W(\bar{x},t) \tag{90}$$

Now assume that the power is uniformly generated across the core such that $T_f(t) = T_f(\bar{x},t)$ and $T_m(t) = T_m(\bar{x},t)$. Now further assume that the bulk moderator is uniformly mixed such that $\delta T_B(t) = \delta T_B(\bar{x},t)$. Mixing is such in the GTRR that this assumption is probably very reasonable. Since the inlet coolant temperature is constant, $\delta T_{m_i}(t) = \delta T_{m_i}(\bar{x},t)$. This latter condition is a physical requirement of the system.

Now further assume that $\delta T_{W_i}(t) = 0$, i.e. the return water temperature from the cooling tower remains a constant. This condition implies that the cooling tower has an excess cooling capacity such that slight variations in power have no decisive effect on the return water temperature. This capacity is determined primarily by weather and atmospheric conditions, but this assumption should be reasonably correct.

Based on the foregoing assumptions it becomes straightforward to substitute equations (87) through (90) into equations (79) through (86), subtract the steady state portions, and take the Laplace transforms in the conventional manner.

Consider first the moderator temperature feedback transfer function. The input disturbance is the $\delta P(\bar{x},j\omega)$ and the system output is the $\delta T_M(\bar{x},j\omega)$ which is a slight temperature variation characteristic of the moderator. For the GTRR analysis no single temperature variation is characteristic of the moderator since each fuel cell has a volume fraction

with fuel cell moderator and another surrounding volume fraction of bulk volume moderator. The characteristic moderator is volume weighed such that the moderator $\delta T_{\overline{M}}(\overline{x}, j\omega)$ is defined

$$\delta T_{\overline{m}}(\overline{x}, j\omega) = VFE\ \delta T_{m}(\overline{x}, j\omega) + VFB\ \delta T_{B}(\overline{x}, j\omega) \tag{91}$$

where

VFE is the volume fraction of the moderator in the fuel element per unit cell

VFB is the volume fraction of the moderator in the bulk moderator per unit cell.

The moderator feedback transfer function is then expressed as follows:

$$FM(\overline{x}, j\omega) = \text{Moderator temperature feedback transfer function} \tag{92}$$

$$= \delta T_{\overline{m}}(\overline{x}, j\omega)/\delta P(\overline{x}, j\omega)$$

$$= (VFE)\ \delta T_{m}(\overline{x}, j\omega)/\delta P(\overline{x}, j\omega) + (VFB)\ \delta T_{B}(\overline{x}, j\omega)/\delta P(\overline{x}, j\omega)$$

The moderator feedback transfer function can be directly solved from simultaneous solution of the eight heat transfer equations with the eight unknowns. The solution for $FM(\overline{x}, j\omega)$ is as follows.

$$FM(\overline{x}, j\omega) = \left(VFB\ \frac{\delta T_{B}(\overline{x}, j\omega)}{\delta P(\overline{x}, j\omega)}\right) + \left(VFE\ \frac{\delta T_{m}(\overline{x}, j\omega)}{\delta P(\overline{x}, j\omega)}\right) \tag{93}$$

$$= \left(\frac{1}{H(\overline{x})(\tau_{f} j\omega + 1)}\right)\left(\frac{1}{CDENOM}\right)\left(VFE(\overline{x})(RTMTB) + VFB(\overline{x})\right)$$

where

$$CDENOM = (TMPTM*RTMTB) + 2\frac{F(\bar{x})C_m}{H(\bar{x})}(\tau_B j\omega+1)$$

$$TMPTM = \tau_m j\omega+1 - 2\frac{F(\bar{x})C_m}{H(\bar{x})} - (1/(\tau_f j\omega+1))$$

$$TMPTXX = \tau_{XX} j\omega+1 - 2\frac{F(\bar{x})C_m}{H_X} - (1/(\tau_W j\omega+1+2F_W C_W/H_X))$$

$$RTMTB = ((2F(\bar{x})C_m/H_X) + (\tau_B j\omega/2)(TMPTXX))/(TMPTXX)$$

$$\tau_f = M_f(\bar{x})/H(\bar{x})$$
$$\tau_m = M_m(\bar{x})/H(\bar{x})$$
$$\tau_B = M_B(\bar{x})/(F(\bar{x})(C_m)$$
$$\tau_W = M_W/H_X$$
$$\tau_{XX} = M_X/H_X$$

The fuel feedback transfer function is denoted by $FF(\bar{x},j\omega)$ and is defined as follows

$$FF(\bar{x},j\omega) = \frac{\delta T_f(\bar{x},j\omega)}{\delta P(\bar{x},j\omega)} \tag{95}$$

where $\delta T_f(\bar{x},j\omega)$ is the slight variation of the fuel temperature which is the fuel response to the input $\delta P(\bar{x},j\omega)$.

As before, the equation is lengthy; however, the solution is again straightforward.

$$FF(\bar{x},j\omega) = (1/(H(\bar{x})(\tau_f j\omega+1)))(CNUM/CDENOM) \tag{96}$$

where

$$CNUM = (\tau_m j\omega+1 - 2F(\bar{x})\ C_m/H(\bar{x}))(2F(\bar{x})\ C_m/(H_X*TMPTXX) + \tau_B j\omega/2) + (2F(\bar{x})\ C_m/H(\bar{x}))(\tau_B j\omega+1)$$

with CDENOM and TMPTXX as defined in equation (94).

This approach provides a spatial solution for the moderator and fuel feedback transfer functions; however, the conditions imposed in this derivation result in constant values for these feedback transfer functions over the limits of the reactor core. This condition is true for a first order approximation much in the manner that the thermal flux is assumed constant across the reactor core.

APPENDIX B

PSEUDO-RANDOM BINARY SIGNAL FOR FREQUENCY RESPONSE TESTING

An experimental tool commonly used for determining the dynamic behavior of a reactor system is the frequency-response measurement. These measurements are useful because they indicate changes in system stability under varying conditions.[52]

A number of different testing procedures may be used to measure the frequency response. These methods include sine-wave testing, binary approximation to sine-wave signals, pseudo-random binary sequences, pseudo-random ternary sequences, and various non-periodic test signals. Each method has particular advantages for certain experiments depending on experiment requirements. For the purpose of this research a pseudo-random binary sequence was chosen. This approach for this experiment has several advantages. First, this approach is simple and hence relatively easy to implement. Second, this technique permits investigation over a band of frequencies rather than a single frequency for a given experimental run. Third, this approach is quite applicable to low frequency testing which is the frequency band of interest for this investigation.

A pseudo-random binary sequence is a special sequence of equal-amplitude positive and negative pulses that are applied in "step" fashion. Hence, the term binary indicates that such a procedure or sequence has two levels (positive or negative) applied as a step function. The term pseudo-random is a bit misleading. The signal has a definite wave form

and is strictly periodic. The reason for this term in the title is due to the characteristics of the sequence. For example, the autocorrelation function of the sequence is similar to the autocorrelation function of a random signal. In addition, the power spectrum for a large bit sequence is similar in form to the spectral density of a random signal.[84]

The pseudo-random binary sequence is characterized by the number of bits in the sequence and the period of the sequence. A bit is defined as a minimum width pulse. All pulses in the sequence are minimum width or multiples thereof. A typical pseudo-random sequence (referred to as PRB sequence) is shown in Figure 40.

Algorithms are known for generating PRB sequences, but sequences can be generated only with a certain number of bits, Z, in the sequence. Two different methods[85] can be used for generating a sequence of length Z, either $Z = 2^m-1$ or $Z = 4m-1$ where m is an integer. A technique for generating signals will be presented later.

Frequency Spectrum

The equation for a period of the autocorrelation function of the general PRB sequence[85] is

$$C_{XX}(\tau) = 1 - \left(\frac{Z+1}{T}\right)\tau \quad , \qquad 0 \leqq \tau \leqq T/Z \tag{97}$$

$$= -1/Z \quad , \quad \frac{T}{Z} \leqq \tau \leqq (Z-1)\frac{T}{Z} \tag{98}$$

$$= -Z + \left(\frac{Z+1}{T}\right)\tau \quad , \quad (Z-1)\frac{T}{Z} \leqq \tau \leqq T \tag{99}$$

where

τ = variable correlation time

Z = number of bits in the sequence

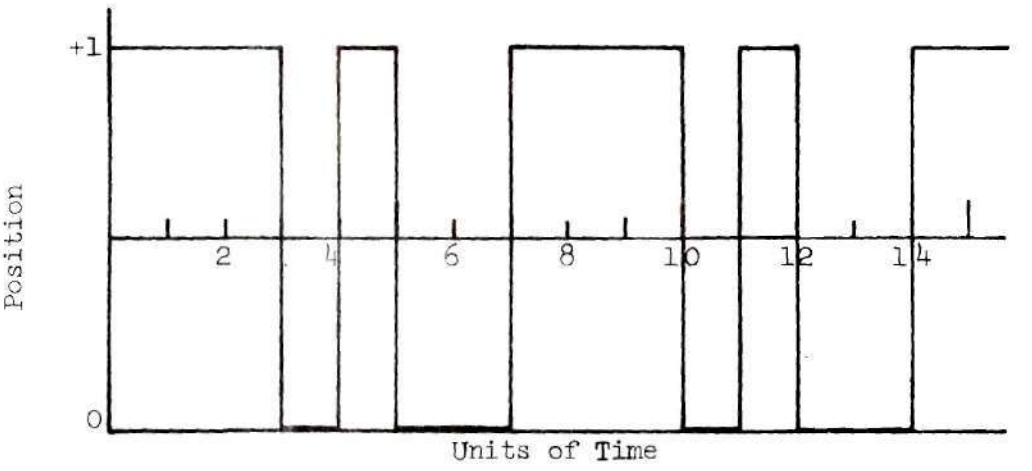

Figure 40. A Seven-Bit Pseudo-Random Binary Sequence

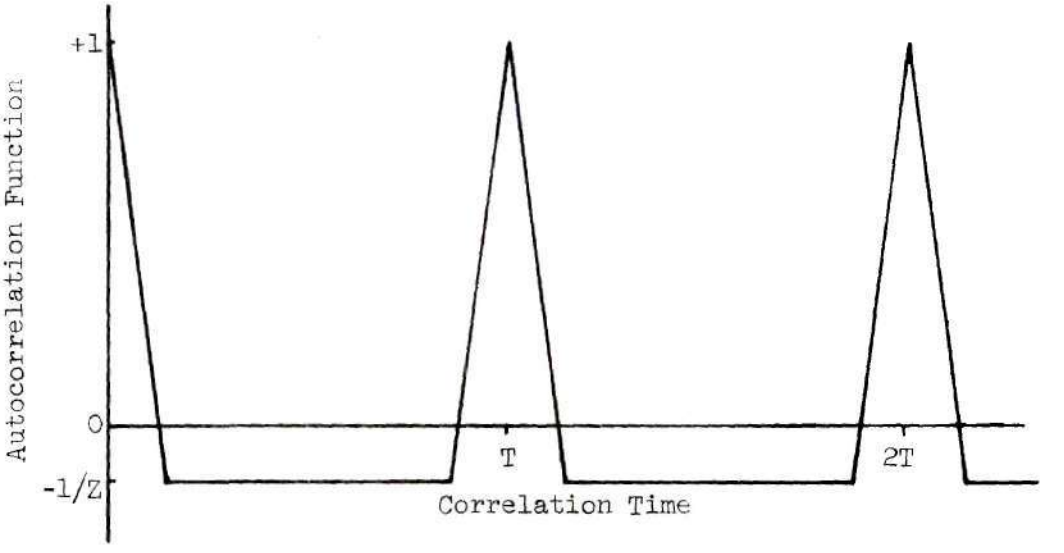

Figure 41. Autocorrelation Function[85] of PRB Sequence with Z Bits and Periodicity T

T = period of the sequence

Δt = minimum pulse width.

The general form of the autocorrelation function for a sequence of Z bits and a periodicity T is shown in Figure 41. It has the general features of one spike per period which is somewhat similar to a delta function.

Using the properties of the PRB sequence and its autocorrelation function, $C_{XX}(\tau)$, a brief discussion will be presented on the frequency spectrum of the signal. The essential point to be covered is that frequency spectrum or the spectral power, denoted by $P(f_n)$, varies with the number of bits in the sequence. A small number concentrates the signal power in a few harmonics, whereas a larger value of Z tends to distribute the signal power over more harmonics. As Z approaches a large number the frequency spectrum approaches a constant value.

From Wiener's theorem the signal spectral power is related to the autocorrelation function for a periodic function in the following manner.

$$P(f_n) = \int_{-T/2}^{T/2} C_{XX}(\tau) \exp(-j\omega_n \tau)\, d\tau \quad , \quad \omega_n = 2\pi f_n \tag{100}$$

In order to bring out certain pertinent points it will be necessary to express the $C_{XX}(\tau)$ value as a Fourier series. This can be expressed by the following equation

$$C_{XX}(\tau) = \tfrac{1}{2}a_o + \sum_{k=1}^{\infty} a_k \cos\omega_k t \tag{101}$$

where a_k coefficients are the standard Fourier series coefficients. The

b_k term equation is zero since the equations for the autocorrelation function are even. This property can be seen from Figure 41.

Substituting $C_{XX}(\tau)$ in Wiener's equation yields the following relationship.

$$P(f_k) = a_k(T/2) \tag{102}$$

where

$$a_k = 2/T \int_{-T/2}^{+T/2} C_{XX}(\tau) \cos\omega_k \tau \, d\tau \quad , \quad k \geq 1 \tag{103}$$

The spectral power density, $P(f_n)$ is therefore directly proportional to the coefficient a_k.

The a_k coefficient can be determined by the above equation in conjunction with the $C_{XX}(\tau)$ equations which are a function of T and Z.

Carrying out the integration one solves for a_k.

$$a_k = \frac{2(Z+1)}{Z^2} \left[\frac{\sin k\pi/Z}{k\pi/Z}\right]^2 \quad , \quad k \geq 1. \tag{104}$$

The spectral power density $P(f_k)$ is therefore related to Z and k by this unusual equation. This equation now permits one to evaluate a given sequence for the distribution of the spectral power density. The total spectral power P_t is therefore

$$P_t = \sum_{k=1}^{\infty} P(f_k) \tag{105}$$

By the selection of Z one is able to obtain the distribution of the spectral power and with the selection of Δt ($T=Z\Delta t$) one selects fre-

quencies of interest.

The effect of varying Z can be seen from the envelopes of the power spectrum plots for several sequences shown in Figure 42. These curves are for the same period, T, but for different numbers of bits, Z, in the sequence.

The effect of the number of bits per sequence is clear from this figure. For sequences with few bits per sequence, the signal strength is concentrated in the low frequency end of the spectrum. For sequences with many bits per sequence, the amplitudes change less from harmonic to harmonic, but the low frequency amplitudes are lower than for the sequences with few bits per sequence. It should be pointed out that this scheme provides and contains information related to harmonic frequencies only. No information is available for non-harmonic frequencies.

It is frequently useful to know the harmonic number at which the harmonic amplitude is down to half of the amplitude of the first harmonic. This value can be determined by solving the following expression for k.

$$a_k/a_1 = \frac{\left(\frac{\sin \frac{\pi k}{Z}}{\frac{\pi k}{Z}}\right)^2}{\left(\frac{\sin \frac{\pi}{Z}}{\frac{\pi}{Z}}\right)^2} = 0.5 \qquad (106)$$

For Z greater than 20, the following relation holds

$$k_h \simeq 0.44Z \qquad (107)$$

where

k_h = harmonic number of the harmonic whose amplitude is half the amplitude of the fundamental

Z = number of bits in the sequence.

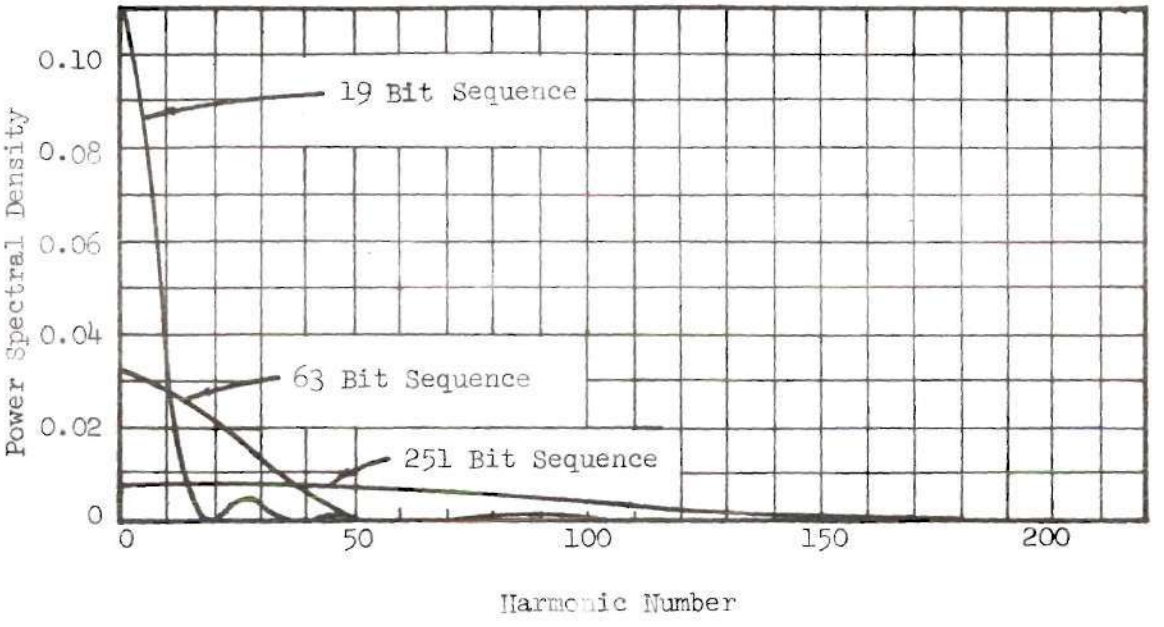

Figure 42. Comparison of Spectra[85] for Sequences with Different Numbers of Bits

Another quantity that is useful for evaluating the test signal is the fraction of the signal power concentrated in the desired frequencies. Considering those harmonics at which the amplitudes are at least half as large as for the fundamental than the total spectral power in these harmonics, $P_{\frac{1}{2}}$ is given by

$$P_{\frac{1}{2}} = \sum_{k=1}^{0.44Z} P(f_k) \tag{108}$$

The average power per harmonic in this range is given by

$$\overline{P}_{\frac{1}{2}} = P_{\frac{1}{2}}/0.44Z$$

For a study of several sequence lengths it was observed that the harmonics with amplitudes at least half as large as the amplitude of the fundamental contain about 71 percent of the total signal power.

Implementing the PRB Signal

There are two procedures which may be used to generate PRB sequences.[85] In each method, the number of bits is restricted to certain specific values. For one type the allowable number of bits, Z, is given by

$$Z = 2^m - 1 \tag{109}$$

where m is an integer.

The allowable values of Z are 3, 7, 15, 31, 63, 127, 255, 511, 1023, etc.

The other type of sequence permits values for the number of bits, Z, given by

$$Z = 4m-1 \qquad (110)$$

where m is an integer.

The allowable values of Z are 3, 7, 11, 19, 23, etc. Algorithms for generating both sequences are available.

The method for computing the sequence with lengths, $Z = 2^m-1$, lends itself quite readily to generation with the use of a digital computer. This sequence may be generated by employing modulo-2 adder feedback.

Consider the 3 registers (1, 2, and 3) shown below.

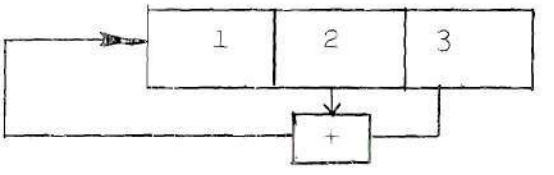

Generation of a sequence proceeds in the following manner.[85]

1. Set initial values (0 or 1) for each register. Selection may be arbitrary, however, one of them must be 1.

2. Generate a new set of digits for each register as follows

   a. Add modulo-2 the values in the registers specified for feedback.

   b. Shift all existing register values one stage to the right and insert the feedback term from step (a) into register. Note that the value in the last register is removed when shifting is accomplished.

3. Repeat until the initial values reappear in all registers.

This set of operations produces a series of digits (0 or 1) for each stage in a pattern which repeats periodically. The pattern in each stage is the same, but they are offset relative to one another. The 0 and 1 indicate which value of the two-level input signal to use. Either 0 or 1

may be interpreted as the high level input or the low level input. The correlation functions and power spectra are identical in each case.

As an example consider the following sequence where the number of registers is 3 with modulo-2 feedback from registers 1 and 3.

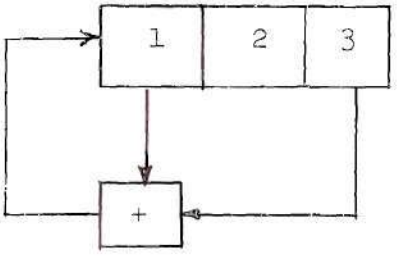

initial values	1	0	0	
1st shift	1	1	0	
2nd shift	1	1	1	
3rd shift	0	1	1	
4th shift	1	0	1	
5th shift	0	1	0	
6th shift	0	0	1	
7th shift	1	0	0	cycle repeats

Thus a 7 bit PRB sequence is (1 1 1 0 1 0 0).

It is known that the maximum number of bits in such a periodic sequence generated by n-stage registers with modulo-2 adder feedback is 2^n-1. Other shorter periodic sequences are obtained for certain feedback connections, but only the maximum length sequence has the desired pseudo-random character. The arrangement of the feedback registers needed to generate maximum length sequences has been determined for a number of sequences. Some of the sequences may be generated with one modulo-2 adder

and others require several. Table 1 gives feedback registers which require only one modulo-2 adder for sequences up to m = 20.

Table 1. Data for Generating PRB Sequences[85]

m (registers)	Z (bits/sequence)	Stages to be added Modulo-2
2	3	1, 2
3	7	1, 3
4	15	1, 4
5	31	3, 5
6	63	1, 6
7	127	1, 7
9	511	4, 9
10	1,023	3, 10
11	2,047	2, 11
15	32,767	1, 15
17	131,071	3, 17
18	262,143	7, 18
20	1,048,575	3, 20

APPENDIX C

GTRR AND NORA REACTOR DATA AND CONSTANTS

The Georgia Tech Research Reactor

The GTRR is a heavy-water moderated and cooled reactor consisting of enriched U-235 fuel in an aluminum-uranium alloy. A description of the reactor is presented in the chapter on Instrumentation and Equipment. The intent of this appendix is to present the two-group cross sections and heat transfer data used for the diffusion and source transfer function calculations in the program SPARE.

Neutronic data came primarily from a Technical Report on Reactor Physics Calculations[72] for the 5 MW GTRR and are presented in Table 2. The reactor was divided into four zones. Zone 1 consisted of a D_2O and aluminum mixture. Zone 2 consisted of a homogenized region of fuel (U-235), D_2O, and aluminum. Zone 3 consisted primarily of D_2O with some graphite and aluminum. Zone 4 consisted of the graphite reflector.

Table 3 contains the heat transfer parameters most of which were taken from the Safeguards Report[70] for the GTRR. The heat transfer coefficient between the fuel and moderator was calculated using the Dittus-Boelter equation. It is interesting to note that this particular calculation was quite similar to some earlier independent calculations using the modified Colburn equation.

The feedback coefficients are tabulated in Table 4. In each case the computation of the coefficients was based on two assumptions. The

Table 2. Two-Group Constants[72] for the GTRR Analysis

Zone	Temp (°C)	D_1 (cm)	D_2 (cm)	Σ_{a_1} (cm^{-1})	Σ_{a_2} (cm^{-1})	Σ_r (cm^{-1})	$\nu\Sigma_{f_1}$ (cm^{-1})	$\nu\Sigma_{f_2}$ (cm^{-1})
Zone 1 Al-D_2O R=8.00 cm	35	1.3280	0.8482	1.620×10^{-4}	5.853×10^{-4}	9.243×10^{-2}	0.0	0.0
Zone 2 U-235, D_2O, and Al R=34.89 cm	22	1.3281	0.8880	7.551×10^{-4}	1.405×10^{-2}	7.934×10^{-3}	9.006×10^{-4}	2.277×10^{-2}
	35	1.3220	0.8961	7.539×10^{-4}	1.393×10^{-2}	7.902×10^{-3}	8.994×10^{-4}	2.253×10^{-2}
	45	1.3900	0.9012	7.521×10^{-4}	1.383×10^{-2}	7.861×10^{-3}	8.972×10^{-4}	2.233×10^{-2}
Zone 3 D_2O, Al, and Graphite R=90.5 cm	35	1.322	0.8747	1.610×10^{-4}	7.689×10^{-4}	8.299×10^{-3}	0.0	0.0
Zone 4 Graphite R=154.5 cm	35	1.111	0.8620	0.00	2.537×10^{-4}	2.338×10^{-3}	0.0	0.0

Additional Two-Group Values: $\bar{V}_1 = 2.000 \times 10^6$ cm/sec $\bar{V}_2 = 2.550 \times 10^6$ cm/sec

$(B_Z)_1^2 = 7.216 \times 10^{-4}$ cm^{-2} $(B_Z)_2^2 = 7.216 \times 10^{-4}$ cm^{-2}

Table 3. GTRR Core Data

Number of Fuel Elements	18
Mass (lb):	
Fuel aluminum matrix	122.4
Moderator in fuel cells	130.0
Moderator in reactor vessel (1100 gal)	10,000.0
Moderator in heat exchanger and adjoining pipe	4,960.0
Secondary water in heat exchanger	2,170.0
Flow Rates (gpm):	
Primary coolant	1,280
Secondary coolant	1,050
1 MW Temperature Differentials (°C):	
Moderator in/out fuel elements	2.71
Moderator in/out heat exchanger	2.71
Primary/secondary water in heat exchanger	3.38
Heat Transfer Coefficient (Btu/hr ft^2°F):	
Fuel-Moderator	1,275
Moderator Temperature Coefficient @ 100°F ($\Delta k/k/°C$)	-3.3×10^{-4}
Area (cm^2):	
Fuel Cell	201.3
Fuel element	58.1
Moderator in fuel element	39.1
Metal area in fuel element	19.0
Heat transfer area per element (ft^2)	8.82

Table 4. Parameter Temperature Coefficients

Parameter	Coefficient	Temperature Coefficient (Range 22-45°C)
D_1	$K^M_{D_1}$	$+ 3.435 \times 10^{-4}$
D_2	$K^M_{D_2}$	$+ 5.739 \times 10^{-4}$
Σ_r	K^M_r	$- 3.174 \times 10^{-6}$
Σ_{a_1}	$K^M_{a_1}$	$- 1.304 \times 10^{-7}$
Σ_{a_2}	$K^M_{a_2}$	$- 9.565 \times 10^{-6}$
Σ_{f_1}	$K^M_{f_1}$	$- 6.059 \times 10^{-8}$
Σ_{f_2}	$K^M_{f_2}$	$- 7.840 \times 10^{-6}$

first assumption is that the change in a given parameter with temperature is due wholly to the moderator temperature, i.e. to assume the fuel feedback term is always zero. For this highly enriched thermal reactor this should prove to be a reasonable assumption. Second, the average value for the coefficient over the entire temperature range is the most appropriate value. The parameters have been evaluated in an earlier study at three temperatures, 22°C, 35°C, and 45°C. The experiments in most cases were in the range of or close to 35°C for the moderator. The coefficients for a parameter then were evaluated in the following manner

$$K^{M}_{(\text{parameter})} = \left(\frac{(\text{parameter value @ } T=45^{\circ}C) - (\text{parameter value @ } T=22^{\circ}C)}{23^{\circ}C}\right) \quad (111)$$

This served to provide somewhat of an average value for the parameter change with temperature.

The GTRR delayed neutron constants are tabulated in Table 5 and are based on studies by Graham.[86]

The NORA Reactor

NORA is a critical assembly using natural and enriched uranium fuel in D_2O and mixed D_2O/H_2O moderators with a graphite reflector.

This facility, located in Kjeller, Norway, is used for reactor physics and kinetics studies. Some of the experimental investigations at NORA in spatial reactor kinetics were amenable to a one-dimensional digital analysis. This was done by Johnson[33] in earlier studies for a zero-power or no feedback case. The one-dimensional calculations by Johnson proved to be very close to the experimental values. Johnson used the diffusion

Table 5. Delayed Neutron Constants[86] for the GTRR

Group	β_i	λ_i (sec^{-1})
1	1.85×10^{-3}	1.96
2	6.12×10^{-4}	4.41×10^{-1}
3	2.06×10^{-3}	2.88×10^{-1}
4	1.21×10^{-3}	1.17×10^{-1}
5	1.50×10^{-3}	3.05×10^{-2}
6	2.54×10^{-4}	9.25×10^{-3}
7	2.33×10^{-5}	2.27×10^{-3}
8	1.51×10^{-5}	7.73×10^{-4}
9	1.07×10^{-5}	3.15×10^{-4}
10	1.70×10^{-6}	1.18×10^{-4}
11	3.79×10^{-6}	5.85×10^{-5}
12	2.10×10^{-7}	1.37×10^{-5}

$\beta_{total} = 0.007558$

programs CHARLIE and CRAM in his method for the complex calculations. In an attempt to test SPARE, calculations were done on the NORA reactor using the data used by Johnson. This provided an experimental check in addition to a separate independent analytical calculation.

The two-group data used by Johnson[33] for NORA are tabulated in Table 6. The delayed neutron constants for NORA are presented in Table 7.

Table 6. Two-Group Constants[34] for the NORA Analysis

Zone	D_1 (cm)	D_2 (cm)	Σ_{a_1} (cm^{-1})	Σ_{a_2} (cm^{-1})	Σ_r (cm^{-1})	$\nu\Sigma_{f_1}$ (cm^{-1})	$\nu\Sigma_{f_2}$ (cm^{-1})
Reactor Core R=59.7 cm	1.292	0.8180	2.382×10^{-4}	3.654×10^{-3}	9.676×10^{-3}	0.00	5.560×10^{-3}
D_2O Reflector R=112.5 cm	1.305	0.8255	0.00	1.110×10^{-4}	1.090×10^{-2}	0.00	0.00
Graphite Reflector R=162.5 cm	1.192	1.050	0.00	8.250×10^{-4}	2.820×10^{-3}	0.00	0.00

Additional Two-Group Values: $\bar{V}_1 = 2.00 \times 10^6$ cm/sec $\bar{V}_2 = 2.20 \times 10^5$ cm/sec

$(B_Z)_1^2 = (B_Z)_2^2 = 5.536 \times 10^{-4}$ cm^{-2}

Table 7. Delayed Neutron Constants[33] for the NORA Reactor

Group	β_i	λ_i (sec^{-1})
1	2.500×10^{-4}	1.270×10^{-2}
2	1.400×10^{-3}	3.170×10^{-2}
3	1.250×10^{-3}	1.150×10^{-1}
4	2.700×10^{-3}	3.110×10^{-1}
5	8.700×10^{-4}	1.400×10^{0}
6	1.800×10^{-4}	3.870×10^{0}
7	4.800×10^{-4}	2.780×10^{-1}
8	1.500×10^{-4}	1.690×10^{-2}
9	5.000×10^{-5}	4.900×10^{-3}
10	3.000×10^{-5}	1.520×10^{-3}
11	2.000×10^{-5}	4.300×10^{-4}
12	2.000×10^{-5}	1.200×10^{-4}
13	2.000×10^{-6}	4.000×10^{-5}
14	7.000×10^{-7}	3.700×10^{-6}

$\beta_{total} = 0.0073907$

APPENDIX D

SCHEMATIC DIAGRAMS OF ELECTRONIC EQUIPMENT

The electronic circuits for the pile oscillator solenoid drive units and the electrometers used in this research are presented on the following pages. The solenoid drive units were designed by Mr. John Alderman of the Georgia Tech Nuclear Research Center. These drive units were built and tested by Mr. Jay Noble and the author. The electrometer units were procured commercially, but were built to the experimental specifications by Mr. J. C. Gundlach of Reactor Controls, Inc.

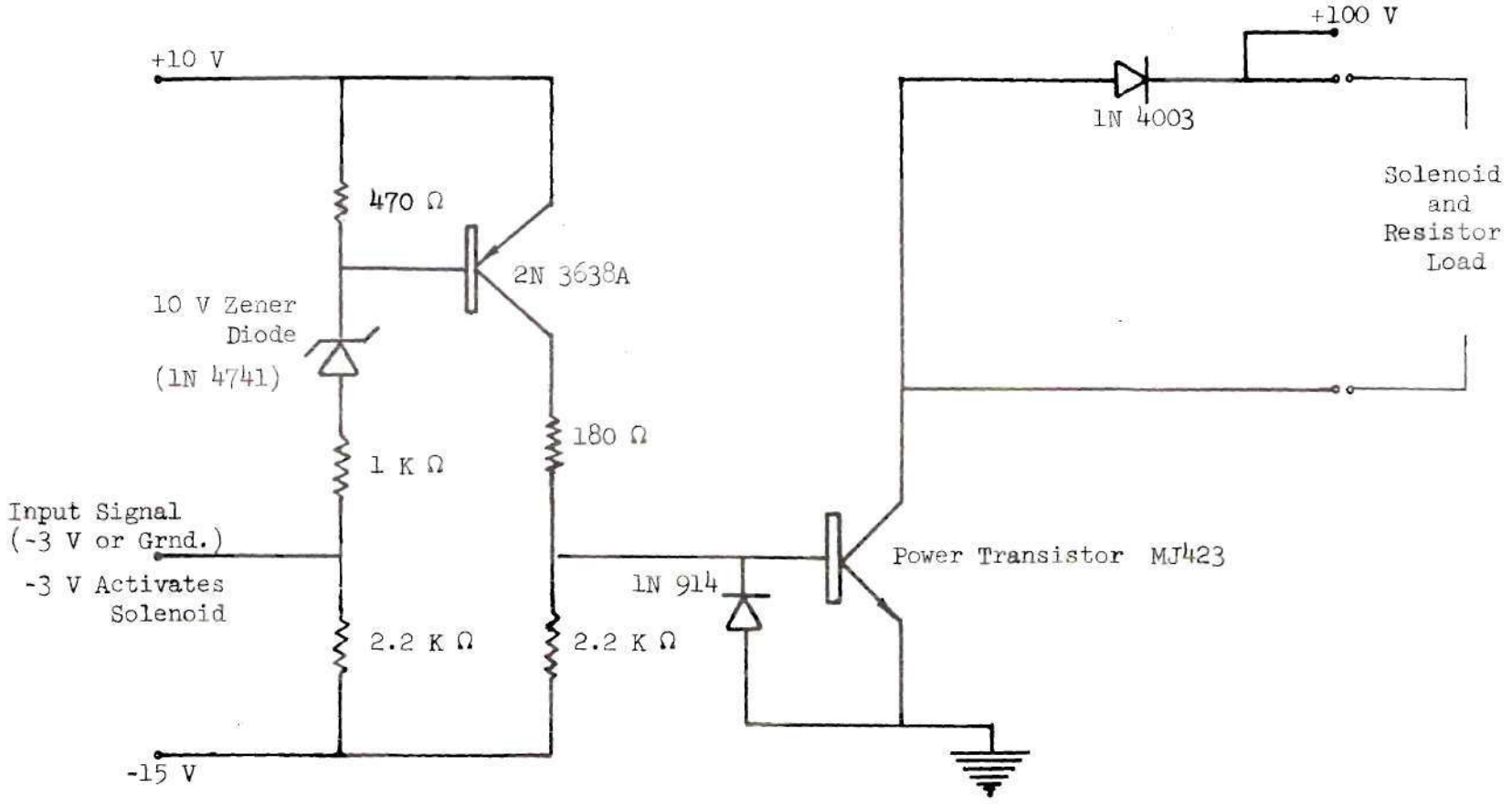

Figure 43. Schematic Diagram of Drive Unit for One of the Pile Oscillator Solenoids

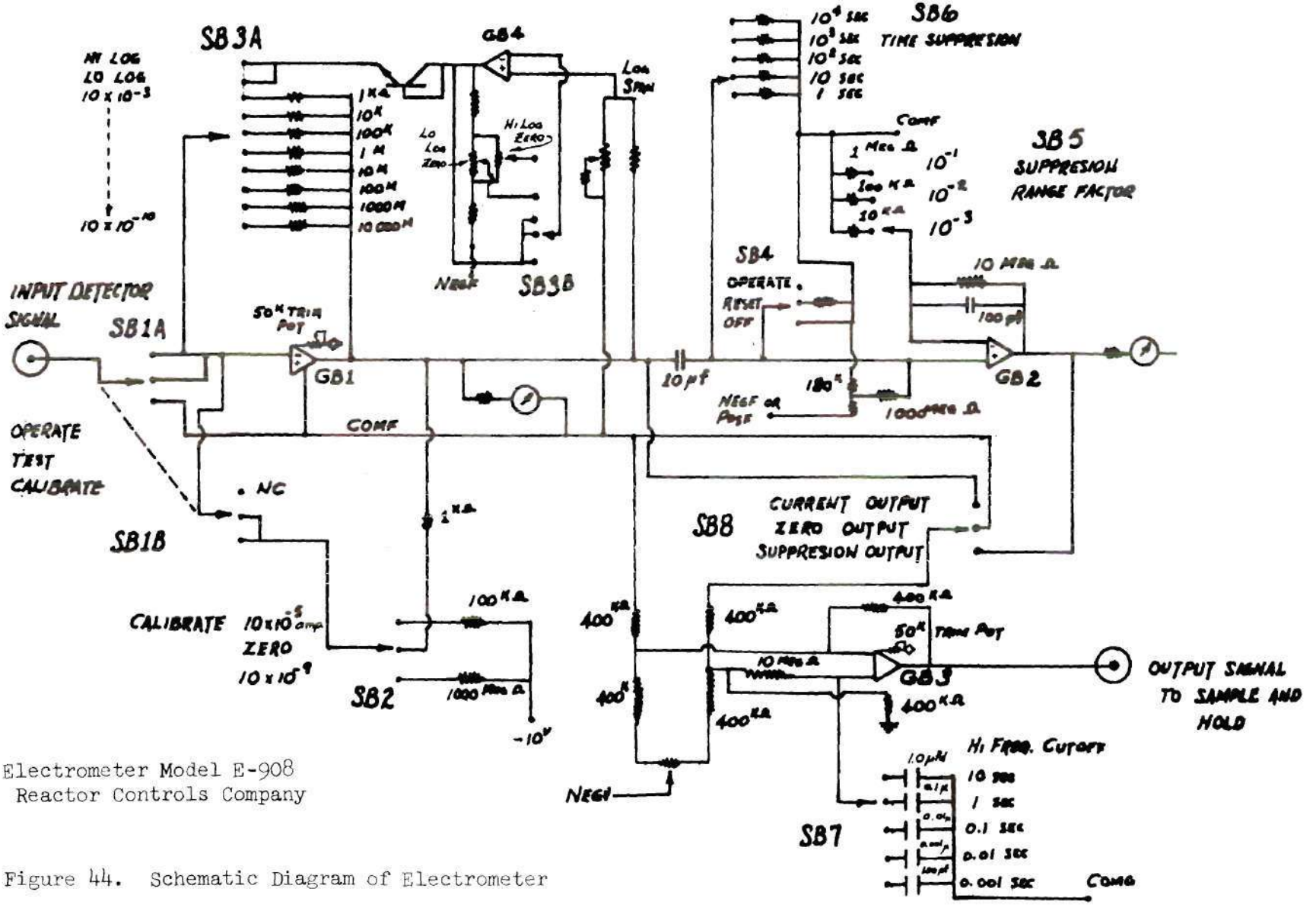

Electrometer Model E-908
Reactor Controls Company

Figure 44. Schematic Diagram of Electrometer

APPENDIX E

A POINT MODEL STUDY OF THE GTRR TRANSFER FUNCTION AT ZERO POWER AND FULL POWER

The purpose of this appendix is to present the point model studies of the GTRR transfer function for full-power (1000 kW) and for zero-power conditions. This work was completed early in the overall investigation in order to establish the presence of temperature feedback and to determine the feasibility of attaining the low frequencies required in such an experimental investigation.

Define now a system with a forward transfer function, $KG(j\omega)$, and a temperature feedback transfer function $FD(j\omega)$. The closed loop transfer function $TF(j\omega)$, can be shown from elementary servo theory to respond in the following manner.

$$TF(j\omega) = \frac{KG(j\omega)}{1 - FD(j\omega)\ KG(j\omega)} \qquad (112)$$

The feedback term is assumed to be positive in this derivation.

For the particular case of a reactor the output or response is the fractional change in neutron population, $\delta n(j\omega)/n_o$, and the input is the small sinusoidal introduction of reactivity, $\delta k(j\omega)$, where $j\omega$ is the frequency of interest. For the point model reactor[63]

$$KG(j\omega) = 1/(\ell^* j\omega^*(1 + \Sigma_i\ (\beta_i/\ell(j\omega+\lambda_i)))) \qquad (113)$$

where

ℓ is the prompt neutron lifetime

β_i is the percent of group i delayed neutrons

λ_i is the decay constant for the group i neutrons.

Assuming that feedback is primarily due to the moderator, then $FD(j\omega)$ is proportional to $FM(j\omega)$ which was derived in Appendix A.

The constants of proportionality necessary are a power term which serves to relate the moderator temperature change to a fractional change in power as in the case of $\delta n(j\omega)/n_o$, and a coefficient which corrects for the units and makes the denominator dimensionless. Therefore,

$$FD(j\omega) = \alpha P_o \; FM(j\omega) \qquad (114)$$

where

α is a coefficient relating the reactivity change to the change in temperature

P_o is the steady state power level

$FM(j\omega)$ is the moderator transfer function defined as $\delta T_M(j\omega)/\delta P(j\omega)$

$FD(j\omega)$ is the moderator transfer function derived for a point model case.

With the terms defined clearly and related to the various reactor parameters which are tabulated in Appendix C, the transfer function values can be evaluated for the zero-power and high-power cases over a wide range of frequencies. The results of this work are shown in Figures 45 and 46 for P_o = 1000 kW, 900 kW, and zero power.

From these calculations and the figures it can be ascertained that

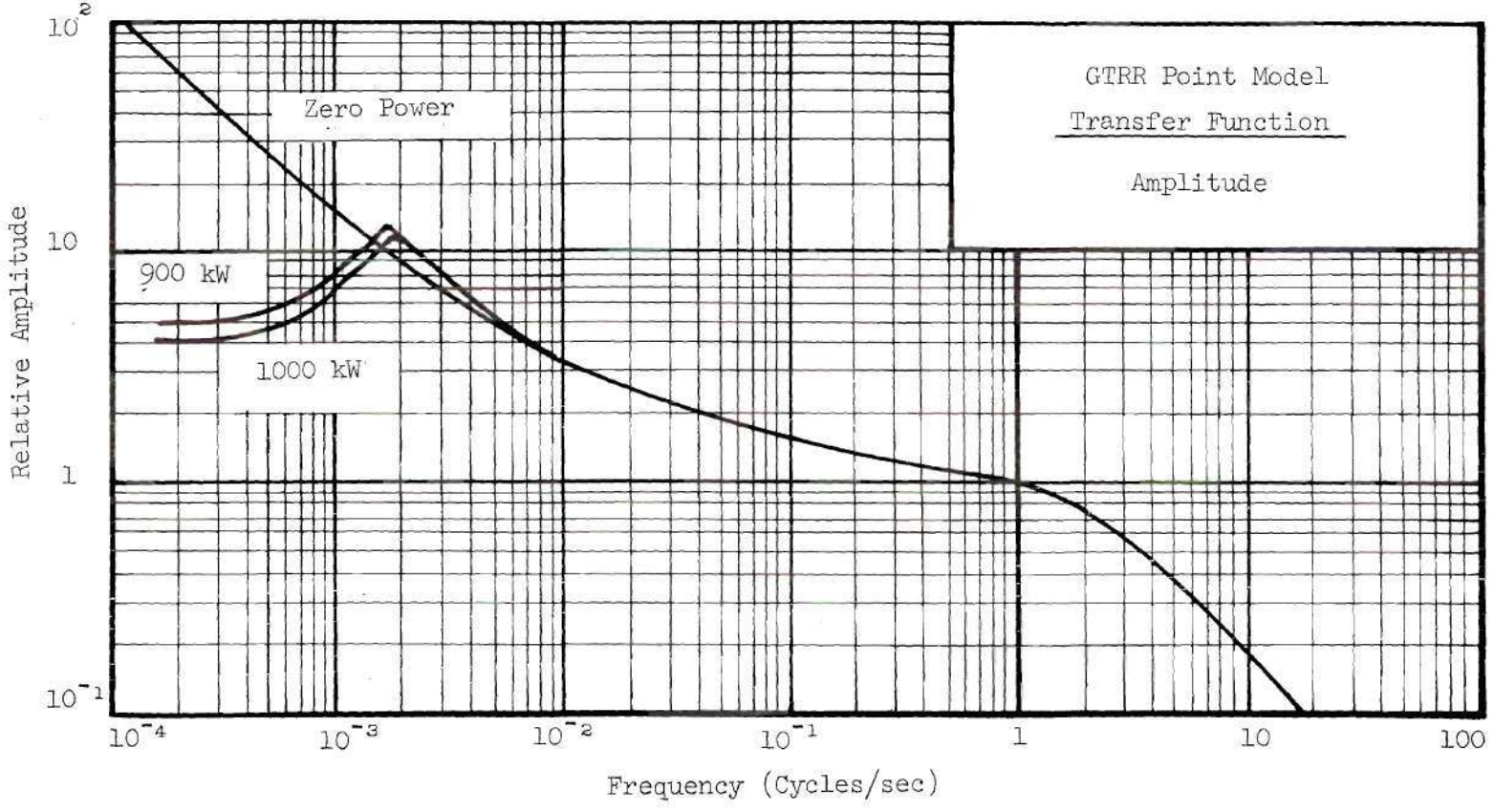

Figure 45. Amplitude of Transfer Function for GTRR Point Model

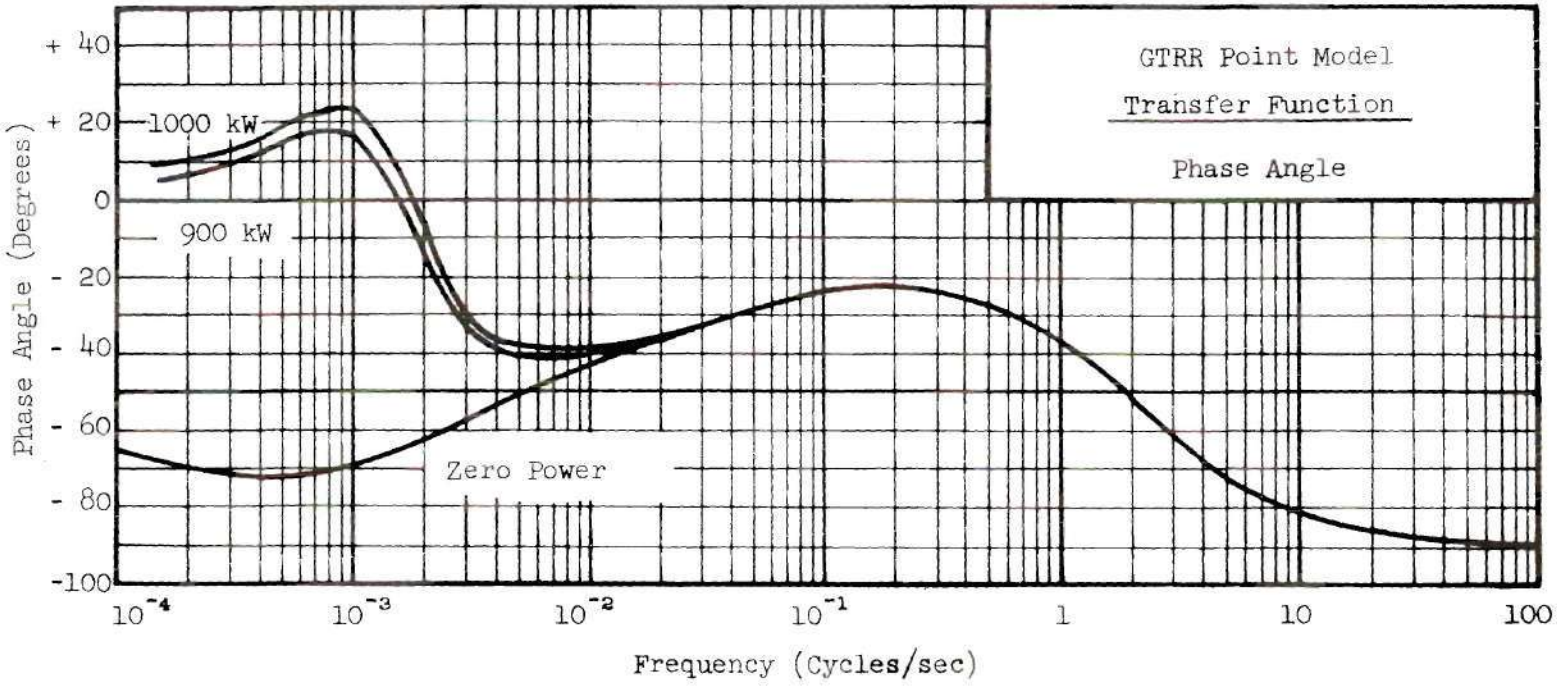

Figure 46. Phase Angle of Transfer Function for GTRR Point Model

temperature feedback becomes significant only at frequencies of 2×10^{-2} Hz and less. Pronounced effects occur at frequencies below 1×10^{-3} Hz.

This computation served to point out that significant temperature feedback effects were present and could be observed at reasonably low frequencies with the proper experimental planning and execution.

APPENDIX F

EXPERIMENTAL DATA COLLECTION PROGRAM FLOWCHARTS

Two programs were required for the collection and storage of the experimental data. The program ACQUIRE was used in the PDP-8 computer and generally was used to establish experimental parameters, document the experiment, drive the oscillator, control the ADC operation by the sample-and-hold unit, temporarily store in-core the data from the ADC operation, and transmit these data to the PDP-8/I computer. The program HANDLE was used in the PDP-8/I computer and generally was used to accept the data from the PDP-8, store these data temporarily in-core, write the data on magnetic tape, and perform miscellaneous magnetic tape functions such as writing end-of-files and rewinding the tape. Both programs are written in PAL (Program Assembly Language). Flowcharts for the two programs are shown in Figures 47 and 48.

In addition, the subroutine in ACQUIRE for driving the oscillator in accordance with the desired PRB sequence is shown in Figure 49. The teletype input to ACQUIRE determines the length and type of sequence. This was made variable in order to make the program more flexible.

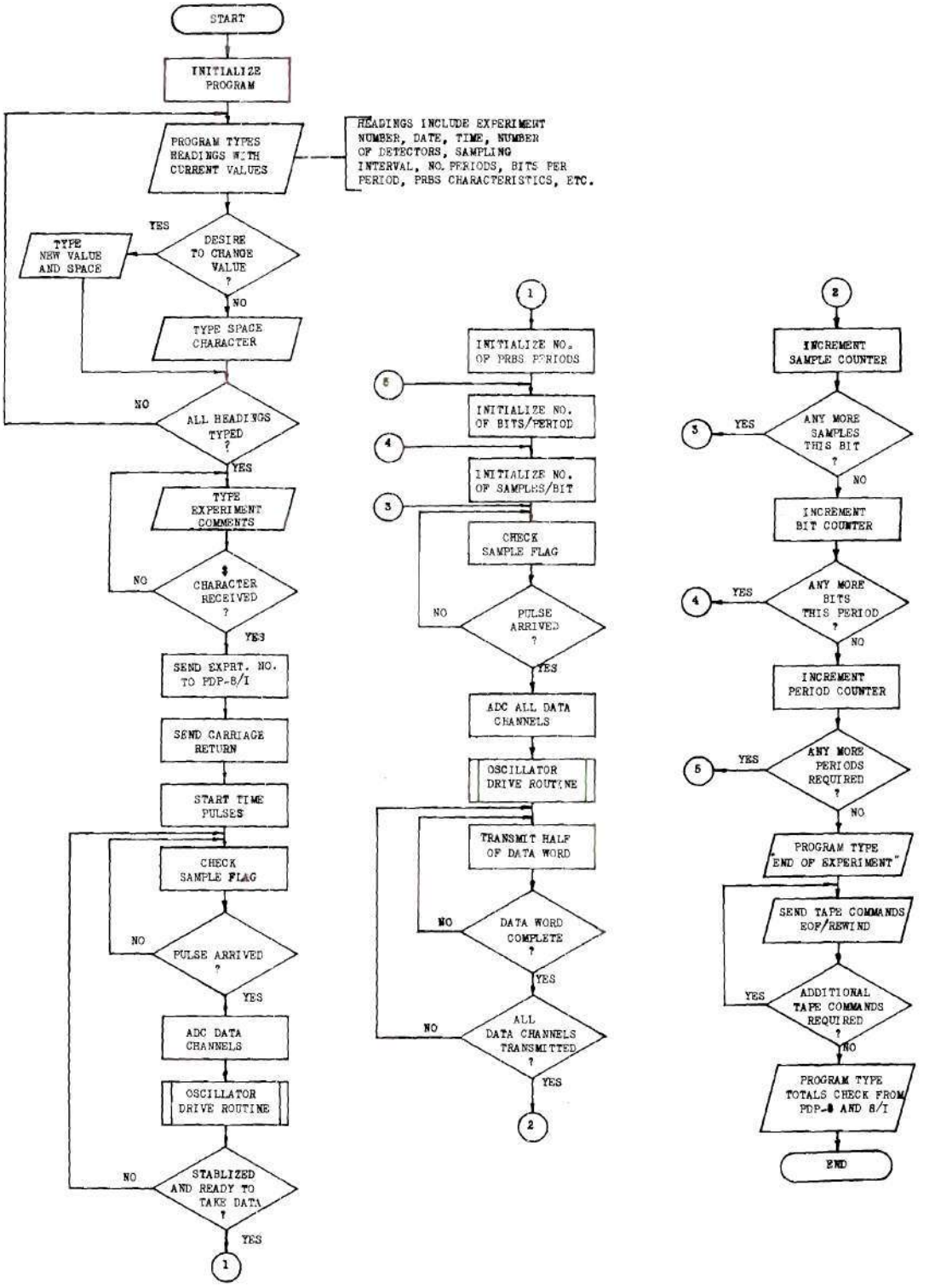

Figure 47. Flowchart for the Data Collection Program ACQUIRE

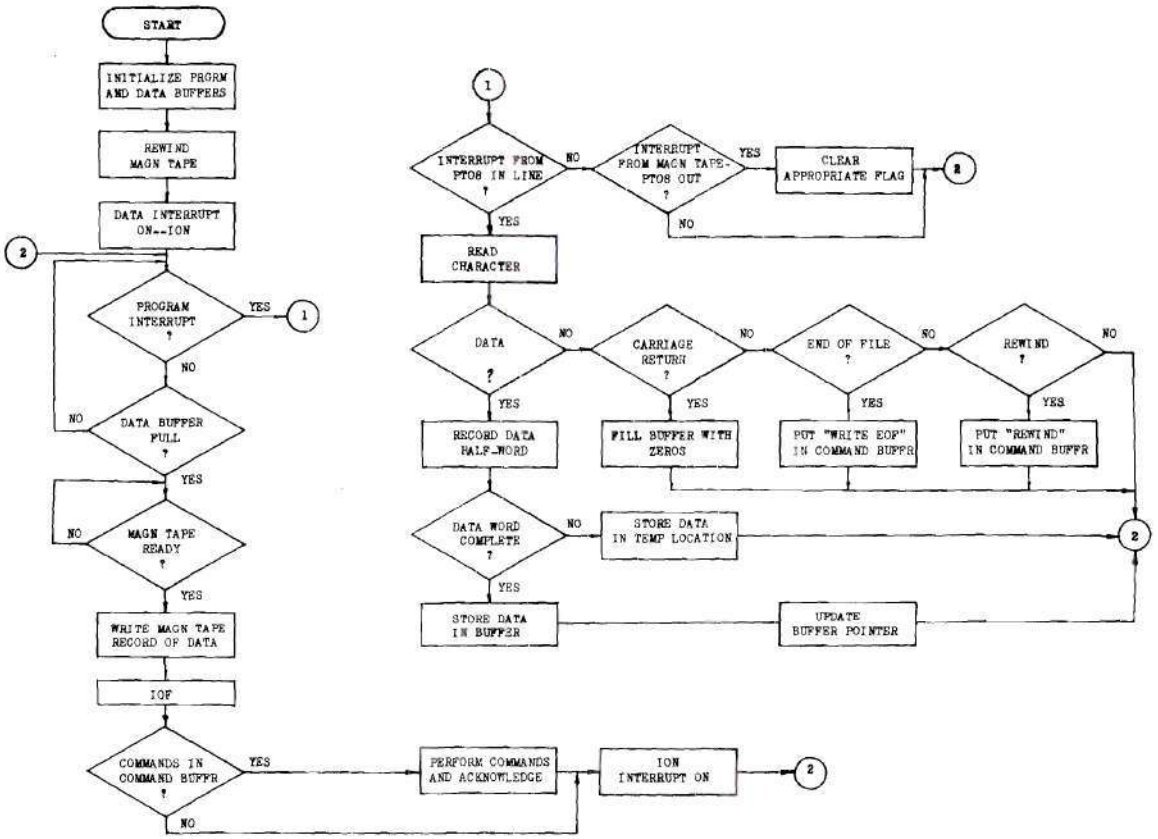

Figure 48. Flowchart for the Data Handling Program HANDLE

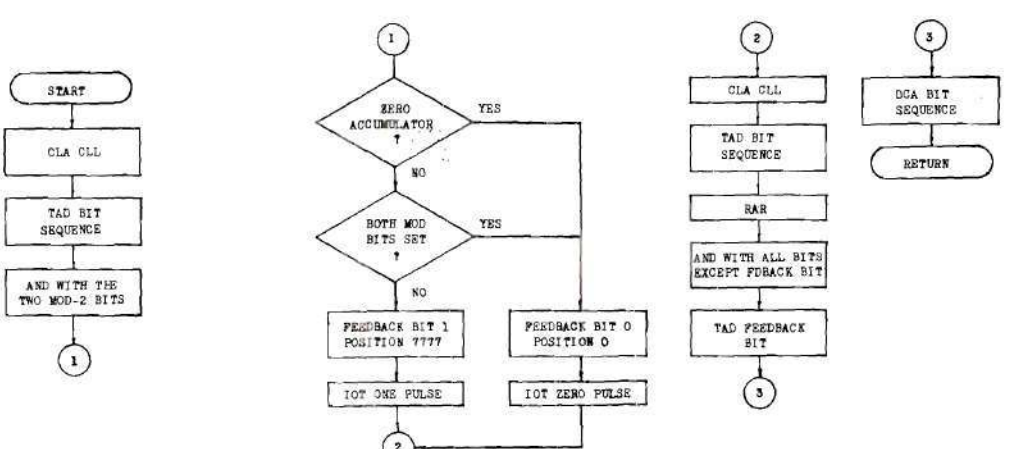

Figure 49. Flowchart for the Pile Oscillator Drive Routine

APPENDIX G

FREQUENCY RESPONSE MEASUREMENTS OF THE OSCILLATOR AND DATA COLLECTION EQUIPMENT

In the earlier discussion on the theoretical basis for experimental measurements and the experimental techniques, it was pointed out that, over certain frequency ranges, both the frequency response of the oscillator and the electrometers must be considered in the system analysis. This is particularly true for high frequencies for obvious reasons. In the case of the pile oscillator the physical movement occurs in a finite time period rather than a step fashion; therefore, studies relating system response to this movement must be related to the true movement rather than an assumed step function. In the case of the electrometers, actual filters are employed to filter out undesirable high frequency components. This reduction of equipment frequency response or electronic filtering is likewise not a step function and varies with frequency. High frequency filters were used in this experiment to rid the experiment of such factors as AC 60 Hz components and practically all frequency components in excess of the Nyquist frequency.

The purpose of this appendix is to present the results of studies made in this general area. The conclusion generally made from these measurements for the conditions of this experimental program is that significant corrections were necessary only for frequencies of one Hz and greater.

The first result discussed is for the actual movement of the oscil-

lator versus the theoretical movement. The measurements were made by attaching a position detector (Schavitz Engineering Company 200 DC Linear Variable Differential transformer) to an oscillator drive solenoid in the same manner that the drive solenoid is attached to the oscillator rotor. The output voltage signal from the position detector was then a function of the solenoid position. The output signal from the position detector was then wired directly to the sample-and-hold unit. The solenoid was driven in a typical experimental manner with a given PRB sequence and the actual response as measured by the position detector versus the theoretical response was investigated over a wide frequency range. The frequency range specifically investigated varied from 4×10^{-2} to 11 Hz. These limits varied from the lower frequency limit with practically no correction factors necessary to the highest frequency of interest for this investigation where there is a reasonably significant correction factor necessary. The frequency response of the physical movement is shown in Figure 50. The amplitude is only slightly affected at the highest frequency with an amplitude attenuation of five percent. However, the phase angle lag is appreciable with a phase angle shift of 40° at 11 Hz.

The amplitude and phase angle correction factors for the solenoid and rotor physical movement become quite large for frequencies in excess of 20 Hz. This feature makes the PRB sequence method of frequency response testing less desirable in the higher frequency ranges. In addition, for the very high frequencies introduced with very short bit times the two drive solenoids had a tendency to "jam up" since time was not permitted for one solenoid to deactivate and the other solenoid to activate. This investigation was limited to a maximum frequency of approximately ten Hz

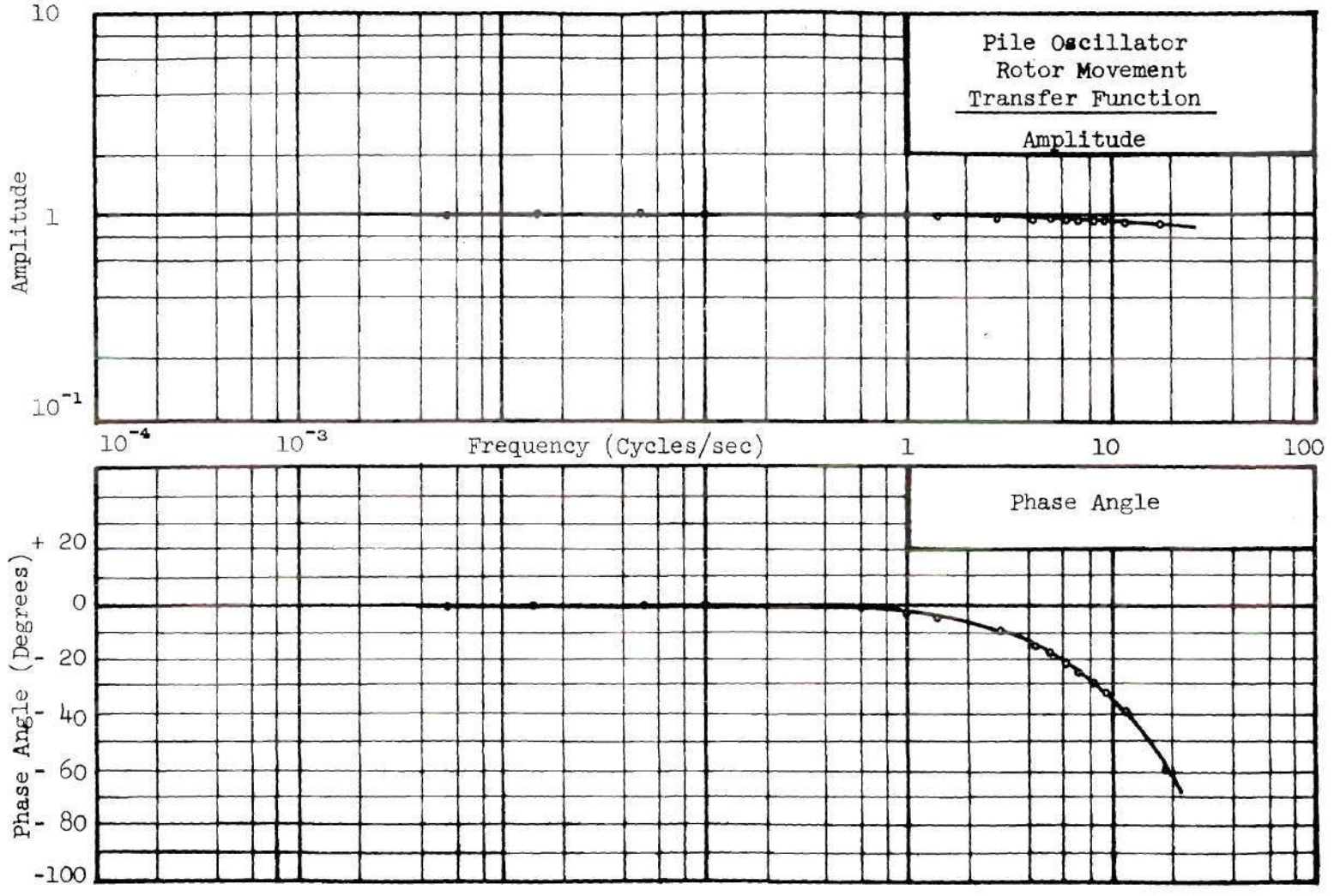

Figure 50. Transfer Function Measurements of the Pile Oscillator Rotor Movement (Measured Movement Response to Theoretical Movement Input Signal)

therefore, the solenoid "jam up" did not occur and the corrections for the rotor movement were made directly from the graphs in Figure 50.

The next area of interest was that of the frequency response of the electrometers. It has been pointed out that the electrometers had several settings for the low pass filters for the filtering or removal of unwanted high frequency components. Transfer function measurements were made for all range or current settings and several values of the low pass filters. The transfer function for the electrometer settings with the physical movement attenuation included is shown in Figure 51. This combination of factors was done as a matter of experimental ease since the position detector signal from the solenoid drive was attached to the electrometer with the appropriate settings and the resultant electrometer signal given to the sample-and-hold. By comparing this resultant output signal to the theoretical signal, one then gets the transfer function that includes attenuation and phase shift from both the finite movement time and electrometer response. This result provides the data of interest since it is much more inclusive and includes the information for the true correction. The transfer function amplitude of the electrometer filtering is equal to the amplitude of the combined effect divided by the amplitude of the finite movement. Likewise, the phase angle shift due to the electrometer filtering is the difference in phase angles between the combined effect and finite movement alone.

The electrometer transfer function studies were conducted with the current range set at 10^{-4} amp with the low pass filter set at 100 rad/sec. The low pass filter is a first order filter, therefore the amplitude attenuation should be 20 decibels per decade with the amplitude reduced by

a factor of three decibels ($\sqrt{2}$) at the break frequency of 15.9 Hz (100 rad/sec) with a 45° phase shift. From an analysis of the two graphs, it can be seen that the electrometer amplitude of 0.707 with a phase shift of 45° occurs close to the designed value of 15.9 Hz. To further check the amplitude attenuation through the electrometer, a sinusoidal wave generator was used as an electrometer input signal with the output from the instrument measured on an oscilloscope. The resulting ratio of output to input signals at various frequencies produced a curve similar to the curve shown in Figure 51. The resultant curve plotted was duplicated by the oscilloscope measurements within the accuracy of the scope readings.

Very little of this information could be used in the main experimental investigation since only a limited amount of the work was concerned with measurements above one Hz.

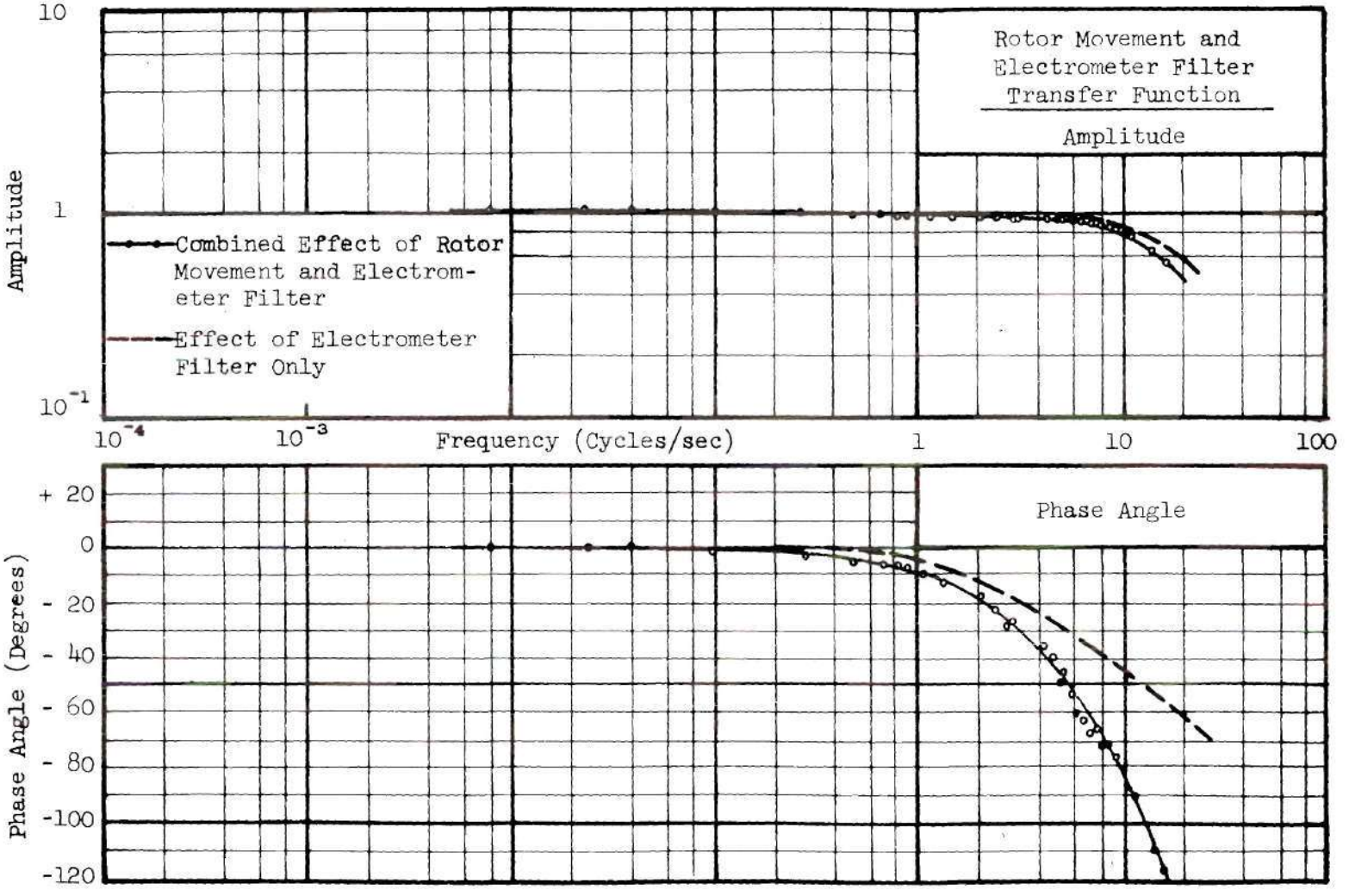

Figure 51. Transfer Function Measurements of the Rotor Movement and the Electrometer Filter (Measured Output Signal to Theoretical Movement Input Signal)

BIBLIOGRAPHY

1. J. N. Grace, "Reactor Kinetics," Selected Basic Techniques, Naval Reactors Physics Handbook, A. Radkowsky (Ed.), Vol. I, U. S. Atomic Energy Commission (1964).

2. P. R. Kasten, "Space-Dependent Reactor Kinetics," Nuclear Safety, 7 (2), 162-165 (Winter 1965-1966).

3. R. S. Stone, "Xenon Instability," Nuclear Safety, 1 (2), 35-37 (December 1959).

4. J. V. Wilson, "Xenon Instabilities," Nuclear Safety, 5 (4), 345-354 (Summer 1964).

5. Chun Hsu and T. P. Mulcahey, "Methods for Studying Space-Dependent Reactor Dynamics," Reactor and Fuel-Processing Technology, 11 (4), 172-179 (Fall 1968).

6. J. B. Yasinsky and A. F. Henry, "Some Numerical Experiments Concerning Space-Time Reactor Kinetics Behavior," Nuclear Science and Engineering, 22 (2), 171-181 (June 1965).

7. S. O. Johnson, E. P. Gyftopoulos, and M. E. Radd, "Effect of Flux Shape Changes on Power Excursions Behavior," Transactions American Nuclear Society, 8 (1), 221 (June 1965).

8. T. W. Kerlin, "Status of Space-Time Analysis," Nuclear Safety, 6 (4), 395-398 (Summer 1965).

9. A. F. Henry, "Neutron Kinetics," Selected Basic Techniques, Naval Reactors Physics Handbook, A. Radkowsky (Ed.), Vol. I, U. S. Atomic Energy Commission (1964).

10. A. F. Henry, "The Application of Reactor Kinetics to the Analysis of Experiments," Nuclear Science and Engineering, 3 (1), 52-70 (January 1958).

11. A. F. Henry and N. J. Curlee, "Verification of a Method for Treating Neutron Space-Time Problems," Nuclear Science and Engineering, 4 (6), 727-744 (December 1958).

12. A. M. Weinberg and E. P. Wigner, The Physical Theory of Neutron Chain Reactors, University of Chicago Press, Chicago, Illinois, 1958.

BIBLIOGRAPHY (Continued)

13. S. Kaplan, O. J. Marlowe, and J. Bewick, "Application of Synthesis Techniques to Problems Involving Time Dependence," Nuclear Science and Engineering, 18 (2), 163-176 (February 1964).

14. C. Hsu and R. E. Bailey, "Stability Analysis of Nonlinear Reactor Systems," Transactions American Nuclear Society, 9 (2), 457 (1966).

15. J. Chernick, A Review of Nonlinear Reactor Dynamics Problems, USAEC Report BNL-774, Brookhaven National Laboratory (July 1962).

16. P. N. Haubenreich, "Power-Reactor Stability," Nuclear Safety, 5 (4), 354-356 (Summer 1964).

17. J. P. Franz, "Pile Transfer Function," AECD-3260 (1949).

18. J. M. Harrer, R. C. Boyer, and D. Krucoff, "Transfer Function of Argonne CP-2 Reactor," Nucleonics, 10 (8), 32 (1950).

19. E. P. Gyftopoulos, "Transfer Function Representation of Nuclear Power Plants," Proceedings of the Conference on Transfer Function Measurement and Reactor Stability Analysis, ANL-6205, Argonne National Laboratory (May 1960).

20. A. M. Weinberg and H. C. Schweinler, "Theory of Oscillating Absorber in a Chain Reactor," Physical Review, 74, 851-863 (1948).

21. J. A. DeShong, "Power Transfer Functions of the EBWR Obtained Using a Sinusoidal Reactivity Driving Function," ANL-5798, Argonne National Laboratory (1957).

22. J. A. DeShong and W. C. Lipinski, "Analysis of Experimental Power-Reactivity Feedback Transfer Functions for a Natural Circulation Boiling Water Reactor," ANL-5850, Argonne National Laboratory (1957).

23. V. Rajagopal, Experimental Study of Nuclear Reactor Internal Noise and Transfer Function Using Random Reactivity Variations and Correlation Analysis, Ph.D. Thesis, Rensselaer Polytechnic Institute, Troy, New York (1960).

24. T. F. Parkinson, "Measurements of the Transfer Function of the University of Florida Training Reactor," Research Reactor Journal, AMF Atomics, 3 (3), 14-20 (Spring 1963).

25. V. Rajagopal and G. E. Swen, "Saxton Chemical Skim Kinetic Experiments," WCAP 3269-44, Westinghouse (June 1965).

BIBLIOGRAPHY (Continued)

26. P. T. Hansson and L. R. Foulke, "Investigations in Spatial Reactor Kinetics," Nuclear Science and Engineering, 17 (4), 528-533 (December 1963).

27. T. Nomura, "Some Aspects of Zero Power Reactor Transfer Functions," Journal of Nuclear Science and Technology (Tokyo), 1 (2), 41-50 (1964).

28. C. K. Sanathanan, "On the Synthesis of Space Dependent Transfer Functions," Inst. Elec. Electron. Eng. Trans. Automat. Contr., AC-11 (4), 724-729 (October 1966).

29. W. E. Loewe, "Space Dependent Effects in the Response of a Nuclear Reactor to Forced Oscillations," Nuclear Science and Engineering, 21, 536-549 (1965).

30. C. D. Kylstra and R. E. Uhrig, "Spatially Dependent Transfer Function for Nuclear Systems," Nuclear Science and Engineering, 22, 191-205 (1965).

31. T. Hoshino, J. Wakabayashi, and S. Hayashi, "New Approximate Solution of Space- and Energy-Dependent Reactor Kinetics," Nuclear Science and Engineering, 23 (2), 170-182 (October 1965).

32. C. E. Cohn, R. J. Johnson, and R. N. Macdonald, "Calculating Space-Dependent Reactor Transfer Functions Using Statics Techniques," Nuclear Science and Engineering, 26, 198-206 (1966).

33. R. J. Johnson, Investigation of the Space-Dependent Zero Power Reactor Source Transfer Function, Ph.D. Thesis, Georgia Institute of Technology, Atlanta, Georgia (September 1966).

34. R. N. Macdonald, A Method for the Analysis of Modulated Neutron Experiments, Ph.D. Thesis, Georgia Institute of Technology, Atlanta, Georgia (June 1966).

35. C. G. Poncelet, "Space Dependent Reactor Transfer Functions," WCAP 2873, Westinghouse (March 1966).

36. C. G. Poncelet, "Solution of the Multi-group Space-Time Diffusion Equations," International Conference on the Utilization of Research Reactors and Reactor Mathematics and Computation, Mexico City, Mexico (May 1967).

37. D. N. Bridges, J. D. Clement, J. P. Renier, "A Method for Calculating Space-Dependent Reactor Source Transfer Functions with Feedback," Nuclear Science and Engineering, 36 (1), 122-125 (April 1969).

BIBLIOGRAPHY (Continued)

38. E. P. Gyftopoulos, "General Reactor Dynamics," The Technology of Nuclear Reactor Safety, Reactor Physics and Control, T. J. Thompson and J. G. Beckerly (Eds.), Vol. 1, The MIT Press, Cambridge, Massachusetts, 1964.

39. F. de Hoffman, "Intensity Fluctuations of a Neutron Chain Reactor," USAEC Report MDDC-382 (LADC-256), Los Alamos Scientific Laboratory (1946).

40. E. D. Courant and P. R. Wallace, "Fluctuations of the Number of Neutrons in a Pile," Physical Review, 72 (11), 1038-1048 (1947).

41. M. N. Moore, "The Determination of Reactor Transfer Functions from Measurements at Steady Operation," Nuclear Science and Engineering, 3 (4), 387-394 (April 1958).

42. J. A. Thie, "Theoretical Reactor Statics and Kinetics of Boiling Reactors," Proceedings of the Second United Nations International Conference on the Peaceful Uses of Atomic Energy, Geneva, 1958, Vol. ii, 440-446, United Nations, New York (1958).

43. C. E. Cohn, "Determination of Reactor Kinetics Parameters by Pile Noise Analysis," Nuclear Science and Engineering, 5, 331-335 (1959).

44. C. E. Cohn, "Reflected-Reactor Kinetics," Nuclear Science and Engineering, 13 (1), 12-17 (1962).

45. Noise Analysis in Nuclear Systems, TID-7679, U. S. Atomic Energy Commission Symposium Series 4 (1964).

46. J. A. Thie, "Statistical Analysis of Power Reactor Noise," Nucleonics, 17 (10), 102-108 (October 1959).

47. J. D. Balcomb, H. B. Demuth, and E. P. Gyftopoulos, "A Crosscorrelation Method for Measuring the Impulse Response of Reactor Systems," Nuclear Science and Engineering, 11 (2), 159-166 (October 1961).

48. M. Hara and N. Suda, "Some Investigations into the Application of Pseudorandom Binary Signals to Reactor-Synamics Measurements," Proceedings of the Symposium on Neutron Noise, Waves, and Pulse Propagation, University of Florida, Gainesville, Florida, 247-270, February 1966.

49. J. Miida, K. Sumita, and Y. Kuroda, "Noise Analysis of Nuclear Reactor Systems in Japan," Noise Analysis in Nuclear Systems, TID-7679, 155-168 (1964).

BIBLIOGRAPHY (Continued)

50. P. Meyer and E. Garelis, "Use of a Pseudorandom Source Input in the Measurement of Impulse-Response Functions," Proceedings of the Symposium on Neutron Noise, Waves, and Pulse Propagation, University of Florida, Gainesville, Florida, February, 1966.

51. R. E. Uhrig and M. J. Ohanian, "Pseudorandom Pulsing of Subcritical Systems," Proceedings of the Symposium on Neutron Noise, Waves, and Pulse Propagation, University of Florida, Gainesville, Florida, February, 1966.

52. T. W. Kerlin, "Frequency-Response Testing," Nuclear Safety, 8 (4), 339-345 (Summer 1967).

53. W. T. Cochran, et al., "What is the Fast Fourier Transform?," IEEE Transactions on Audio and Electroacoustics, AU-15 (2), 45-55 (June 1967).

54. R. Klahn and R. R. Shively, "FFT-Shortcut to Fourier Analysis," Electronics, 124-128 (April 1968).

55. J. W. Cooley, "Applications of the Fast Fourier Transform Method," Proceedings of the IBM Scientific Computing Symposium, Yorktown Heights, New York, June, 1966.

56. J. M. Reynolds, Private Communication on unpublished research on Georgia Tech Research Reactor (March 1970).

57. J. A. Thie, Reactor Noise, Rowman and Littlefield, New York, New York, 1963.

58. J. A. Thie, "Noise Analysis in Reactor Safety," Nuclear Safety, 7 (3), 271-278 (Spring 1966).

59. M. Otsuka, "Theoretical Phases of Neutron Fluctuation Research in Japan," Preprints of the Japan-United States Seminar on Nuclear Noise Analysis, Tokyo and Kyoto, Japan, September, 1968.

60. J. A. Thie, "Noise in Power Reactors--A Review of Experiment, Analysis, and Theory," Preprints of the Japan-United States Seminar on Nuclear Reactor Noise Analysis, Tokyo and Kyoto, Japan, September, 1968.

61. K. Saito, "Input Noise Source of At-Power Reactors with Temperature Feedback Effect," JAERI Memo Number 3265 (Unpublished), Japan Atomic Energy Research Institute (October 1968).

BIBLIOGRAPHY (Continued)

62. M. W. El-Wakil, Nuclear Power Engineering, McGraw-Hill Book Company, New York, New York, 1962.

63. M. A. Schultz, Control of Nuclear Reactors and Power Plants, McGraw-Hill Book Company, Inc., New York, 1961.

64. C. E. Cohn, "A Simplified Theory of Pile Noise," Nuclear Science and Engineering, 7 (5), 472-475 (1960).

65. R. V. Meghreblian and D. K. Holmes, Reactor Analysis, McGraw-Hill Book Company, New York, 1960.

66. J. Macphee, "The Relative Stability of Boiling and Pressurized Light Water Moderated Reactors," IRE Transactions on Nuclear Science, NS-4 (1), 25-29 (March 1957).

67. M. Hara, et al., "Application of the Pseudo Random Binary Signals to JRR-3 High Power Dynamics Measurements," Journal of Nuclear Science and Technology, 5 (2), 79-85 (February 1968).

68. D. Little and M. A. Schultz, "Designing Heterogenous Reactors for Stability," IRE Transactions on Nuclear Science, NS-4 (1), 30-33 (March 1957).

69. C. Hsu, "Control and Stability Analysis of Spatially Dependent Nuclear Reactor Systems," ANL-7322, Argonne National Laboratory (July 1967).

70. "Safeguards Report for the Georgia Tech Research Reactor," Georgia Institute of Technology, Atlanta, Georgia (Unpublished)(January 1960).

71. W. W. Graham and D. M. Walker, Safety Analysis Report for the 5 MW Georgia Tech Research Reactor, Technical Report No. GT-NE-7, Nuclear Engineering Series, Georgia Institute of Technology, Atlanta, Georgia (December 1967).

72. J. J. Seidler, J. D. Clement, and W. R. Klein, Reactor Physics Calculations for the 5 MW Georgia Tech Research Reactor, Technical Report GT-NE-9, Nuclear Engineering Series, Georgia Institute of Technology, Atlanta, Georgia (September 1968).

73. R. S. Kirkland, Private Communication (June 1970).

74. M. Clark and K. R. Hansen, Numerical Methods of Reactor Analysis, Academic Press, Inc., New York, 1964.

BIBLIOGRAPHY (Concluded)

75. G. H. Weaver, Private Communication (June 1969).

76. "Small Computer Handbook," Digital Equipment Company, Maynard, Massachusetts, 1970.

77. V. Rajagopal, "Determination of Reactor Transfer Functions by Statistical Correlation Methods," Nuclear Science and Engineering, 12, 218-224 (1962).

78. J. A. Thie, Reactor Noise, Rowman and Littlefield, New York, 1963.

79. R. B. Blackman and J. W. Tukey, The Measurement of Power Spectra, Dover Publications, Inc., New York, 1958.

80. R. E. Uhrig, "Noise Analysis Notes," Unpublished notes (1968).

81. J. W. Cooley and J. W. Tukey, "An Algorithm for the Machine Calculation of Complex Fourier Series," Mathematics of Computation, 19 (90), 297-301 (April 1965).

82. N. R. Goodman, On the Joint Estimation of the Spectra, Cospectrum and Quadrature Spectrum of a Two-Dimensional Stationary Gaussian Process, Ph.D. Thesis, Princeton University (1957).

83. R. D. Evans, The Atomic Nucleus, McGraw-Hill Book Company, Inc., New York, 1955.

84. T. W. Kerlin, "Deterministic Signals for Frequency Response Measurements in Reactor Systems," Preprints of the Japan-United States Seminar on Nuclear Reactor Noise Analysis, Tokyo and Kyoto, Japan, September 1968.

85. T. W. Kerlin, "The Pseudo Random Binary Signal for Frequency Response Testing," USAEC Report ORNL-TM-1662, Oak Ridge National Laboratory, 1966.

86. W. W. Graham, III, The Determination of Effective Delayed Neutron and Photoneutron Kinetics Parameters in a Highly Enriched Heavy-Water Reactor, Ph.D. Thesis, Georgia Institute of Technology, Atlanta, Georgia (August 1965).

VITA

Donald Norris Bridges was born in Cleveland County, North Carolina, on August 13, 1936. He attended Shelby (N.C.) High School and graduated in 1954. Mr. Bridges attended North Carolina State University where he received the degree of Bachelor of Civil Engineering "with High Honors" in June, 1958. He attended graduate school in Civil Engineering at North Carolina State University and received a Master of Science degree in June, 1960.

In January, 1961, he was employed by the DuPont Company at the Savannah River Plant as a project engineer. The type of work at the Savannah River Plant was general engineering in support of the plant's nuclear facilities. In August, 1962, Mr. Bridges began four years of active duty in the United States Navy Civil Engineer Corps. The first tour of duty after Officer Candidate School was as a project management officer for the Public Works Center in Guantanamo Bay, Cuba. The second tour of duty was as a planning officer for the Public Works Center in Pensacola, Florida. Both of these jobs were primarily related to the management, maintenance, and construction of the Naval Shore Establishment facilities.

Mr. Bridges left active duty in 1966 to attend graduate school at the Georgia Institute of Technology. He received the Master of Science in Nuclear Engineering degree in 1968 and continued studies for a doctorate. The graduate study by Mr. Bridges at Georgia Tech was supported

by a Special Atomic Energy Commission Fellowship and a Graduate Research Assistantship.

Mr. Bridges is a member of the American Nuclear Society and the honor societies, Tau Beta Pi, Phi Kappa Phi, Sigma Xi, and Chi Epsilon. Mr. Bridges is active in the Naval Reserve and holds the rank of Lieutenant Commander.

Mr. Bridges is married to the former Charlene Kiser of Shelby, North Carolina. They have two children, Denise and David.